

TECHNISCHE UNIVERSITÄT MÜNCHEN

Department Chemie

Lehrstuhl für Biotechnologie

**Mechanistic Analysis of the Hsp70/ Hsp90
Co-chaperone Sti1**

Gordon Hack

Vollständiger Abdruck der von der Fakultät für Chemie der Technischen Universität München zur Erlangung des akademischen Grades eines Doktors der Naturwissenschaften genehmigten Dissertation.

Vorsitzender: Prof. Dr. Michael Sattler

Prüfer der Dissertation:

1. Prof. Dr. Johannes Buchner

2. Prof. Dr. Matthias Rief

Die Dissertation wurde am 08.07.2019 bei der Technischen Universität München eingereicht und durch die Fakultät für Chemie am 13.12.2019 angenommen.

Abstract

Hsp70 and Hsp90 are molecular chaperones which jointly assist the folding of many cellular proteins including kinases, transcription factors and E3 ligases. The collaboration between Hsp70 and Hsp90 is facilitated by the adapter protein Sti1, which physically connects the chaperones allowing for transfer of substrate proteins, termed clients, between them. Sti1 is an elongated protein composed of two modules connected by a flexible linker. These modules are in turn composed of multiple TPR and DP domains, with the N-terminal module comprising TPR1-DP1 and the C-terminal module comprising TPR2A-TPR2B-DP2. The TPR domains harbour the primary binding sites for Hsp70 (TPR1 and TPR2B) and Hsp90 (TPR2A) however the way in which the modules of Sti1 collaborate to bind the chaperones remains unclear. In this work an *in vitro* FRET system was developed to pinpoint the interaction between the C-terminus of the Hsp70 substrate binding domain (SBD) and TPR1 and TPR2B of Sti1. This revealed collaboration between the two domains in Hsp70 binding as well as a function for TPR1 in loading TPR2B via transfer of the Hsp70 C-terminus. An *in vitro* method for generating Sti1 labelled with different dyes at both domains within the same molecule was also developed for use in single-molecule FRET experiments. Biochemical and biophysical techniques were used to characterise the interaction of Sti1 with Hsp70 and Hsp90, in combination with Sti1 mutants and domain-swapped constructs. These experiments revealed an interdependency between Sti1 modules in chaperone binding. They further demonstrated the importance of the surface geometry of the C-terminal module of Sti1 in Hsp90 binding and in forming a ternary complex with both chaperones. Collaboration between the two modules of Sti1 was found to be critical for complex formation with Hsp70, Hsp90 and a model client protein, highlighting a role for the N-terminal module in loading complexes formed on the C-terminal module.

Contents

1 Introduction	1
1.1 Protein folding and molecular chaperones.....	1
1.1.1 Protein folding.....	1
1.1.2 Molecular chaperones.....	2
1.2 The Hsp70 chaperone	5
1.2.1 Functional diversity of the Hsp70 family	5
1.2.2 Structure and mechanism of Hsp70.....	8
1.2.3 Interaction with NEFs and J-proteins.....	10
1.3 The Hsp90 chaperone	11
1.3.1 Structure and mechanistic cycle of Hsp90.....	12
1.3.2 Hsp90 co-chaperone interactions.....	13
1.3.3 Hsp90 client interactions	15
1.4 Sti1: Bridging the gap	16
1.4.1 Architecture of Sti1	16
1.4.2 Interactions of Sti1 with Hsp70 and Hsp90	18
1.5 Aims	21
2 Results and Discussion	22
2.1 A FRET system to study Sti1 TPR domain interactions.....	22
2.1.1 Design of FRET system and Sti1 FRET mutants.....	22
2.1.2 Equilibrium FRET between Ssa1-SBD and Sti1 TPR domains	25
2.1.3 Kinetic analysis of TPR domain association measured by FRET	30
2.2 Towards a three colour FRET system to study the Sti1-Hsp70 Interaction.....	35
2.2.1 Design of Sti1 labelled independently at two sites.....	35
2.2.2 Generation of double labelled Sti1 via sortase-mediated ligation	38
2.3 TPR domain swaps: function within the context of full-length Sti1	42
2.3.1 Design of Sti1 TPR domain-swapped constructs.....	42
2.3.2 Functional analysis of Sti1 domain-swapped constructs	43
2.3.3 Contributions of TPR domains to the binding of labelled Hsp70	45

2.3.4 TPR domain contributions to ternary complexes with Hsp90 and labelled Hsp70	47
2.3.5 Contributions of TPR domains to the binding of labelled Hsp90	48
2.3.6 TPR domain contributions to ternary complexes with Hsp70 and labelled Hsp90	50
2.3.7 Complex formation between Sti1 domain-swapped constructs and the Ssa1-SBD.....	54
2.4 Complex formation with the client protein GR.....	60
2.4.1 Formation of GR-LBD-Hsp70-Hsp40 oligomeric complexes	60
2.4.2 Formation of quaternary GR-LBD complexes in the absence of ATP.....	63
3 Conclusions and Perspectives	68
3.1 TPR domain collaboration in EEVD binding revealed by FRET	68
3.2 Collaboration in EEVD binding requires context within Sti1.....	69
3.3 New insights into the Sti1-Hsp90 interaction	70
3.4 New insights into Hsp70-Sti1-Hsp90 ternary complex formation.....	71
3.5 Sti1 contributions to GR maturation <i>in vivo</i>	72
3.6 Sti1 inter-domain communication in GR-LBD quaternary complex formation	73
4 Materials and Methods	76
4.1 Materials and equipment.....	76
4.2 Primers	80
4.3 Plasmids.....	81
4.4 Molecular biology	82
4.4.1 Primer design.....	82
4.4.2 General PCR	82
4.4.3 Restriction digestion and ligation	82
4.4.4 Agarose gel electrophoresis.....	83
4.4.5 Site-directed mutagenesis	83
4.4.6 Restriction-free cloning	83
4.4.7 SLIC cloning.....	84
4.4.8 <i>E.coli</i> culture media.....	85
4.4.9 <i>S. cerevisiae</i> culture media	85
4.4.10 <i>P. pastoris</i> culture media.....	86
4.4.11 Cultivation of <i>E. coli</i> strains.....	86
4.4.12 Transformation of chemically competent <i>E. coli</i> strains.....	87
4.4.13 Cultivation of yeast strains	87

4.4.14 Transformation of <i>S. cerevisiae</i> strains.....	88
4.5 Protein expression and purification	88
4.5.1 Purification buffers	88
4.5.2 Protein expression	90
4.5.3 Cell disruption	91
4.5.4 Protein purification.....	91
4.6 Protein biochemistry.....	92
4.6.1 SDS polyacrylamide gel electrophoresis.....	92
4.6.2 Protein labelling	94
4.6.3 Sortase-mediated in vitro protein ligation	94
4.7 Protein analytical methods.....	95
4.7.1 Circular dichroism spectroscopy.....	95
4.7.2 UV/ Vis spectroscopy	96
4.7.3 Equilibrium FRET spectroscopy	96
4.7.4 Stopped-flow FRET spectroscopy.....	98
4.7.5 Fluorescence anisotropy	98
4.7.6 Analytical ultracentrifugation.....	99
4.8 Activity assays.....	100
4.8.1 Steady state regenerative ATP activity assay.....	100
4.8.2 Glucocorticoid receptor activity assay	101
Bibliography.....	103
Publications.....	117
Acknowledgements.....	119

Introduction

1.1 Protein folding and molecular chaperones

1.1.1 Protein folding

The rich diversity of life is made possible by the variety of folded structures adopted by proteins across living organisms. The information that governs these structures is contained within the sequence of a protein's constituent amino acids, the so called primary structure (Anfinsen, 1973). The attainment of 3D structure based on a given sequence is non-trivial due to the immense number of available degrees of freedom: a protein of 100 amino acids would take longer than the age of the universe to sample all the conformations available to it (Levinthal, 1968). Several mechanisms have been proposed to explain the fact that in reality, proteins are able to fold in tens of microseconds, including hierarchical folding initiated by secondary structure nucleation, or initial formation of unfolded states with broadly native-like topologies (Dill *et al*, 2008). One widely adopted view is that the conformational space available to a protein is thermodynamically constrained, giving rise to an energy surface or folding landscape. Starting from a large set of unfolded states, the folding polypeptide chain explores this surface, being funnelled through defined intermediates down a free energy gradient to arrive at the lowest energy conformation, the native state (Figure 1.1) (Dill & Chan, 1997; Dinner *et al*, 2000). The driving force behind this process is the burial of hydrophobic residues within protein cores, reorientation of hydrophilic residues to the aqueous environment, and a large entropic benefit from the reorganisation of associated water molecules (Levy & Onuchic, 2006). Proteins may however become kinetically trapped in metastable states, and prolonged exposure of hydrophobic residues may give rise to non-productive interactions with neighbouring chains resulting in amorphous aggregates (Figure 1.1). This risk is especially high considering the crowded environment of the cell, whose macromolecular concentration can reach up to 300-400 mg/ ml (Zimmerman & Trach, 1991). An additional challenge is posed by the changing environment of the cell under cellular stress conditions (Gidalevitz *et al*, 2011). Rapid or prolonged changes in temperature, pH, the local concentration of other molecules or chemicals, and osmotic and oxidative stresses can all have deleterious effects on protein folding. Furthermore mutations within the protein sequence can significantly alter the folding

landscape, giving rise to a loss of function if the native state cannot be achieved, or causing a build-up of toxic misfolded proteins or disease-causing amyloid fibril formations (Chiti & Dobson, 2006).

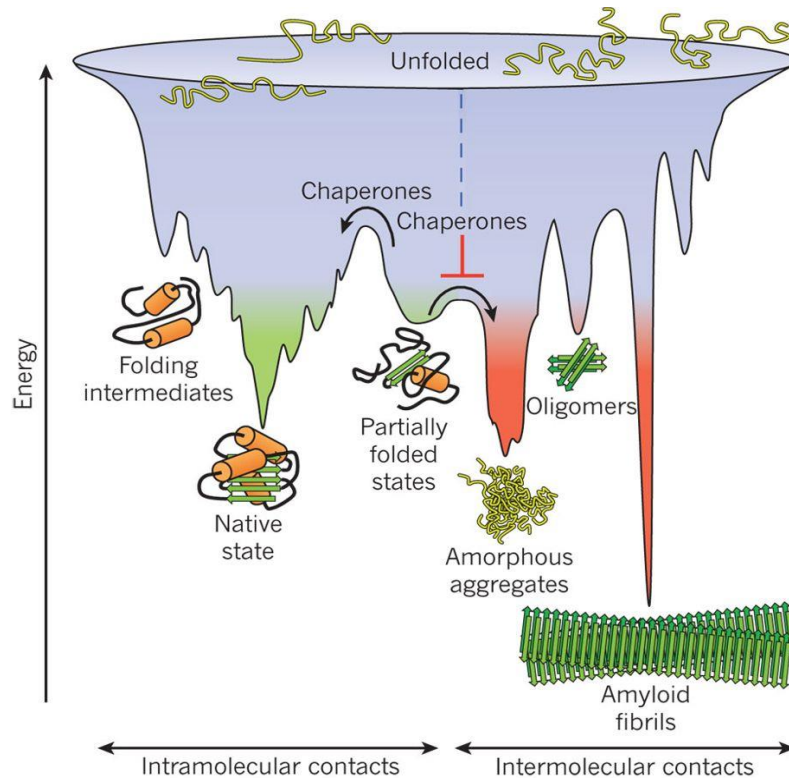


Figure 1.1 The protein folding energy landscape. Beginning from an initial unfolded state, a protein must fold by sampling through the metastable folding intermediates which define its folding landscape, gradually moving towards its most thermodynamically stable native state. Proteins can however become trapped in metastable states which can lead to the formation of toxic aggregates and amyloid fibrils. Molecular chaperones augment folding by promoting on-pathway interactions, resolving intermediates, refolding misfolded proteins and disassembling aggregates and amyloid fibrils. Adapted from Hartl et al., (2011).

1.1.2 Molecular chaperones

To address the challenges outlined in the previous section, nature has evolved a specialised set of proteins termed molecular chaperones, which play an indispensable role in protein folding across all forms of life. Chaperones function by binding hydrophobic residues and sequestering folding intermediates, allowing for formation of on-pathway contacts leading to the native state, while suppressing off-pathway intra- and inter-molecular contacts leading to misfolded states (Figure 1.1) (Hartl *et al*, 2011). Further, they form an integral part of the cellular protein quality

control, actively disassembling misfolded proteins and aggregates for degradation and recycling (Bukau *et al*, 2006). In analogy to enzymes and their substrates, chaperones can greatly enhance the thermodynamics of folding for proteins, lowering energy barriers between intermediate states (Takagi *et al*, 2003).

Most chaperones were found to be upregulated in response to heat stress and were thus termed heat shock proteins (HSPs) (Lindquist & Craig, 1988). Based on sequence homology and molecular weight they can be identified into five main classes: Hsp60/ chaperonin, Hsp70, Hsp90, Hsp100/ Clp and the so-called small heat shock proteins (sHsp). All classes except the small heat shock proteins are ATPases. Termed 'foldases', they exhibit cycles of substrate binding and release, coupling the energy from ATP hydrolysis to drive folding of the substrate in the process (Saibil, 2013). Small heat shock proteins however are ATP-independent, and their chaperoning capacity derives from their ability to dynamically assemble into poly-disperse oligomers. These bind to partially folded client proteins to suppress aggregation, prompting the term 'holdases' (Haslbeck *et al*, 2005). Their most prominent member is α -crystallin, a major structural protein in the vertebrate eye, whose conserved core α -crystallin domain represents the defining feature among sHsps (Horwitz, 1992). Structural and functional

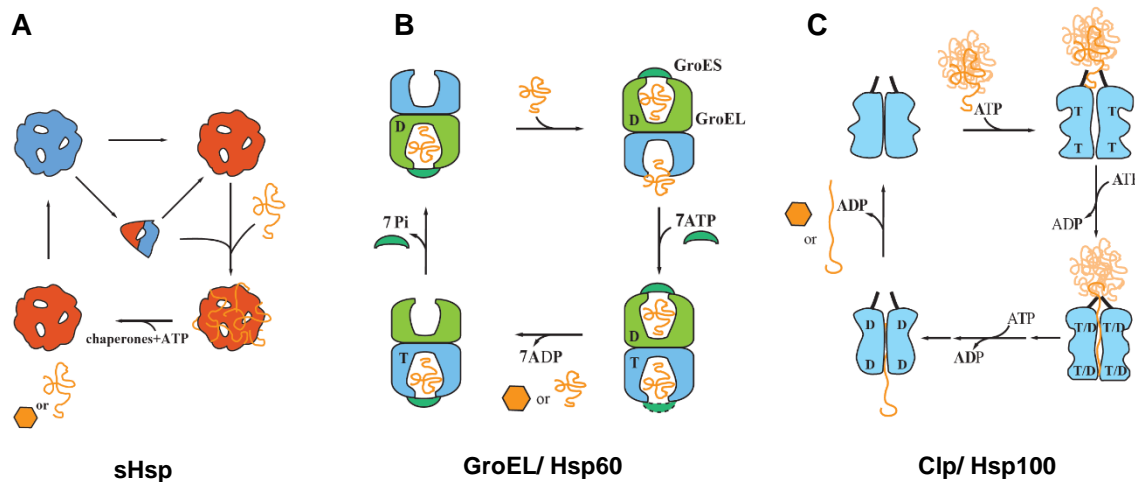


Figure 1.2 The diversity of molecular chaperones. (A) Small heat shock proteins (sHsp) form oligomeric structures which bind to and sequester unfolded proteins. These can then be refolded with the help of ATP-dependent chaperones. (B) Group I chaperonins such as GroEL provide a central cavity with the co-chaperone GroES in which substrate proteins are folded in an ATP-dependent manner. (C) The Clp/ Hsp100 chaperones couple ATP hydrolysis with the threading of misfolded substrates through a central pore for subsequent refolding or degradation. Adapted from Richter *et al.*, (2010).

variation across the family is provided by variability in the flanking N- and C-terminal regions, which evolved independently of the core domain (Kriehuber *et al*, 2010). Functionally speaking sHsps provide a temporary reservoir for unfolded proteins to prevent further aggregation (Figure 1.2, A). Misfolded substrates can then be refolded or disaggregated by coupling with other ATP-dependent chaperones such as Hsp70 and Hsp100/Clp (Mogk *et al*, 2003).

While the other four chaperone classes, the foldases, share a common dependence on ATP for their folding activity, their structures and mechanisms differ greatly. Hsp60s, also termed the chaperonins, are a class of chaperones characterised by their formation of large oligomeric ring structures. Unfolded peptide chains bind to, and are subsequently sequestered within a central ring cavity, whereupon ATP-dependent folding is promoted in a cooperative manner (Spiess *et al*, 2004). Chaperonins are classified structurally into group I and group II. The group I chaperonins are found in bacteria and endosymbiotic organelles and are exemplified by GroEL from *Escherichia coli* (Figure 1.2, B). GroEL forms two stacked homo-heptameric rings into which substrates bind, before being capped by a heptameric ring-shaped cofactor, Gro-ES (Braig *et al*, 1994; Xu *et al*, 1997). Group II chaperonins such as TRiC/ CCT (TCP-1 ring complex/ chaperonin-containing TCP1) form stacked heterooligomeric ring complexes of eight to nine subunits per ring, and are found in archaea and the cytosol of eukaryotic cells (Valpuesta *et al*, 2002). Group II chaperonins have a built-in lid and their constituent paralogous subunits possess differential net charge and ATP binding affinity, providing functional asymmetry across the complex (Reissmann *et al*, 2012; Leitner *et al*, 2012). Folding takes place via a nucleotide driven conformational cycle, involving highly coordinated allosteric communication between subunits, which induces global expansion and contraction of the complex (Lopez *et al*, 2015).

The Hsp100/ Clp chaperone family form homohexameric ring structures and have a demonstrated function in disassembling higher order protein structures and aggregates (Schirmer *et al*, 1996; Doyle & Wickner, 2009). Their mechanism involves ATP-dependent threading of a substrate polypeptide chain through a central pore (Figure 1.2, C) (Weber-Ban *et al*, 1999). In the case of bacterial ClpA, the unfolded substrate is transferred directly into the double-ring serine protease ClpP for degradation (Reid *et al*, 2001). Alternatively, substrates can be immediately refolded as in the case of ClpB/Hsp104. These have been shown to associate with the Hsp70 chaperone system forming a “bi-chaperone” network capable of disassembling, unfolding and refolding large aggregates (Goloubinoff *et al*, 1999; Mogk *et al*, 2015).

Hsp70 is the most extensive class of molecular chaperones, with homologues expressed in all three kingdoms of life as well as in various eukaryotic compartments. It consists of an N-terminal nucleotide binding domain (NBD) and a C-terminal substrate binding domain (SBD). ATP turnover in the NBD is intricately coupled to coordinated binding and release of peptide substrates in the SBD (Jiang et al., 2005; Mayer et al., 2019). Nature has adapted this basic mechanism for deployments in a broad range of functions, ranging from co-translational folding of nascent polypeptide chains, to refolding of protein aggregates, to translocation of polypeptide chains across membranes into cellular compartments (Döring et al., 2017; Nelson et al., 1992; Neupert et al., 2007). After folding to an intermediate stage, substrates are handed over from Hsp70 to the Hsp90 chaperone, facilitated by the bridging co-chaperone Sti1/Hop (Röhl et al., 2015; Schmid et al., 2012; Wegele et al., 2006).

Hsp90 acts at the later stages of folding, associating with a set of client proteins including transcription factors, kinases and E3 ligases to facilitate their maturation and regulate their stability (Taipale *et al*, 2012). Hsp90 functions as a homodimer with each subunit consisting of a C-terminal dimerization domain (CTD), middle domain (MD) domain and N-terminal domain (NTD) which possesses ATPase activity. It undergoes a conformational chaperone cycle augmented by a range of co-chaperones, which bind at defined stages and confer specificity for particular client proteins (Röhl *et al*, 2013). Hsp90 clients are involved in a broad range of cellular networks and the chaperone plays a central role in cellular protein homeostasis (Taipale *et al*, 2010).

1.2 The Hsp70 chaperone

1.2.1 Functional diversity of the Hsp70 family

Hsp70 is perhaps the most functionally versatile of all the molecular chaperones. Consisting of a nucleotide binding domain (NBD) and a substrate binding domain (SBD) tethered by a short linker, it functions through cycles of ATP hydrolysis coupled to the binding and release of substrates. This process is augmented by two principal classes of cochaperones: J-proteins (Hsp40) play a dual role in delivering substrates to Hsp70 and stimulating its ATPase activity, while nucleotide exchange factors (NEFs) displace ADP to facilitate subsequent re-binding of ATP (Figure 1.3, A) (Zuiderweg *et al*, 2017). Evolution has adapted this process to serve many cellular functions through a diversification of the hsp70 gene family, and an even greater

diversification of the accompanying co-chaperones (Kampinga & Craig, 2010). One factor underscoring the functional diversity of Hsp70 is its degenerate substrate recognition mechanism. The consensus motif consists of a short stretch of five amino acids enriched in hydrophobic residues, flanked by positive residues. Such non-stringency means that these sequence requirements are almost ubiquitous across the proteome, occurring on average every 30 – 40 amino acids in most proteins (Rüdiger *et al*, 1997). Indeed 15 – 20 % of newly synthesised polypeptides are chaperoned by Hsp70 (Thulasiraman *et al*, 1999).

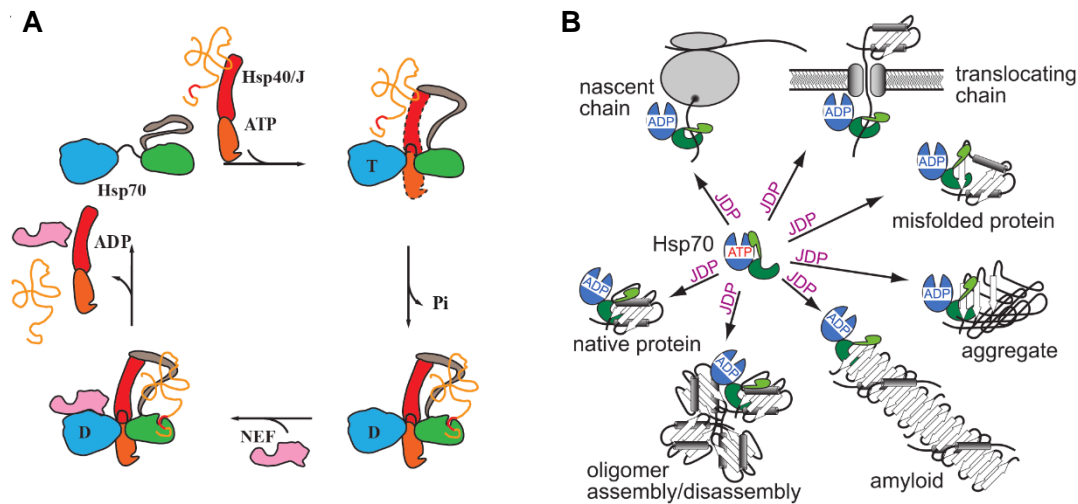


Figure 1.3 Functional diversity of Hsp70. (A) Mechanistic cycle of Hsp70 (blue: NBD, green: SBD, grey: lid) depicting the influence of J-domain proteins (Hsp40/ J) which deliver substrates and stimulate ATPase activity. Following substrate binding and ATP hydrolysis, nucleotide exchange factors (NEF) assist ADP release, followed by release of the substrate. Adapted from Richter *et al.*, (2010). (B) Schematic representation of the wide array of chaperone functions in which Hsp70 participates. J proteins (JDP) assist in loading substrates and provide functional specificity. Adapted from Mayer *et al.*, (2019).

The archetypal Hsp70 is bacterial DnaK. Being both constitutively expressed as well as heat-inducible, it carries out the folding of newly synthesised substrates, refolding of misfolded and aggregated proteins as well as roles in protein transport and quality control (Mayer & Bukau, 2005). Bacteria contain two further Hsp70 isoforms, HscA and HscC. HscA appears to function specifically in the assembly of iron-sulphur cluster-containing proteins, while HscC appears to lack general chaperone activity but may play a role in heavy metal stresses and UV-irradiation damage (Hoff *et al*, 2000; Kluck *et al*, 2002).

A dramatic expansion of isoforms reflects the high level of specialisation of Hsp70 within eukaryotic cells and across eukaryotic compartments (Figure 1.3, B). Yeast contain 14 Hsp70-encoding genes, and express 20 J-proteins as well as three NEFs, while humans contain at least thirteen Hsp70-encoding genes, and express a total of 50 J-proteins along with seven NEFs (Mayer & Bukau, 2008; Kampinga *et al*, 2009). In the human cytosol two major Hsp70 isoforms are present, the constitutively expressed Hsc70 (HSPA8) and the stress induced Hsp70 (HSPA1). These 'generalists' carry out the major folding activities, unfolding substrates for transport into organelles, as well as diverting terminally misfolded substrates for proteasomal degradation, or lysosomal translocation in the chaperone-mediated autophagy pathway (CMA) (Kaushik & Cuervo, 2012). Specificity in these activities is imparted by the rich repertoire of J proteins, NEFs and co-chaperones with which Hsp70 associates. For example the ribosome-associated J-protein DNAJC2 recruits Hsc70 to newly synthesised clients, while another J-protein, scHlj1, recruits Hsp70 to polypeptides exiting the ER during ER-associated degradation (ERAD) (Hundley *et al*, 2005; Nakatsukasa *et al*, 2008). The BAG proteins are NEFs which, in addition to exerting NEF activity through their common BAG domain, provide adaptor functions through additional protein-protein interaction motifs. BAG3 for example contains multiple PXXP motifs, IPV motifs and a WW domain, which bind to PpxY, SH3 and small heat shock proteins respectively (Kabbage & Dickman, 2008). The co-chaperone Sti1/ Hop connects Hsp70 to the Hsp90 system while CHIP (C-terminal of Hsp70 interacting protein) mediates Hsp70's role in proteasomal degradation by binding the Hsp70 C-terminal tail before recruiting ubiquitin ligases through a U-box domain (Jiang *et al*, 2001; Johnson *et al*, 1998). Compartment-specific chaperone functions are carried out by specialised Hsp70 isoforms within eukaryotic organelles. BiP (immunoglobulin binding protein) (HSPA5) is located in the lumen of the endoplasmic reticulum where it facilitates folding, translocation of newly synthesised proteins and retrotranslocation of misfolded proteins for proteasomal degradation (Wang *et al*, 2017). An analogous role is played by mitochondrial Hsp70 (mtHsp70, HSPA9 or mortalin) in stabilising mitochondrial pre-proteins as they are imported into the mitochondrial matrix (Ungermann *et al*, 1994; Craig, 2018). Indeed such pre-proteins will have been delivered to the mitochondrial import receptor Tom70 by cytosolic Hsp70 in collaboration with Hsp90 (Young *et al*, 2003).

Yeast express 9 cytosolic Hsp70 isoforms. Ssa1 – 4 are the classical Hsp70 chaperones, essential for viability and responsible for general protein folding and housekeeping. They are activated by the J-proteins, Ydj1 and Sis1 (Lu & Cyr, 1998). Ssb1 and Ssb2 are non-essential and serve a

more specialised role in assisting folding of nascent polypeptide chains, associating directly with the ribosome (Nelson *et al.*, 1992). The homologue Ssz has a similarly specialised role in nascent chain folding. It forms a stable complex with the Hsp40 homologue zuotin which binds almost exclusively to the ribosome; giving it the term ribosome-associated-complex (RAC) (Gautschi *et al.*, 2001). RAC acts in concert with Ssb1 and Ssb2 in processing nascent polypeptide chains as they exit the ribosome (Gautschi *et al.*, 2002). The two remaining isoforms, Sse1 and Sse2 have diverged into their own sub-family, named Hsp110 after the mammalian counterpart. The main function of Hsp110 appears to be to serve as NEFs for the canonical Hsp70s (Raviol *et al.*, 2006; Dragovic *et al.*, 2006). More recently however they have been shown to possess independent chaperone activity, and to take part in targeting substrates for proteasomal degradation (Mattoo *et al.*, 2013; Kandasamy & Andréasson, 2018).

1.2.2 Structure and mechanism of Hsp70

Over recent decades multiple structural, biochemical and computational studies have helped to build a picture of the conformational landscape of this highly dynamic chaperone. The 45 kDa Nucleotide binding domain (NBD) is divided into two lobes, I and II, each comprising two subdomains, IA, IB, IIA, IIB (Figure 1.4). These form a deep central cleft in which nucleotides bind and make contact with all four subdomains (Flaherty *et al.*, 1990). The NBD connects to a 25 kDa substrate binding domain (SBD) via a short linker which itself plays a central role in mediating allosteric communication (Swain *et al.*, 2007). The SBD is further subdivided into a 15 kDa β -sandwich subdomain (SBD β) which harbours the substrate binding site, and a C-terminal 10 kDa α -helical subdomain (SBD α) which acts a lid that reversibly closes over the substrate during the mechanistic cycle (Zhu *et al.*, 1996). The final 15 – 25 residues (varying between homologues and organisms) form a disordered region of unclear function which terminates with the highly conserved EEVD motif, important for TPR-co-chaperone binding (Brinker *et al.*, 2002; Smock *et al.*, 2011).

Structural studies have helped define two major conformational states adopted by Hsp70. In the presence of ADP or in the absence of nucleotide, a so-called ‘high affinity’ state is adopted in which the NBD and SBD exist as separated, independently tumbling units constrained by the linker (Figure 1.4, left) (Bertelsen *et al.*, 2009). In this state substrate association and dissociation is slow and the first two helices of SBD α pack tightly on the SBD β , forming a lid that encloses the substrate. In the presence of ATP Hsp70 undergoes dramatic structural rearrangements to a low affinity state in which SBD α and SBD β separate from one another and

dock onto opposing side of the NBD (Figure 1.4, Right). This provides a structural basis for the low substrate affinity observed in the ATP state (Kityk *et al*, 2012).

In addition to ATPase activity in the NBD regulating substrate binding in the SBD, substrate binding in the SBD reciprocally stimulates ATPase activity in the NBD (Flynn *et al*, 1989). Multiple residues have been identified in contributing to inter-domain communication, both through functional genetic screens and mutational analysis of surface exposed residues (Jiang *et al*, 2005; Montgomery *et al*, 1999). Many of these map to the extensive hydrogen bond network which is observed at the NBD/ SBD interface in the ATP-open conformation (Kityk *et al*, 2012). More recently, independent networks of residues leading away from this interface in both directions have been identified, highlighting signal transmission pathways that extend directly from the nucleotide binding pocket in the NBD, through to the substrate binding pocket in SBD β (Kityk *et al*, 2015; Mayer & Gierasch, 2019).

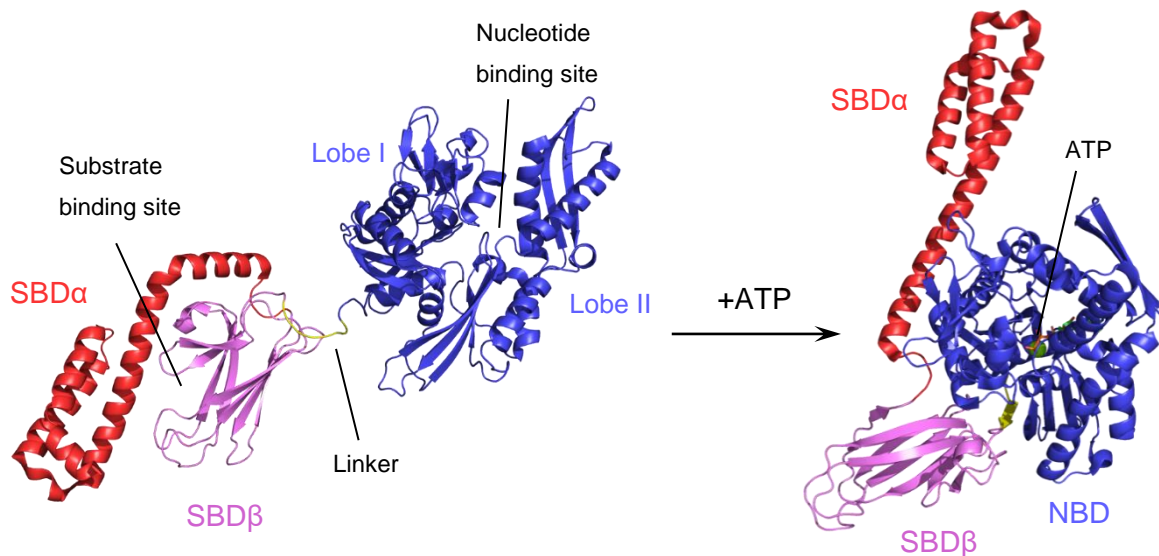


Figure 1.4 Hsp70 conformational transitions. Left: NMR solution structure (PDB: 2KH0) of Hsp70 in the 'high affinity' state showing the SBD α (red) closed over the SBD β (magenta) to form the substrate binding site. The linker (yellow) connects the NBD (blue) with the nucleotide binding site located between the two lobes. Right: crystal structure (PDB: 4B9Q) of Hsp70 in the 'low affinity' state in complex with ATP. SBD α and SBD β separated and docked onto opposing sides of the NBD, leading to low substrate affinity. Structures generated using PyMOL.

1.2.3 Interaction with NEFs and J-proteins

The conformational landscape of Hsp70 can be altered by NEFs and J-proteins, which bind respectively to modulate nucleotide-releasing and ATPase-activating effects (see Figure 1.3, A) (Liberek *et al*, 1991; Schröder *et al*, 1993). NEFs possess diverse structures yet all bind to the NBD of Hsp70, inducing relative movement of its constituent lobes to promote a conformation with lower nucleotide affinity (Figure 1.5, A) (Bracher & Verghese, 2015). Both GrpE, the sole bacterial NEF which is also located in mitochondria and chloroplasts, and the BAG proteins, a eukaryotic NEF class, induce the same 14 degree rotation of subdomain IIB of Hsp70-NBD, despite their unrelated structures and evolutionary histories (Sondermann *et al*, 2001; Harrison *et al*, 1997). The third eukaryotic NEF class comprises the cytosolic HspBP1 and the ER-resident Bap/ Sil1 (mammalian/ yeast). These bind to lobe II of the Hsp70-NBD via an armadillo repeat domain, inducing partial displacement (Shomura *et al*, 2005). More recently Bap has been shown to act as a conformational regulator of the ER-resident Hsp70 BiP, with an additional

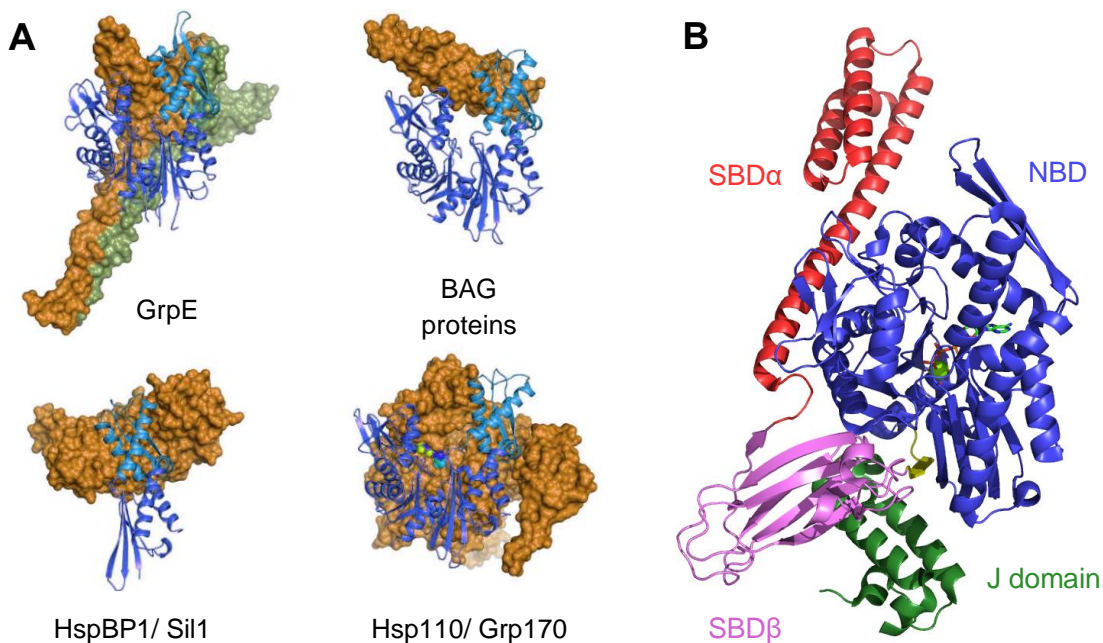


Figure 1.5 Hsp70 co-chaperone interactions. (A) Representative structures of the four NEF classes (surface representation) bound to Hsp70 NBD (ribbon representation). Top left: GrpE dimer bound to Hsp70-NBD (PDB:1DKG), top right: BAG domain bound to Hsp70-NBD (PDB:1HX1), bottom left: HspBP1 bound to Hsp70-lobe II (PDB: 1XQS), bottom right: Sse1p bound to Hsp70-NBD (PDB: 3D2F). (B) Crystal structure of a J domain bound to Hsp70 in the ATP state at a key interface for allosteric regulation (PDB: 5NRO). Structures generated using PyMOL.

function in inducing substrate release (Rosam *et al*, 2018). As mentioned in Section 1.2.1, the final eukaryotic NEF class Hsp110/Grp170 is an evolutionary offshoot of Hsp70 itself and shares the same molecular architecture. The structure of Hsp70 in complex with the yeast Hsp110 homolog Sse1 shows the two NBDs bound face to face, with nucleotide-displacing movements induced in lobe II of Hsp70-NBD (Polier *et al*, 2008).

In contrast to the divergent NEFs, members of the J protein family are united by their conserved J-domain, through which they bind to and modulate the activity of Hsp70. Functional diversity in this large family is provided by variable regions outside of the J-domain which can have little to no sequence relationship (Kampinga & Craig, 2010). J proteins play a joint role in delivering client proteins to Hsp70 while stimulating its ATPase activity. ERdj3, the major Hsp40 in immunoglobulin folding, transiently stimulates the ATPase activity of the ER-Hsp70 BiP, and forms a stable complex with BiP-ADP which has increased substrate affinity (Marcinowski *et al*, 2011). The J domain has been shown to stimulate Hsp70 ATPase activity by binding to the NBD, affecting the NBD-SBD linker conformation and inducing docking of the linker into a hydrophobic patch in the NBD (Jiang *et al*, 2007). A recent crystal structure of a J domain complexed with Hsp70-ATP shows the domain positioned at a key interface, simultaneously contacting the NBD, SBD- β and linker (Figure 1.5, B). This area is a Hsp70 allosteric commutation hotspot, suggesting a mechanism by which J proteins can feed into the Hsp70 allosteric network (Kityk *et al*, 2018). A group of small molecules has been discovered to bind to the J-protein/ Hsp70-NBD interface, providing the possibility to selectively target this interaction with therapeutics (Wisén *et al*, 2010).

1.3 The Hsp90 chaperone

Hsp90 is an essential protein which plays a central role in modulating a broad range of cellular processes. Originally discovered in the heat shock response in yeast, Hsp90 is now known to associate with several hundred client proteins involved in stress regulation, development, DNA repair and neuronal signalling as well as many other processes (Borkovich *et al*, 1989; Echeverría *et al*, 2011). Hsp90 plays a role at the later stages of folding and is generally required for the final stages of activation of its client proteins. Examples include hormone binding by steroid hormone receptors (SHRs), the loading of siRNA into the Argonaute 2 complex, or promoting an active conformation with client kinases (Grammatikakis *et al*, 1999;

Pratt & Toft, 1997; Iwasaki *et al*, 2015). In addition Hsp90 plays a role in the assembly of diverse complexes such as the telomere complex, kinetochore, RNA polymerase II, RNA induced silencing complexes (RISC) and the 26S proteasome (Makhnevych & Houry, 2012). To facilitate such diverse processes, Hsp90 associates with a large complement of co-chaperones which augment its mechanistic cycle and influence interactions with different clients (Röhl *et al*, 2013). Hsp90 has also been shown to facilitate genetic variation by associating with and buffering proteins with destabilising mutations, thereby allowing for their expression within a population (Jarosz & Lindquist, 2010; Rutherford & Lindquist, 1998). This activity however represents a double-edged sword, since Hsp90 is able to chaperone oncoproteins, allowing them to retain or even gain function in cancer cells (Whitesell & Lindquist, 2005). This has led to a burgeoning field of anti-cancer therapeutics which specifically target and inhibit Hsp90 (Butler *et al*, 2015; Neckers & Workman, 2012).

1.3.1 Structure and mechanistic cycle of Hsp90

Hsp90 exists as a homodimer, with each subunit consisting of an N-terminal domain (NTD) connected to a middle domain (MD) by a charged flexible linker, followed by a C-terminal domain (CTD) (Figure 1.6, A). The NTD is the site of ATP binding and hydrolysis while the charged linker modulates contact between the NTD and MD, important for the ATPase mechanism and function (Prodromou *et al*, 1997; Jahn *et al*, 2014). The MD mediates interaction with client proteins while the CTD is the site of Hsp90 dimerisation (Wayne & Bolon, 2007). At the end of a flexible tail at the very C-terminus lies the MEEVD sequence, to which a variety of co-chaperones possessing TPR domains bind to modulate Hsp90 function.

Hsp90 is a member of the gyrase, HSP90, His kinase and MutL (GHKL) superfamily of split ATPases, and docking of the MD onto the NTD is required to complete formation of the split ATPase domain and enable ATP hydrolysis (Meyer *et al*, 2003; Dutta & Inouye, 2000). In the absence of nucleotide, Hsp90 adopts an open V-shaped conformation (Shiau *et al*, 2006). Nucleotide binding induces closure of the subunits through a succession of defined intermediate states, to reach a final closed state in which the subunits are twisted with respect to one another (Figure 1.6, B) (Ali *et al*, 2006). Hsp90 ATPase activity is low, ranging from 0.1 ATP min⁻¹ in humans to 1 ATP min⁻¹ in yeast, however rather than ATP hydrolysis itself, the conformational changes leading to the final closed state have been shown to be rate-limiting (McLaughlin *et al*, 2002; Hessling *et al*, 2009). Furthermore the precise amount of time spent in each of these conformational states has been shown to be important for function (Zierer *et al*,

2016). The natural products geldanamycin and radicicol specifically inhibit Hsp90 by blocking the binding of ATP within the NTD and have spawned many promising therapeutics which target this site (Neckers & Workman, 2012).

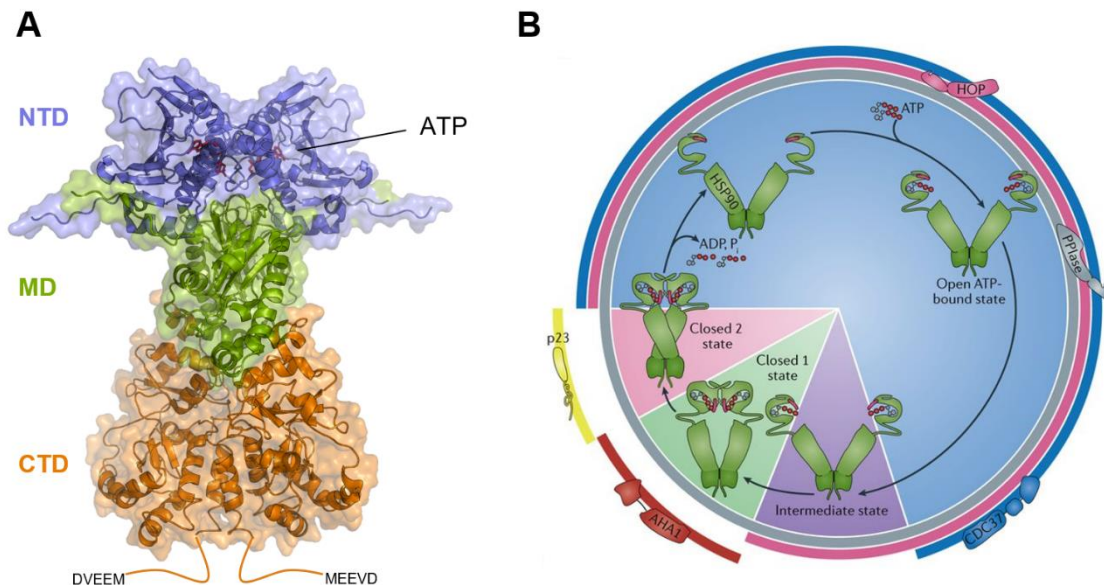


Figure 1.6 Structure and mechanistic cycle of Hsp90. (A) Crystal structure of yeast Hsp90 (PDB: 2CG9) in the final closed conformation. ATP (red) is bound within the NTD (blue), which is connected by the linker (disordered in the crystal structure) to the MD (green), followed by the CTD (orange), which terminates in the MEEVD motif connected by a flexible tail. (B) Progression of the Hsp90 ATPase cycle through defined conformational states, with the size of each coloured segment indicating the amount of time spent in each conformation. Coloured bars around the outside depict the stages of the cycle at which the co-chaperones HOP, Cdc37, PPIases, AHA1 and p23 bind. Adapted from Schopf et al., (2017).

1.3.2 Hsp90 co-chaperone interactions

Co-chaperones are important auxiliary proteins which bind to Hsp90 at the various stages of the conformational cycle outlined in the previous section. Bacteria possess no Hsp90 co-chaperones and the bacterial Hsp90 orthologue HtpG cycles in a deterministic, ratchet-like mechanism (Ratzke *et al*, 2012). In eukaryotes on the other hand, co-chaperones modify the Hsp90 cycle to impart specificity for particular functions, or interaction with particular clients. Many possess tetratricopeptide (TPR) domains which bind to the Hsp90 C-terminal EEVD motif, while others bind to surfaces across the MD and NTD, and the multiplicity of binding modes allows co-chaperones to bind in a sequential or synergistic manner (Schopf *et al*, 2017).

Ser/Thr protein phosphatase T (Ppt1; PP5 in humans) for example is a TPR-containing co-chaperone that binds to and dephosphorylates Hsp90, thereby regulating its conformational cycle (Wandinger *et al*, 2006). Cell division cycle 37 (CDC37) is a non-TPR co-chaperone that binds Hsp90 jointly across the MD and NTD and specifically mediates the maturation of kinase clients and (Stepanova *et al*, 1996; Verba *et al*, 2016). Simultaneous binding of PP5/ Ppt1 and CDC37 allows for dephosphorylation of CDC37, providing extra regulation of Hsp90-mediated kinase maturation (Vaughan *et al*, 2008). One of the best characterised Hsp90 co-chaperones is the Hsc70/ Hsp90-organizing protein (HOP; Sti1 in yeast) (discussed further in Section 1.4). HOP/ Sti1 contains a total of three TPR domains and facilitates simultaneous binding of Hsp70 and Hsp90 through their EEVD motifs (Johnson *et al*, 1998; Scheufler *et al*, 2000). Further it serves to hold Hsp90 in an open conformation, inhibiting its ATPase activity and allowing for delivery of client proteins from Hsp70 (Figure 1.7) (Richter *et al*, 2003).

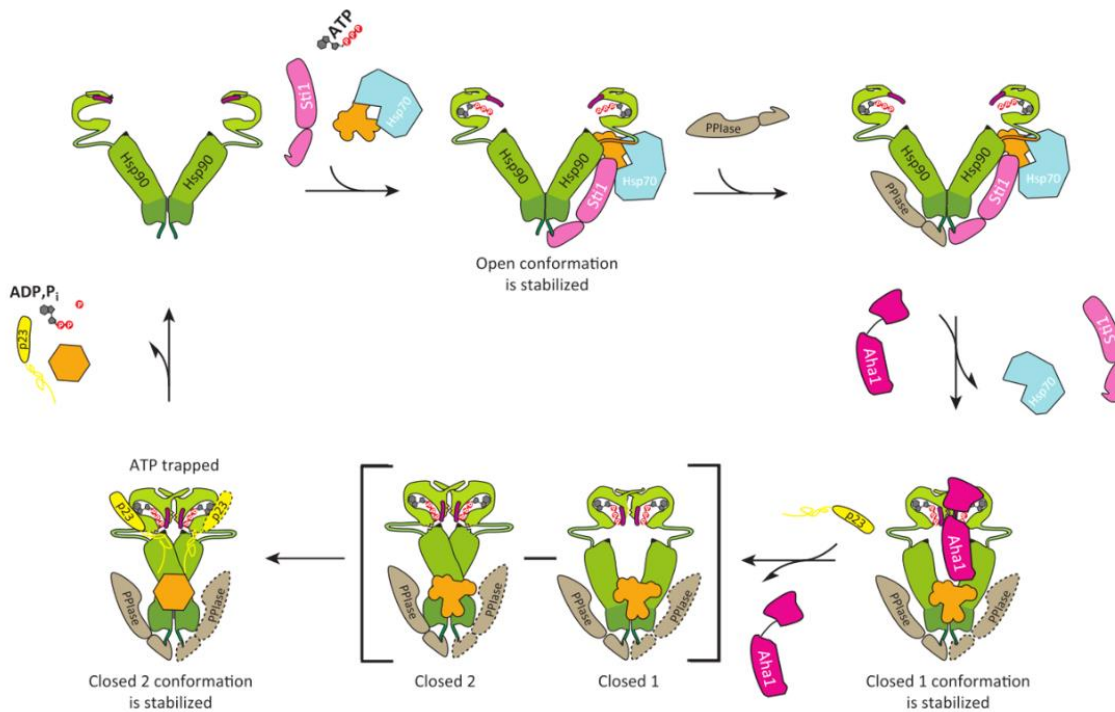


Figure 1.7 Hsp90 co-chaperone cycle. Sti1 binds Hsp90 to inhibit its ATPase activity and facilitate transfer of client proteins from Hsp70. PPIases bind through their TPR domains, forming heterocomplexes with Sti1 which can regulate progression of the cycle. Aha1 displaces Sti1 and induces closure of the Hsp90 dimer, stimulating its ATPase activity. After progressing through an initial closed 1 conformation, Hsp90 arrives at a final closed 2 conformation stabilised by p23/ Sba1. This allows for completion of folding and eventual release of the client protein before the cycle begins again. Adapted from Röhl *et al*, (2013).

The PPIases are cis–trans peptidyl–prolyl isomerases which also associate with Hsp90 through their TPR domains. Also termed immunophilins, In vertebrates they include the 51 kDa FK506-binding proteins FKBP51 and FKBP52 as well as cyclophilin 40 (CYP40), while yeast possess the cyclophilins Cpr6 and Cpr7 (Mayr *et al*, 2000). In addition to possessing chaperone activity, these co-chaperones bind at defined stages of the Hsp90 cycle and thereby regulate its progression (Freeman *et al*, 1996; Bose *et al*, 1996). Activator of Hsp90 ATPase 1 (Aha1) sequentially displaces Hop/ Sti1 to move the chaperone cycle forward (Li *et al*, 2013). Aha1 is a strong stimulator of Hsp90 ATPase activity and promotes a closed state in which one Aha1 is bound asymmetrically across the NTD and MD of a Hsp90 dimer (Retzlaff *et al*, 2010). p23 (Sba1 in yeast) is a late-acting co-chaperone that stabilises the final closed state of Hsp90, binding a groove formed by the dimerised Hsp90 NTDs (Ali *et al*, 2006).

1.3.3 Hsp90 client interactions

Unlike the more indiscriminate binding of Hsp70 to exposed hydrophobic residues, Hsp90 seems to bind to a specific, albeit large sub-section of the proteome. For humans this includes approximately 60 % of all kinases, 30 % of E3 ligases and 7 % of transcription factors (Taipale *et al*, 2012). The general features which define a Hsp90 client remain elusive, however some principles of interaction have been established with model clients. Comparison of the Hsp90 ‘non-client’ cellular Src kinase (c-Src) and its oncogenic counterpart v-Src, a strong Hsp90 client, suggest general intrinsic stability and folding cooperativity as determinants of Hsp90 dependency (Boczek *et al*, 2015). The tumour suppressor protein p53 is a client protein that binds mainly to the Hsp90-MD, with possible contributions from the NTD and CTD (Hagn *et al*, 2011). Whether p53 is fully folded or disordered when bound to Hsp90 however remains controversial (Rudiger *et al*, 2002; Park *et al*, 2011). One of the best studied Hsp90 clients, the glucocorticoid receptor has been shown to bind mainly in the cleft formed by two Hsp90 MDs in a dimer, with small contributions from the flanking NTD and CTD (Lorenz *et al*, 2014). This accords with a mutagenic study in which client-binding residues were found mainly to cluster in the MD (Genest *et al*, 2013). A recent cryo-EM structure of structure of the Hsp90 in complex with Cdc37 and the kinase client cyclin-dependent kinase 4 (CDK4) reveals the client threaded through a closed Hsp90 dimer, making intimate contact with the MDs (Verba *et al*, 2016).

1.4 Sti1: Bridging the gap

Sti1 (Stress-inducible protein 1; in yeast) or Hop (Hsp70-Hsp90 organizing protein; in humans) is a key co-chaperone in the joint functioning of the Hsp70 and Hsp90 systems. It forms a physical bridge between Hsp70 and Hsp90, resulting in a multi-chaperone complex in which delivery of intermediate client proteins from Hsp70 to Hsp90 is facilitated (Chen, 1998; Johnson *et al.*, 1998). Furthermore by inhibiting Hsp90 ATPase activity and preventing N-terminal dimerization, Sti1 regulates timing of the client transfer process (Prodromou *et al.*, 1999; Richter *et al.*, 2003). It is then displaced by PPIases, allowing for the final stages client maturation to continue on Hsp90, assisted by the co-chaperone p23 (Freeman *et al.*, 2000; Li *et al.*, 2011). Unlike many other co-chaperones Sti1 is substantially up-regulated in response to stress and, like Hsp70 and Hsp90 themselves, Hop overexpression has been observed in cancer cells (Ruckova *et al.*, 2012). Thus the targeting of Hop or its chaperone interactions presents an interesting therapeutic strategy (Walsh *et al.*, 2011). *S. cerevisiae* cells lacking Sti1 can grow well under optimal conditions but exhibit severe defects under stress (Chang *et al.*, 1997). In the absence of stress, chaperone function may be provided through a weak direct interaction between Hsp70 and Hsp90, which has been observed both in yeast and bacteria, of which the latter lacks a Sti1/ Hop homologue altogether (Nakamoto *et al.*, 2014; Kravats *et al.*, 2018). No direct interaction between Hsp70 and Hsp90 has thus far been observed in the mammalian system and knockout of Hop in mice is embryonically lethal (Beraldo *et al.*, 2013). In addition to its central role in Hsp70/ Hsp90 mediated chaperoning, Sti1/ Hop has been found to possess an increasing number of independent physiological functions. For example it has been found to be extracellularly secreted by many neuronal cell types (Baindur-Hudson *et al.*, 2015). Here it is involved in diverse neuronal functions in cell growth, survival and differentiation, chiefly through complex formation with the normal cellular prion protein PrPC (Zanata *et al.*, 2002).

1.4.1 Architecture of Sti1

Yeast Sti1 and Human Hop share a high degree of sequence conservation, conserved structure and conserved binding properties with both Hsp70 and Hsp90 (Röhl *et al.*, 2014). Furthermore Hop can functionally substitute for Sti1 in yeast (Carrigan *et al.*, 2004). Sti1 is an elongated protein consisting of a number of consecutively arranged globular domains connected by linkers: three tetratricopeptide (TPR) domains, TPR1, TPR2A and TPR2B as well as two aspartate- and proline-rich (DP) domains, DP1 and DP2. These are arranged into an N-terminal

module comprising TPR1 and DP1, connected by a flexible 60 amino acid linker to a C-terminal module comprising TPR2A, TPR2B and DP2 (Figure 1.8). TPR domains are common adapter modules for EEVD-chaperones, consisting of tandem repeats of 34 amino acid sequences which form 3 pairs of antiparallel α -helices, with optional additional flanking helices. Overall these generate a right-handed superhelical amphipathic groove with conserved basic residues which form a 'carboxylate-clamp' important in EEVD binding (Smith, 2004). In Sti1, TPR2A specifically binds the C-terminal tail of Hsp90 while TPR1 and TPR2B bind the Hsp70 C-terminal tail, representing the primary mode of interaction with each of the chaperones (Schmid *et al*, 2012). In addition to interactions forming the carboxylate clamp, specificity for either chaperone is provided by interactions with residues upstream of the EEVD (GPTIEEVD in the case of Hsp70 and DTEMEEVD in the case of Hsp90) (Scheufler *et al*, 2000).

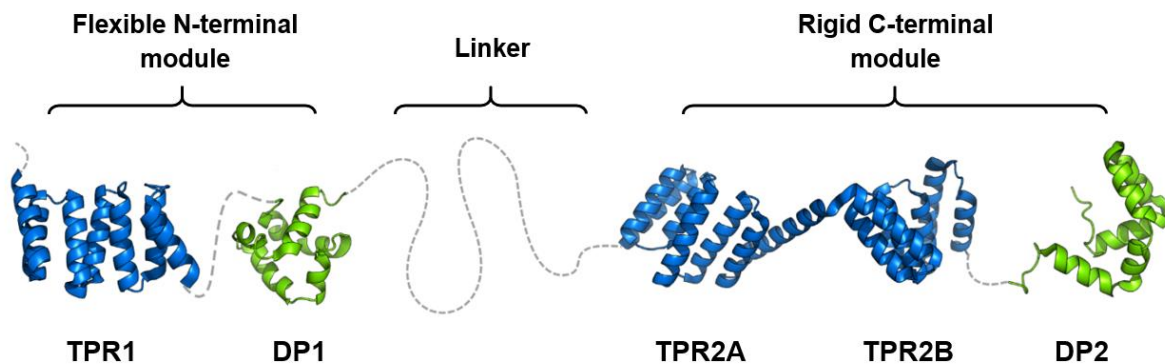


Figure 1.8 Schematic model of Sti1 from structures of individual domains. Sti1 is an extended protein comprising a flexible N-terminal module and a rigid C-terminal module connected by a central, flexible linker region. The N-terminal module consists of TPR1 (PDB:1ELW) and DP1 (2LLV) while the C-terminal module consists of TPR2A-TPR2B (PDB: 3UQ3) and DP2 (PBD: 2LLW).

The function of the DP domains of Sti1 has so far remained less clear. These small α -helical domains have a unique fold shared only with the co-chaperone HIP (Hsp70 interacting protein), although the domains are not functionally interchangeable between the two proteins (Nelson *et al*, 2003). A role for DP2 in client activation has been identified, with mutations in this domain shown to abrogate *in vivo* activation of the glucocorticoid receptor (GR), a model client protein (Carrigan *et al*, 2005; Flom *et al*, 2006). DP1 is however dispensable for client activation and cannot rescue the defect caused by loss of DP2 when the two domains are exchanged in position (Schmid *et al*, 2012). On the C-terminal module, DP2 has been shown to have a fixed orientation

with respect to TPR2A-TPR2B, which themselves form a rigid S-shaped configuration orienting peptide binding grooves on opposing sides (Figure 1.8). The N-terminal module on the other hand is flexible and the both the N- and C-terminal modules are highly flexible with respect to one another via the linker (Röhl *et al*, 2015). TPR2A-TPR2B binds Hsp70 and Hsp90 simultaneously and, with the addition of DP2, is the minimal unit necessary to support GR activation *in vivo*. This has led to the idea that TPR2A-TPR2B-DP2 forms the productive core of Sti1, with the N-terminal module TPR1-DP1 serving an auxiliary role in loading and unloading Hsp70 (Schmid *et al*, 2012). Indeed the *D. melanogaster* Sti1 homologue lacks DP1 and the *C. elegans* homologue lacks TPR1-DP1 altogether (Gaiser *et al*, 2009; Johnson *et al*, 2009).

1.4.2 Interactions of Sti1 with Hsp70 and Hsp90

In addition to the primary Hsp90-EEVD - TPR2A binding mode, a secondary interaction has been defined between the Hsp90-MD and surface across TPR2A-TPR2B (Figure 1.9). This is the minimal unit necessary to inhibit Hsp90 ATPase activity, and may do so by making additional contact with the Hsp90-NTD (Richter *et al*, 2003; Lee *et al*, 2012). The observed FRET association between Sti1 and Hsp90 shows three kinetic phases, leading to a picture where the Hsp90-EEVD - TPR2A interaction engages first, acting as a 'fishing hook', before conformational changes allow engagement of the secondary interaction, and possibly binding of a second Sti1 (Lee *et al*, 2012).

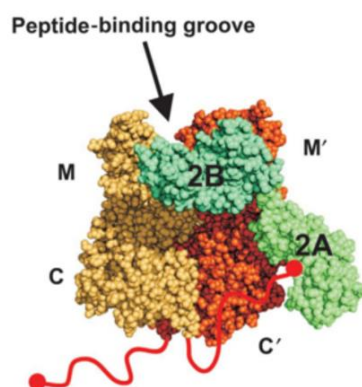


Figure 1.9 Secondary interaction between Sti1 and Hsp90. In addition to the MEEVD peptide interaction (red), Hsp90 (MD and CTD dimer shown in gold and orange) engages a secondary interaction with a joint surface across TPR2A-TPR2B of Sti1 (green). The peptide binding groove of TPR2B faces outwards, making it accessible to Hsp70. Adapted from Schmid *et al*. (2012).

The full nature of interaction between Sti1 and Hsp70 is less clear due to overlapping contributions from TPR1 and TPR2B (Flom *et al*, 2006). Analogous to the case with Hsp90 and TPR2A, the C-terminal EEVD motif of Hsp70 forms a primary interaction with the peptide binding grooves of TPR1 and TPR2B (Demand *et al*, 1998; Flom *et al*, 2007; Schmid *et al*, 2012). While no secondary interaction has thus far been defined between Sti1 and Hsp70, evidence exists of additional contributions to binding outside of the primary EEVD interaction (Carrigan *et al*, 2004; Schmid *et al*, 2012). Ternary complexes are formed between Hsp70, Hsp90 and Sti1 as well as with Sti1 in which either TPR1 or TPR2B are inactivated, although respectively to a lesser and greater extent. Both binding to Hsp70 and ternary complex formation are affected by the presence of the Sti1 linker, indicating a role for conformations in which the modules at either end communicate. Indeed the presence of the Hsp70 and Hsp90 induces significant conformational fluctuations in Sti1 which bring the two modules into close proximity (Röhl *et al*, 2015). A recent electron microscopy study was able to capture ternary complexes between Sti1, Hsp70 and Hsp90 as well as a quaternary complex with the ligand binding domain of GR (Alvira *et al*, 2014). In the major population of the ternary complex, Sti1 occupies one face on an Hsp90 dimer and is bent 180° about the linker (Figure 1.10, A). The Hsp70 NBD protrudes from the top of the complex while the Hsp70 SBD is inserted down between the two lobes of Sti1, seemingly poised for transfer between modules. A small population of ternary complexes were observed in an extended conformation, with mass attributed to Hsp70 bound to TPR1 protruding out to one side (Figure 1.10, B). Taken together these results have built up a picture in which TPR1 functions as a recruitment module, binding an incoming client-bound Hsp70 before loading onto TPR2B, which forms a productive module with Hsp90 bound to TPR2A (Figure 1.10, C). From here the client may transfer directly to Hsp90 to complete its folding.

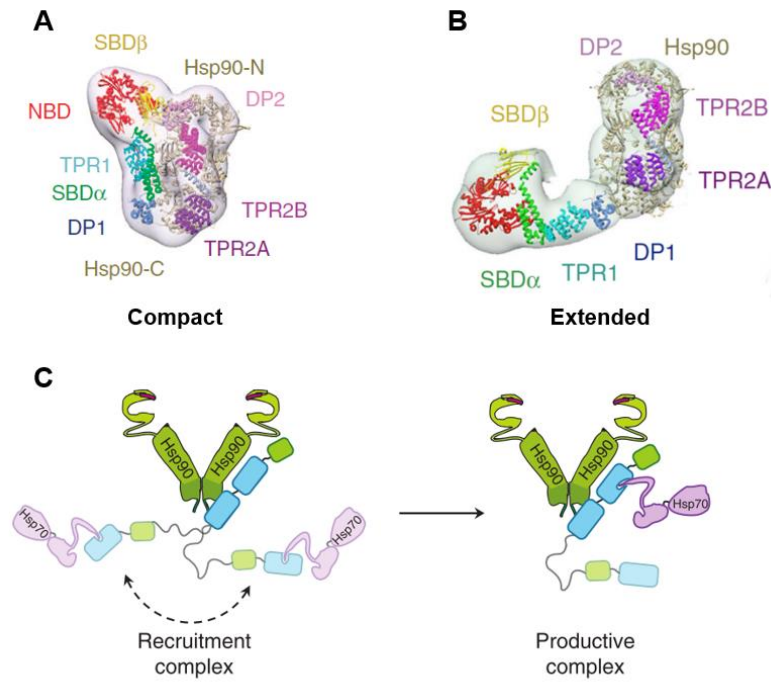


Figure 1.10 Structure of Hsp70-Sti1-Hsp90 ternary complexes. (A) The major population is a compact complex with Hsp70 and Hsp90 bound on opposing sides of Sti1, which itself is bent 180° into a U-shape. (B) The minor population is extended and appears to show Sti1 bent roughly 90° with Hsp70 bound exclusively to TPR1. Adapted from Alvira et al., (2014). (C) Proposed role of TPR1 in loading Hsp70 onto TPR2B in order to interact with Hsp90 and deliver the client protein. Adapted from Röhl et al., (2015).

1.5 Aims

This project aimed to provide a deeper understanding of the central role played by the scaffolding protein Sti1 in assembling multi-chaperone complexes with Hsp70 and Hsp90. In particular, the work aimed to understand the interaction between Sti1 and Hsp70, which has so far been complicated by the presence of two Hsp70 binding sites on Sti1, situated in the TPR domains TPR1 and TPR2B. These are located at opposite ends of the Sti1 protein, which consists of two modules connected by a flexible linker. The project therefore sought to develop strategies to distinguish between these domains, separating contributions to Hsp70 binding as well as to the formation of complexes with Hsp90 and a model client protein.

Firstly, the work aimed to establish an intermolecular FRET system, involving the introduction of probes which could specifically pinpoint the interaction of the Hsp70 C-terminal tail with either TPR1 or TPR2B. By characterising the interaction at each domain under conditions where the other was active or inactive, potential cooperation between them in Hsp70 binding could be investigated. Further the system was sought to be used as a basis for the development of a three-colour FRET system, for future study with single molecule FRET spectroscopy. To this end the project aimed to demonstrate an *in vitro* method for generating a Sti1 molecule in which both TPR1 and TPR2B are labelled specifically with different fluorescent dyes.

The project further aimed to investigate the architecture of Sti1 and in particular, whether the TPR domains could functionally substitute one another in terms of Hsp70 binding and multi-chaperone complex formation. To this end a series of domain-swapped constructs were designed whose functional properties, interaction with Hsp70 and Hsp90, and ternary complex formation with both chaperones could be investigated. Finally, the project aimed to investigate the contribution of Sti1 TPR domains to the chaperoning of a model client protein, the glucocorticoid receptor (GR). This was sought to be achieved by assessing the ability for Sti1 domain-swapped constructs to support GR maturation *in vivo*, as well as examining the determinants of complex formation *in vitro* with the GR ligand binding domain (GR-LBD). Taken together these experiments will provide greater insight into how the TPR domains of Sti1 collaborate in the interaction with Hsp70, Hsp90 and client proteins.

Results and Discussion

2.1 A FRET system to study Sti1 TPR domain interactions

A major aim of this work was to deepen the understanding of how TPR1 and TPR2B cooperate to bind Hsp70, toward formation of the overall multichaperone complex. In contrast to previous work involving isolated Sti1 domains and mutants, a system was sought whereby Hsp70 binding to either TPR could be discriminated while both were active in the full-length protein, allowing contributions from each domain to the other to be separated. To this end fluorescence resonance energy transfer (FRET) was chosen as an ideal tool as it allows for the measurement of interactions between probes introduced at user-designed sites on protein surfaces. A FRET system was therefore designed to pinpoint the primary interaction between the Hsp70 C-terminal EEVD motif, and the peptide binding grooves of TPR1 and TPR2B of Sti1.

2.1.1 Design of FRET system and Sti1 FRET mutants

FRET involves the measurement of energy transfer between a donor fluorophore and an acceptor fluorophore when they come into close proximity. The strength of interaction is very sensitive to distance, as can be seen from the equation for the FRET efficiency, E :

$$E = \frac{1}{1 + (r/R_0)^6}$$

where r is the distance between fluorophores and R_0 is the Förster radius, the distance at which the FRET efficiency is half maximal, characteristic to a particular fluorophore pair. Since in the current application the FRET efficiency was intended to be used to measure the concentration of bound partners, the interaction was designed such that the introduced fluorophores would be less than around 63 Å apart. This is the theoretical R_0 for the ATTO-488 and ATTO-550 dyes, used respectively as donor and acceptor. These were chosen for their good spectral overlap and high photostability and quantum yield. Based on structural information the geometry of the Hsp70-EEVD interaction with TPR1 and TPR2B was estimated, and the donor position was introduced as a cysteine mutation at position E632C in the substrate binding domain of the yeast Hsc70 homologue Ssa1 (Ssa1-SBD), located ten amino acids before the C-terminus (Figure 2.1, A). The SBD was used as a suitable proxy for Ssa1 in this system since it contains no native

cysteines. Ssa1 possesses three native cysteines yet they are all located in the NBD, and replacement of at least one of them was found to lead to structural instability and loss of function (Wang et al. 2012). To detect specific interactions at either TPR1 or TPR2B of Sti1, acceptor sites were introduced via cysteine mutations at positions G88C and K478C

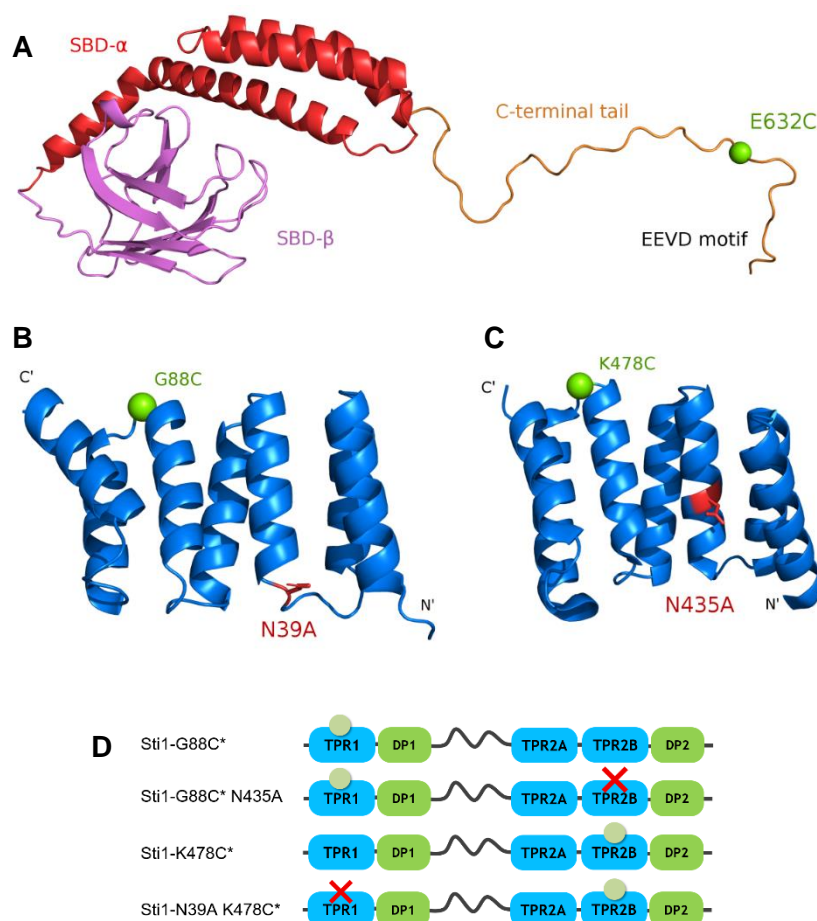


Figure 2.1. Design of the FRET system. (A) Structure of the Ssa1-SBD modelled on the human Hsp70 SBD (PDB: 4PO2) displaying the β -subdomain (magenta), α -helical lid (red), flexible tail (orange) and the position of the E632C FRET mutation (green). (B) Structure of Sti1-TPR1 modelled on HOP TPR1 (PDB:1ELW) showing the position of the G88C FRET mutation (green) and the N39A inactivating mutation (red). (C) Crystal structure of Sti1-TPR2B (PDB: 3UQ3) showing the position of the K478C FRET mutation (green) and the N435A inactivating mutation (red). (D) Schematic representation of the generated Sti1 FRET constructs showing the sites of label introduction (green dot) and inactivating mutation (red cross). Structural homology modelling was carried out using MODELLER and all 3D structures were rendered in pymol (Sali, A. and Blundell T.L. 1993).

respectively, into a cysteine-free variant which was previously shown to be stable and functional (Röhl *et al*, 2015). These positions are at the top, or mouth, of each peptide binding groove and were placed in loop regions to minimise structural perturbation to the domains (Figure 2.1, B, C).

A pair of ‘alternately inactivated’ constructs was also generated in which one domain (TPR1 or TPR2B) was labelled while Hsp70 binding to the other, unlabelled domain was inactivated by mutating the peptide binding groove (N39A and N435A for TPR1 and TPR2B respectively) (Figure 2.1, B, C) (Schmid *et al*, 2012; Röhl *et al*, 2015). The FRET constructs were purified and binding of the unlabelled versions to labelled Ssa1-SBD (Ssa1-SBD*) was verified by AUC (Figure 2.2). All constructs formed a complex with the Ssa1-SBD* that sedimented at around 4.5 S. This represents a binary complex since Sti1 alone sediments at 3.9 S (Li *et al*, 2011). Indeed, Sti1 has previously been observed to form only binary complexes with full-length Ssa1, despite possessing two Hsp70-binding domains (Schmid *et al*, 2012). The peptide binding groove-inactivating mutations served to weaken the affinity, as observed in a tailing off to the left of the distributions for Sti1-N39A K478C and Sti1-G88C N435A, indicating the presence of unbound Ssa1-SBD*.

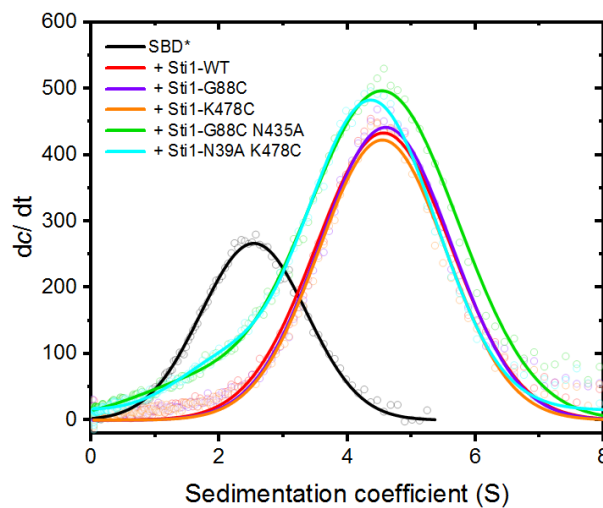


Figure 2.2. Binding of Sti1 FRET constructs to labelled Ssa1-SBD*. AUC Sedimentation velocity analysis was performed on 500 nM SBD* alone (black) or in the presence of 3 μ M Sti1-WT (red), Sti1-G88C (violet), Sti1-K478C (orange), Sti1-G88C N435A (green) or Sti1-N39A K478C.

Dimer- and oligomerisation is a widely observed property of Hsp70. However the Ssa1-SBD construct used here was observed to be monomeric by AUC, ruling out a possible complicating contribution to the analysis of interaction with Sti1 by FRET (Figure 2.3). The capacity for oligomerisation has been shown to reside minimally with the SBD, with necessary regions narrowed down to a portion of the C-terminus and the short linker that connects NBD to SBD (Fouchaq *et al*, 1999; Aprile *et al*, 2013). The current SBD construct lacks the preceding linker which likely explains its monomeric state.

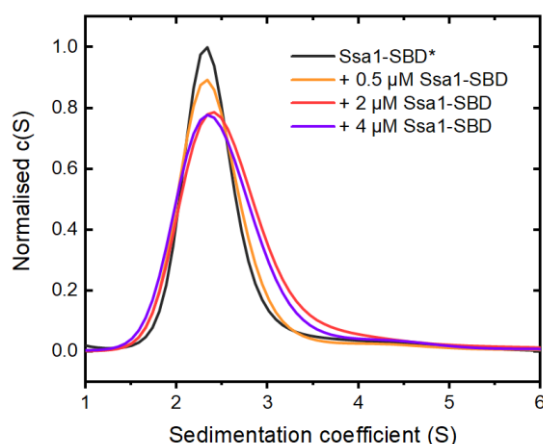


Figure 2.3. Ssa1-SBD* is a monomer. Sedimentation velocity AUC was performed on 500 nM SBD* alone (black) or in the presence of a 1x (orange) 4x (red) or 8x (violet) excess of unlabelled Ssa1-SBD. The resulting traces were analysed as c(S) distributions.

2.1.2 Equilibrium FRET between Ssa1-SBD and Sti1 TPR domains

Initial experiments revealed a functional FRET interaction between SBD* and both acceptor sites at TPR1 and TPR2B of Sti1, indicated by a decrease in donor emission concomitant with an increase in acceptor emission. The effect was reversible by addition of an excess of either unlabelled species (Figure 2.4). To determine the strength of the interaction at either TPR domain, FRET measurements were made over a range of acceptor concentrations.

An initial attempt was made using a serial titration method, involving serial addition of the acceptor to an initial solution of donor within the same cuvette. To control for direct excitation of the acceptor and dilution of the donor, separate titrations of the acceptor into buffer only, as well as of buffer into donor only were made and subtracted from the main series (Martin *et al*, 2008). This however yielded inconsistent results and revealed a high sensitivity of the system to pipetting errors. This method further proved impractical due to the kinetics of the reaction,

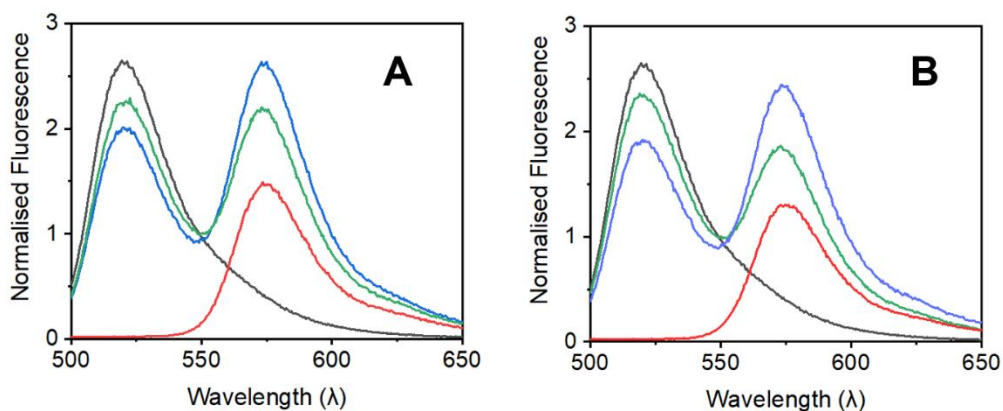


Figure 2.4 Equilibrium FRET interactions with TPR1 and TPR2B. (A) Fluorescence spectra recorded after excitation at 485 nm of 200 nM Ssa1-SBD* alone (black), 500 nM Sti1-G88C* alone (red), both mixed together (FRET) (blue), or both together in the presence of a fivefold excess of unlabelled Sti1-G88C* (green). (B) As in (A) but for Sti1-K478C*.

with binding taking around an hour to approach equilibrium (Section 2.1.3). Experiments were next conducted in a 96-well plate format, using a Jasco FP-8500 fluorimeter equipped with a 96-well plate detector module. These also led to inconsistent results stemming from the temperature fluctuations with the plate setup and significant interference from the optics of the detector module. These initial experiments revealed the extreme sensitivity of the system in general, with a relatively the low signal to noise. This stemmed from the low degree of labelling (DOL) of the donor (56%), which effectively halved the magnitude of any detectable FRET signal. A higher DOL was also unable to be achieved when attempting to label Ssa1-SBD with ATTO-550. The Sti1 FRET constructs on the other hand generally labelled well, with 94 %, 97 % and 100 % achieved respectively with Sti1-G88C, Sti1-G88C N435A and Sti1-K478C, while Sti1-N39A K478C yielded a value of 57 %. Attempts to achieve higher resolution by using higher donor and acceptor concentrations were hampered by the limit of the linear range of the fluorescence detector, which was already approached at around 4-5 μ M Sti1-G88C* or Sti1-K478C*. This meant that in order to achieve a Sti1: Ssa1-SBD ratio high enough to approach binding saturation, it was found that the Ssa1-SBD* donor concentration must be limited to around 200 nM. Reasonable titrations were achieved by carefully mixing individual reactions in a quartz cuvette and incubating for 1 hour at 30°C within the fluorimeter. FRET efficiency was calculated using the ratiometric, double excitation method (Clegg *et al*, 1993). Briefly, after exciting at the FRET wavelength, 485 nm, each sample is excited a second time at 550 nm to

collect emission from the acceptor only. From this, the theoretical acceptor emission at the FRET wavelength can be calculated due to the constant relationship between ϵ_{550} and ϵ_{485} , and then subtracted, along with the donor emission in the acceptor channel, from the raw FRET trace. This method was used to make titrations of TPR1- and TPR2B-labelled Sti1 as well as the alternately inactivated constructs, from which an estimate of the K_d could be made (Figure 2.5 and Table 2.1).

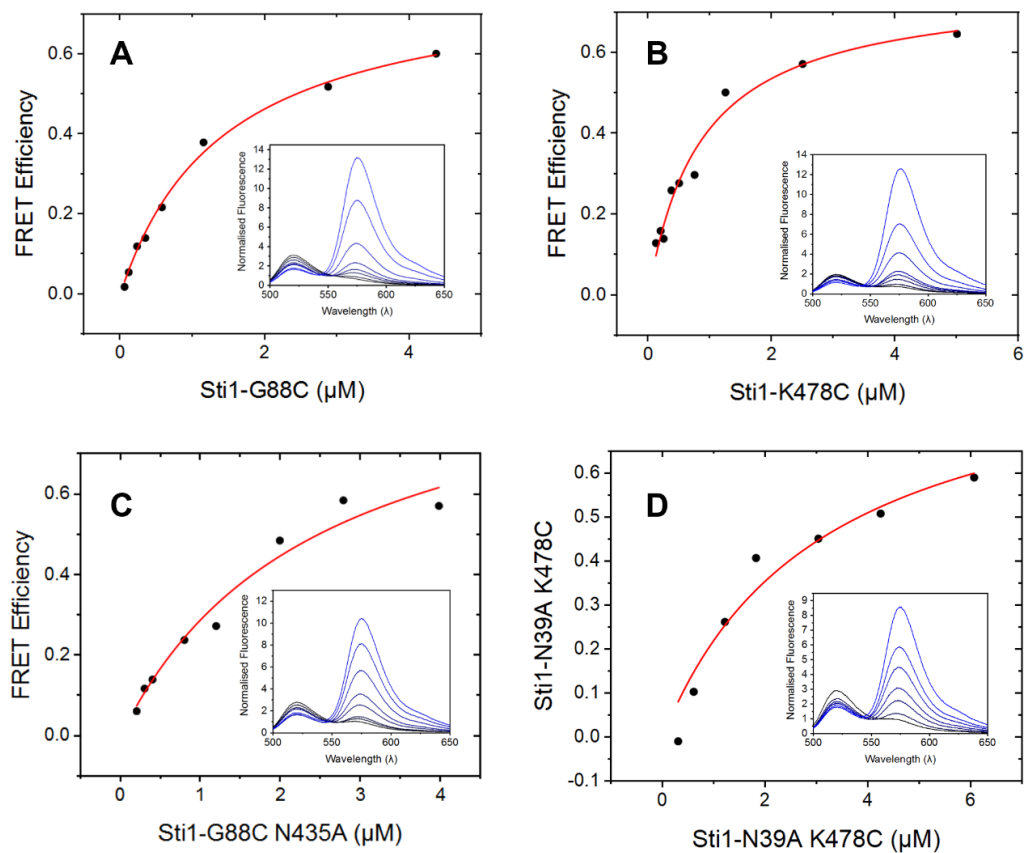


Figure 2.5 Equilibrium FRET titrations. FRET was measured with 200 nM Ssa1-SBD* and increasing concentrations of (A) TPR1-labelled construct, Sti1-G88C*, (B) TPR2B-labelled construct, Sti1-K478C*, (C) TPR1-labelled construct with TPR2B inactivated, Sti1-G88C* N435A and (D) TPR2B-labelled construct with TPR1 inactivated, Sti1-N39A K478C*.

Table 2.1. K_d and maximum binding response values calculated from FRET binding isotherms

	K_d (μM)	E_{MAX}
Sti1-G88C	1.43 ± 0.14	0.79 ± 0.03
Sti1-K478C	0.86 ± 0.14	0.76 ± 0.05
Sti1-G88C-N435A	2.46 ± 0.73	1.0 ± 0.15
Sti1-N39A-K478C	3.12 ± 1.3	0.91 ± 0.18

Binding of Ssa1-SBD* to TPR2B (Sti1-K478C*) was stronger than to TPR1 (Sti1-G88C*), in line with previous observations that TPR2B is the higher affinity site (Schmid *et al*, 2012). For both domains, a decrease in affinity was observed when binding to the opposing domain was inhibited. This provides direct evidence of cooperation between the two domains in binding Ssa1-SBD*, which in turn implies the existence of conformations involving long-range contacts, since the domains are located at opposing ends of Sti1. The effect was more pronounced for the TPR2B system, with Sti1-K78C* and Sti1-N39A K478C* respectively showing the highest and lowest K_d , than for TPR1 (intermediate K_d s). This indicates that TPR2B is more dependent on TPR1 for optimal binding than the other way around, consistent with the idea that TPR1 functions to load Hsp70 onto TPR2B.

As a comparison fluorescence anisotropy was used to analyse the binding of labelled Ssa1-SBD* to unlabelled Sti1-WT along with the TPR1-inactivated variant Sti1-N39A and TPR2B-inactivated Sti-N435A (Figure 2.6). The derived dissociation constants for Sti1-N39A and Sti-N435A are noticeably lower than their counterparts measured with FRET (Table 2.2). While this may indicate interference of the labels introduced in the FRET system, the difference may also indicate a contribution to binding from regions outside the EEVD interaction. The affinity of Sti1 for Ssa1-SBD* was relatively insensitive to TPR domain inactivation, although TPR2B inactivation was slightly more deleterious than TPR1. A much greater impact was observed on the binding capacity, B_{max} , which was reduced by around 30% upon inactivation of either domain. The effect is not purely additive since the Sti1-WT binding capacity is less than the sum of the capacities of the individual domain-inactivated constructs. This shows that when both TPR domains are active, they collaborate to bind the Ssa1-SBD to a limited extent, which aligns with the observation that Sti1-WT only binds Ssa1-SBD with a 1: 1 stoichiometry (section 2.1.1). These findings would be consistent with Sti1 promoting EEVD transfer within the same molecule, rather than binding of a second Ssa1-SBD.

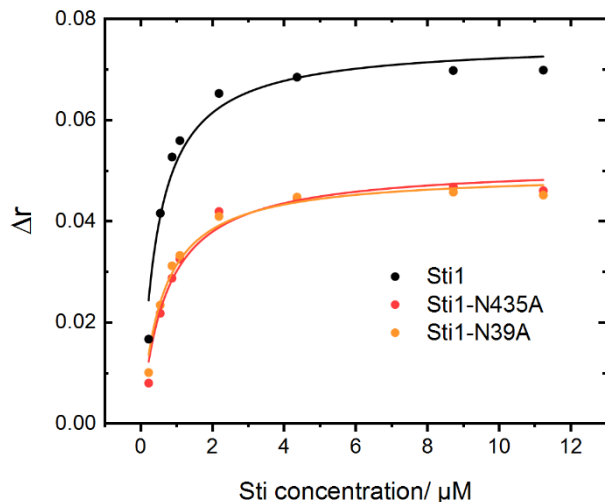


Figure 2.6 Binding of SBD* to unlabelled WT- and TPR-inactivated Sti1. Binding of 200 nM SBD* to increasing concentrations of Sti1-WT (black), Sti1-N39A (orange) or Sti1-N435A (red) was measured by fluorescence anisotropy. Curves were fit using a one site binding equation.

Table 2.2. K_D and maximum binding response values calculated from anisotropy binding isotherms

	K_D (μM)	B_{MAX}
Sti1	0.46 ± 0.07	0.076 ± 0.003
Sti1-N39A	0.58 ± 0.07	0.050 ± 0.001
Sti1-N435A	0.70 ± 0.10	0.051 ± 0.002

Taken together the above results show that EEVD binding to TPR1 and TPR2B is not independent, but rather that there is communication between domains. The fact that the domains are located at distant ends of Sti1 implies compact conformations which bring the two modules of Sti1 together to enable EEVD transfer between domains (Figure 2.7). Such conformations would be mediated by the Sti1 linker and may involve bridging interactions made with Ssa1-SBD. Indeed contributions to Sti1 binding outside of the Ssa1-EEVD have previously been detected, and a direct interaction between a surface on the SBD of Hsc70 and a surface on a TPR domain of the cochaperone CHIP has been reported (Röhl *et al*, 2015; Zhang *et al*, 2015).

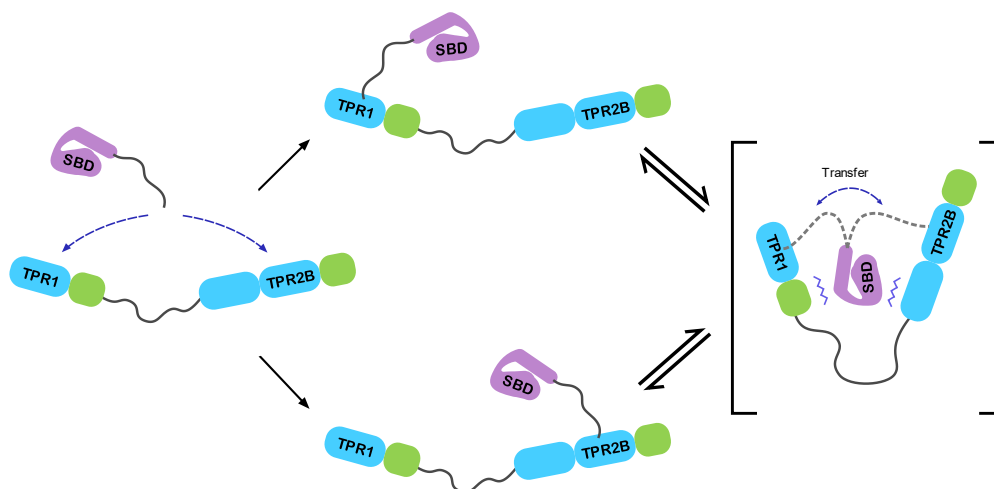


Figure 2.7 Model for the cooperative binding of Ssa1-SBD to Sti1. Ssa1-SBD can bind through its EEVD to TPR1 or TPR2B, however binding to either domain does not take place independently. Instead binding to one domain enables conformations involving additional interactions with the opposing module, which reciprocally enhances interaction with both modules.

2.1.3 Kinetic analysis of TPR domain association measured by FRET

To gain further insight into the binding characteristics of each TPR domain, a kinetic analysis of the association between the Sti1 FRET constructs and Ssa1-SBD* was carried out. Since initial experiments revealed that binding took place in the mixing dead time, measurements were carried out using a stopped flow spectrofluorimeter. Solutions were rapidly mixed, and FRET recorded as an increase in acceptor fluorescence using a 570 nm cut-off filter. The resulting kinetic traces were attempted to be fit to exponential equations requiring the fewest number of phases for a reasonable fit to be achieved (Figure 2.8). For all constructs this resulted in association curves displaying at least three phases, indicating a multi-step binding process:

$$y = A_1 \cdot (1 - e^{-k_1 t}) + A_2 \cdot (1 - e^{-k_2 t}) + A_3 \cdot (1 - e^{-k_3 t})$$

Where the three exponential phases are described by rate constants k_1 , k_2 and k_3 , each with a respective amplitude A_1 , A_2 and A_3 , which equals the contribution of that phase to the overall binding signal. Bi-exponential fits could not faithfully capture the association, giving rise to significant residuals (Figure 2.8, C, D).

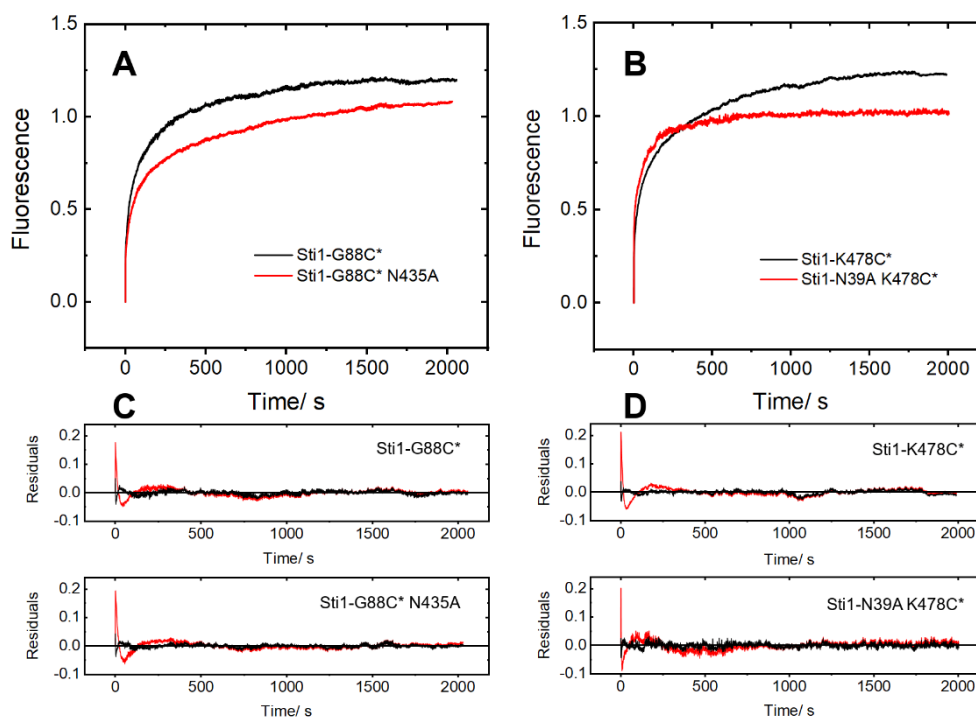


Figure 2.8 Sti1 TPR domain FRET association kinetics. Association between 500 nM Ssa1-SBD* and the Sti1 FRET constructs (500 nM) was measured as an increase in acceptor fluorescence using a stopped flow device. (A) Association at TPR1 with TPR2B either active (black) or inactivated (red). (B) Association at TPR2B with TPR1 either active (black) or inactivated (red). (C, D) Residuals resulting from triple exponential (black), or double exponential (red) fits of the association curves in (A) and (B).

For all constructs the binding comprised a relatively fast phase on the 1/ s timescale, and two slower phases on the 1/ 100 s and 1/ 1000 s timescales. Interestingly, the observation of multiphasic association with the alternately inactivated constructs Sti1-G88C* N435A and Sti1-N39A K478C* reveals the existence of multiple binding contributions to the Hsp70-EEVD – Sti1-TPR interaction, even in the absence of a second functional Hsp70-binding domain. This may be accounted for by initial rapid binding of the Ssa1-EEVD to the Sti1-TPR peptide binding groove, followed by subsequent conformational changes and engagement of additional interactions within the complex which reciprocally enhance the EEVD interaction. Indeed a similar conclusion was drawn for the FRET association between Hsp90 and Sti1 from the observation of three kinetic phases in a previous study (Lee *et al*, 2012).

From the amplitude-weighted average rates it can be seen that binding to TPR2B was faster than to TPR1, and that binding to either TPR domain was faster when the other was inactivated (Figure 2.9, A). Since the average rate is dominated by the fast first phase (see Figure 2.9, B),

and this phase likely arises from the initial EEVD binding interaction, this shows that the two TPR domains effectively compete for the EEVD in the initial binding stage. The higher k_1 observed for TPR2B, with TPR1 both active and inactive, is consistent with the idea that this is the TPR domain essential for client activation, and will out-compete TPR1 for the EEVD. However, the first phase represents less than 30% of the binding signal for the constructs Sti1-G88C*, Sti1-G88C* N435A and Sti1-K478C*, and the majority of binding for these constructs is contributed by the slower phases 2 and 3, with phase three being particularly dominant for Sti1-K478C* (Figure 2.9, C). A previous single molecule FRET study with Sti1 labelled at either end of the linker showed that the molecule was mainly elongated in solution but underwent transient fluctuations to compact conformations (Röhl *et al*, 2015). Upon addition of Hsp70, the fluctuations of Sti1 significantly increased, and three distinct states could be distinguished, corresponding to an elongated, an intermediate and a compact conformation. The population of

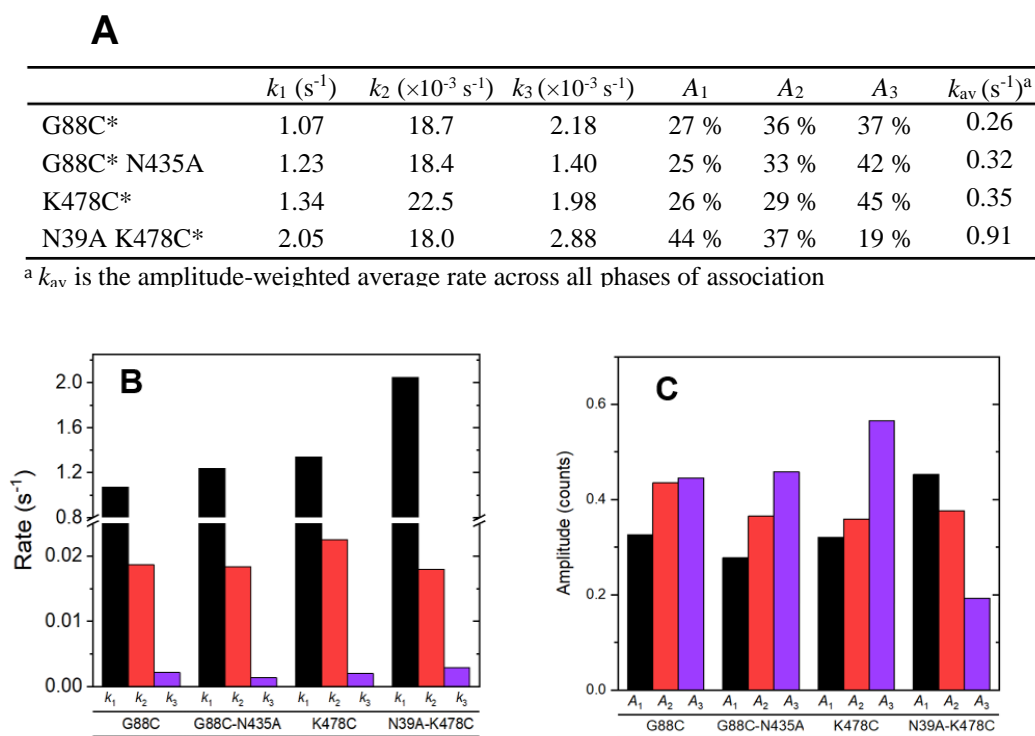
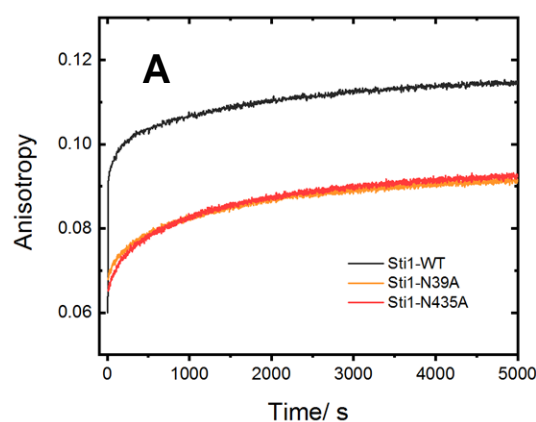


Figure 2.9 Quantification of binding Sti1 TPR domain association kinetics. (A) Table of kinetic parameters resulting from the triple-exponential fits of association curves showing the rate constant (k) and amplitude (A , as percentage) of each phase, along with the amplitude weighted average rate (k_{av}). (B) Plot of the observed rates for the three association phases observed for each construct. (C) Plot of the observed amplitudes (absolute amount) for the three association phases observed for each construct.

these latter conformations would likely make a contribution to the affinity for Hsp70 and may therefore be responsible for association phases 2 and 3 in the current work. After a rapid initial capture of Ssa1-SBD via the EEVD, the complex would be free to sample compacted conformations on a longer timescale, involving potential additional contacts, and gradually move toward a greater population of these states at equilibrium. These phases make the greatest binding contribution in all constructs in which TPR1 is active, suggesting TPR1 plays the decisive role in this phenomenon (Figure 2.9, C). The opposite trend is seen in binding to Sti1-N39A K478C* however, where the first phase dominates and phase three is significantly diminished.

To verify that the observed binding phases were authentic and not an artefact introduced by the FRET system, binding kinetics were measured using anisotropy between labelled Ssa1-SBD and unlabelled wild-type Sti1, Sti1-N39A and Sti1-N435A (Figure 2.10).



B	k_1' (s^{-1})*	k_2' ($\times 10^{-3} s^{-1}$)*	k_3' ($\times 10^{-3} s^{-1}$)*	A_1	A_2	A_3
Sti1-WT	0.11	0.53	6.3	60 %	13 %	28 %
Sti1-N435A	0.05	0.46	2.9	19 %	29 %	52 %
Sti1-N39A	0.12	0.54	3.7	28 %	20 %	53 %

* k' is a lower estimate of true k

Figure 2.10. Association kinetics with unlabelled Sti1 variants. (A) Association between unlabelled Sti1 constructs and Ssa1-SBD* measured by fluorescence anisotropy. 500 nM Ssa1-SBD* was mixed with 500 nM Sti1-WT (black) Sti1-N39A (orange) or Sti1-N435A (red) and association measured as an increase in fluorescence polarization over time. (B) Kinetic parameters resulting from a triple-exponential fit of curves in (A), with rate constants (k) and amplitudes (A , as percentage) of individual phases.

Due to the absence of a stopped flow mixing device, the kinetic parameters could not be quantitatively compared with the FRET system. Nevertheless, the overall form of the association curves agrees well with the FRET experiments, with the same three phases distributed over similar timescales, showing that they reliably capture the binding between Ssa1-SBD and Sti1.

The observed binding behaviour may be rationalised in a scheme in which there is initial rapid binding to either TPR domain via the Ssa1-SBD EEVD motif (state 1), followed by a bridging interaction with the opposing module facilitated by the Ssa1 C-terminal tail and the flexible linker of Sti1 (state 2). This leads to a third, fully compacted state in which transfer of the EEVD between TPR1 and TPR2B is possible (Figure 2.11). Such a scheme explains the three conformational FRET states (low, intermediate and high) previously observed for Sti1 in the presence of Hsp70, and the configuration of Ssa1-SBD wedged between the two modules of Sti1 in the final state is consistent with the EM structure of the Hsp70-Sti1-Hsp90 ternary complex (Alvira *et al*, 2014; Röhl *et al*, 2015). Binding to TPR2B is fast but limited in capacity when TPR1 is inactivated (Sti1-N39A K478C*), leading to a population mainly of states 1 and 2 (Figure 2.11). This can be seen from the association amplitudes (Figure 2.9, C) and observed visually from the shape of the association curves of Sti1 labelled at TPR2B (Figure 2.8, B). Binding to TPR1 is slower and takes place mainly through population of states 2 and 3, with state 3 particularly predominant when TPR2B is inactivated (Sti1-G88C* N435A) (Figure 2.9, C, Figure 2.11). Binding to TPR1 leads to a build-up of state 3, in which transfer of the EEVD is possible, and therefore appears to predispose Sti1 for the transfer of Ssa1-SBD between the modules. The Sti1-K478C* construct displayed the highest overall binding signal (and the lowest K_d , Section 2.1.2) indicating that in the presence of both domains, Sti1 has a preference to load Hsp70 onto TPR2B. This is however achieved with a particularly high contribution from phase 3, which was minimally accessible in the absence of functional TPR1, revealing that state 3 with the EEVD bound to TPR2B is effectively loaded via the TPR1 route, with the EEVD delivered directly from the TPR1-bound state 3 (Figure 2.11). Thus the long range conformations and EEVD transfer play a decisive role in allowing Sti1 to reach full capacity. TPR1 may therefore be viewed as providing a regulatory function to TPR2B, inhibiting its propensity to bind the Hsp70 tail too quickly but ultimately facilitating a higher capacity over a longer timescale. Such a function may serve a role in timing the binding of Hsp90 and other co-chaperones in forming the multi-chaperone complex.

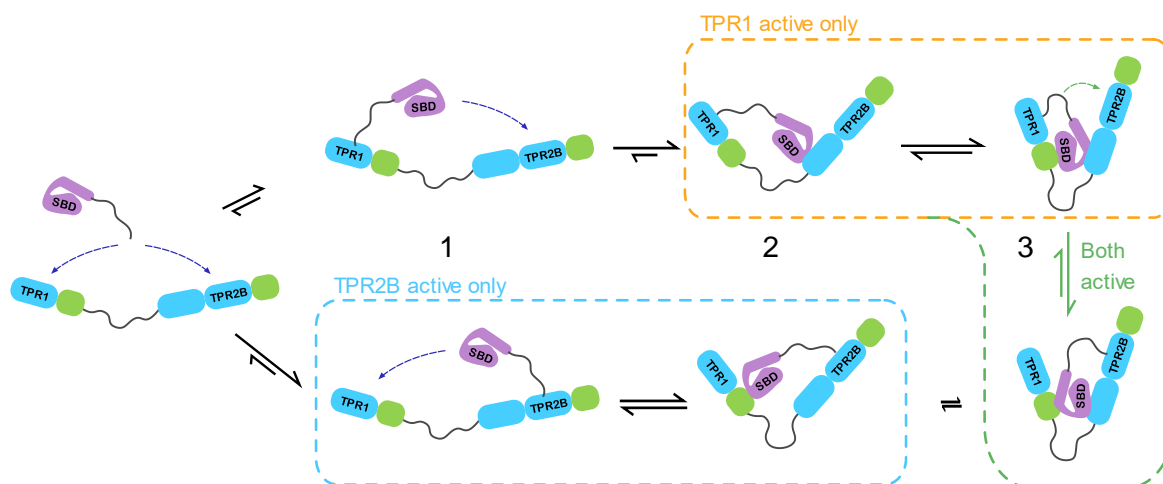


Figure 2.11 Model for the kinetic association of Ssa1-SBD with Sti1. Ssa1-SBD associates with Sti1 through a series of three states. Initially TPR1 and TPR2B compete for fast binding to the Ssa1-SBD EEVD motif, to form state 1. Binding is stabilised by a bridging interaction with the opposing Sti1 module to form state 2. Binding to form state 1 through TPR2B is rapid however state 2 represents a dead-end through this route. State 3 is fully compacted, provides the possibility for transfer of the EEVD motif and is favoured through binding to TPR1. When both TPR1 and TPR2B are active in the wild type molecule, Sti1 efficiently shuttles Ssa1-SBD to the TPR2B-bound state 3 via TPR1.

2.2 Towards a three colour FRET system to study the Sti1-Hsp70 Interaction

2.2.1 Design of Sti1 labelled independently at two sites

To obtain greater insight on the complex manner in which Sti1 binds Hsp70, the FRET system was sought to be extended to study the TPR interactions with three colour single-molecule FRET spectroscopy. Placing a different acceptor label at TPR1 and TPR2B within the same Sti1 molecule would allow for a precise measurement of the Hsp70 dwell time at either domain, providing unprecedented detail on the conformations that enable transfer. To this end, a strategy was sought whereby Sti1 could be divided artificially in two parts, with each part being purified and labelled independently before the two were reconnected. Several in vitro ligation-based strategies exist such as native chemical ligation, protein trans-splicing and expressed protein ligation, however many are inefficient and may require extensive optimization (Xu *et al*, 1999; Muona *et al*, 2010).

For Sti1, an *in vitro* ligation strategy involving the transpeptidase Sortase A (SrtA) from *Staphylococcus aureus* was selected owing to its versatility in ligating structured protein domains. SrtA is responsible for linking surface proteins to the cell wall of gram-positive bacteria. This takes place via cleavage of target proteins at a conserved LPXTG (X= any amino acid) consensus sequence to expose a C-terminal threonine, followed by formation of an amide bond between the threonine and an incoming target glycine (Mazmanian *et al*, 1999). Recombinant SrtA can be used to ligate two proteins of interest by engineering an LPXTG motif at the C-terminus of the first, and one or more glycines at the N-terminus of the second (Mao *et al*, 2004). A number of factors were considered in choosing the site of sortase consensus sequence introduction in Sti1. Namely the sequence should be introduced outside structured domains or in disordered regions to minimise perturbation of the target protein. The site should also be far enough away from structured domains to be accessible to SrtA during the ligation reaction. Satisfying these requirements, the flexible linker within Sti1 was chosen as the site of introduction. Fortuitously the Sti1 linker natively contains the sequence PET, meaning

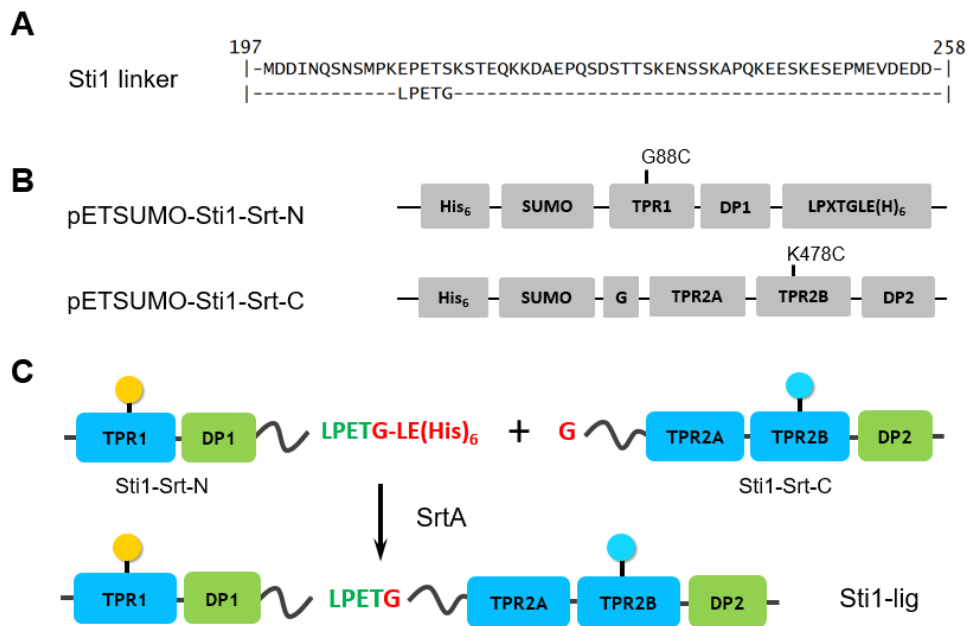


Figure 2.12. Proposed strategy to obtain double labelled Sti1 by *in vitro* ligation with SrtA. (A) Position of the sortase consensus sequence within the Sti1 linker in the ligated construct, bearing a two amino acid substitution. (B) Sti1 is artificially divided into two constructs, Sti1-Srt-N and Sti1-Srt-C, each engineered to contain a single cysteine. (C) Following purification and labelling in independent reactions with different fluorescent dyes, the two constructs are ligated together *in vitro* with SrtA.

that the final construct would remain the same length and contain a substitution of only two amino acids (Figure 2.12, A).

The next step was to devise a practical strategy for the *in vitro* ligation and isolation of the product from the starting materials. A previous approach involving selectively cleavable his-tags was adopted as a starting point, but had to be modified owing to side-reactions leading to undesired products (Freiburger *et al*, 2015). Sti1 was divided within the linker into an N-terminal fragment, Sti1-Srt-N, and a C-terminal fragment, Sti1-Srt-C, which were each cloned into a pETSUMO vector. The sortase consensus sequence followed by a His-tag was engineered at the C-terminus of Sti1-Srt-N while a single glycine was engineered at the N-terminus of Sti1-Srt-C (Figure 2.12, B). The general scheme for sortase mediated ligation of Sti1 is shown in Figure 2.12, C, however a more complicated strategy had to be implemented to isolate only the desired final product (Figure 2.13). In step 1 of the final strategy, the Sti1-Srt-N construct is purified without cleavage of its His₆-SUMO Tag and then reacted with Sti1-Srt-C (purified as normal) in the presence of SrtA. This leads to a mixture of the ligation product, a side product

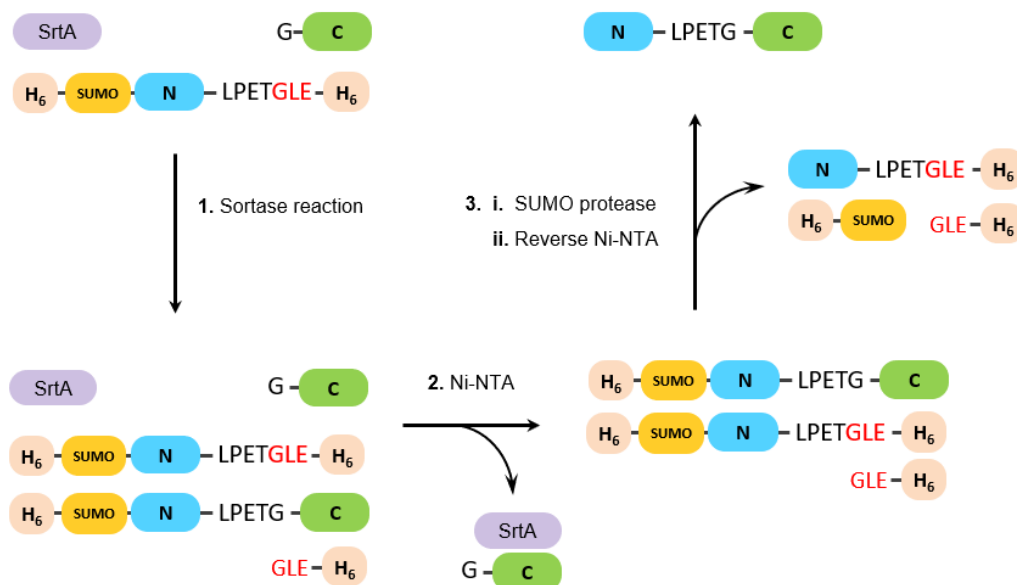


Figure 2.13. Schematic representation of the ligated Sti1 synthesis protocol. In step 1. SrtA facilitates an incomplete ligation between the N-terminal fragment and C-terminal fragment to generate a ligated product, which leaves behind a liberated fragment as well as the starting materials. In step 2. the untagged SrtA and C-terminal fragment are removed by an NiNTA column. In step 3i. SUMO protease cleaves the ligation product and N-terminal fragment. In step 3ii. A second NiNTA column separates the cleaved product from the remaining impurities.

and the starting materials. In the second step the reaction mixture is purified by nickel affinity chromatography to remove the untagged sortase and Sti1-Srt-C. In step three, excess his-tagged SUMO protease is added to cleave the ligation product and remaining Sti1-Srt-N, before the mixture is passed over a second nickel column. This time however the flow-through is collected, which should contain only the desired ligation product and leave the remaining his-tagged species bound to the column.

2.2.2 Generation of double labelled Sti1 via sortase-mediated ligation

The reaction was first tested under various conditions, altering the ratios of each of the fragments or of the enzyme over both fragments. All conditions tested resulted in the fast formation of two labile products which then degraded sequentially on a relatively fast timescale (Figure 2.14, A). The presence of two products was surprising and it was unclear from the molecular weights which, if either, should be the desired product. From the kinetics of the

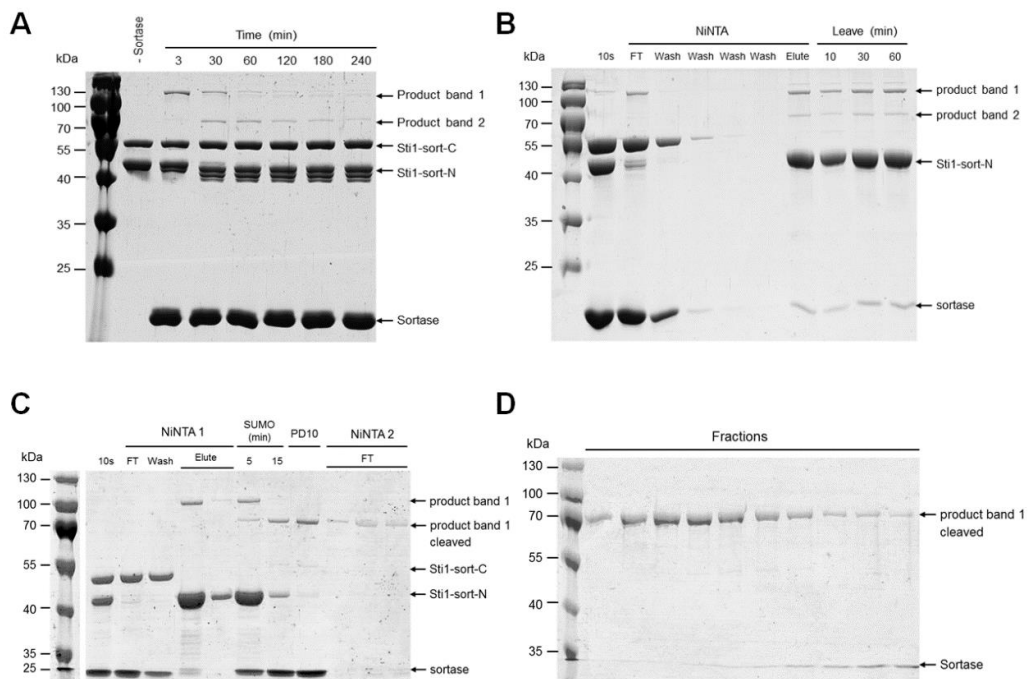


Figure 2.14. Progress of the ligation reaction monitored by SDS-page. Two product bands appear before subsequently disappearing on a relatively fast timescale. (B) Quick loading on to a Ni-NTA column and thorough washing to remove SrtA resulted in stable products. (C) Product band 1 could be separated with a nickel column, cleaved with sumo protease and successfully isolated from all other species with a second nickel column. (D) Cleaved product 1 could be purified to homogeneity with gel filtration chromatography.

reaction it appeared that product 1 may be an intermediate on the pathway to product 2, and an attempt was made to isolate it by rapidly loading the reaction onto a nickel column before washing out SrtA to stop the reaction (Figure 2.14, B). While a small amount of remaining SrtA led to some formation of product 2, the removal of the majority led to both products being stable.

The bands were analysed by peptide mass fingerprinting on a MALDI-TOF device to gain insight into their identity. From a query of the MASCOT database product band 2 yielded a series of hits for Sti1 of mere threshold significance, indicating incomplete coverage of the Sti1 sequence. Product band 1 however yielded a single high significance hit for Sti1 from the *S. cerevisiae* target strain S228C. These data therefore suggest that product 1 was the desired ligated product, while product 2 was an unwanted side product. Product band 2 also appeared concomitantly with a splitting pattern in the Sti1-Srt-N band, and Sti1-Srt-N alone was found to form higher molecular weight species when incubated with SrtA, suggesting that self-ligation of this fragment was responsible for the formation of side products. By scaling up the reaction and decreasing further the handling time, product 1 could be successfully isolated. Lowering the calcium content of the buffer (SrtA is calcium-dependent) also slowed down the reaction and favoured the formation of product 1 over product 2. Product 1 was fully cleavable with SUMO protease and eluted as expected in the flow-through when passed over a second nickel column (Figure 2.14, C). Finally, the cleaved product (termed Sti1-lig) could be isolated by gel filtration chromatography (Figure 2.14, D). Sti1-lig was well folded as analysed by CD spectroscopy and its mass was determined to be 66 kDa by mass spectrometry, in perfect agreement with the expected value for Sti1 (Figure 2.15, A, B). Furthermore in a test for Sti1 functionality, the ligated product inhibited the ATPase activity of Hsp82 to a similar extent as wild type Sti1 (Figure 2.15, C).

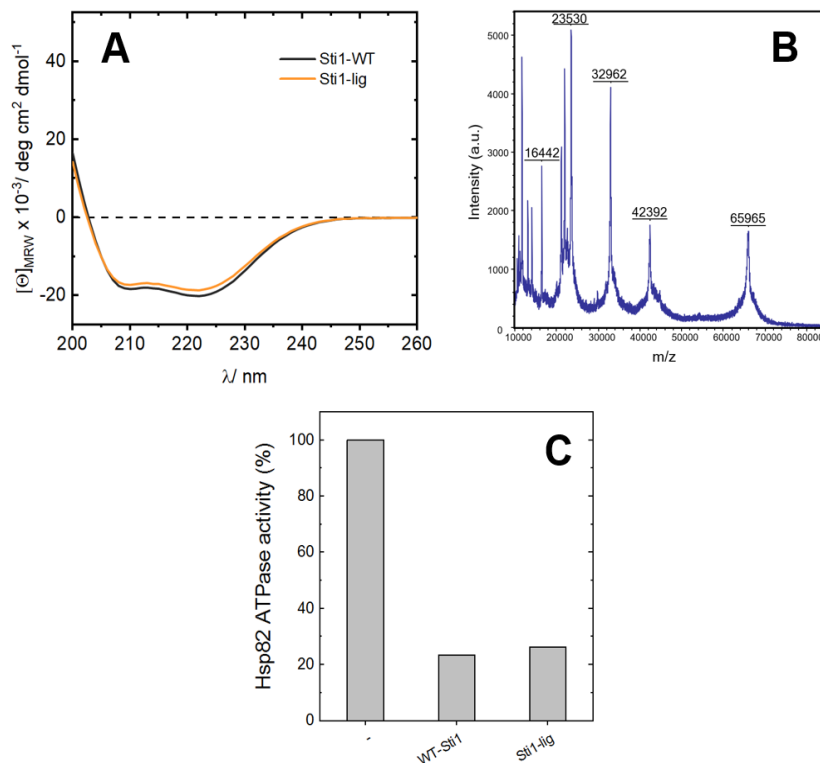


Figure 2.15. Characterisation of Sti1-lig. (A) Far-UV spectrum of Sti1-lig (orange) compared with Sti1-WT (black). (B) Sti1-lig ESI mass spectrum. (C) Inhibition of Hsp82 ATPase activity by Sti1-lig compared with Sti1-WT.

Having established a method for the *in vitro* ligation of Sti1 fragments, the next stage was to use it to produce a version with two independently labelled sites. The selection of dyes for single molecule spectroscopy is restrictive due to the need for compatibility with chemical systems that suppress photophysical side-reactions (Stennett *et al*, 2014). For the current application a label system involving an ATTO-488 donor located on Ssa1-SBD, as well as Cy3b and ATTO-647 acceptors located on TPR1 and TPR2B was selected under advice from Dr. Anders Barth (Laboratory of Prof. Don Lamb, Ludwig-Maximilians-Universität). Progress towards the realisation of this system was however hampered by labelling of the Sti1-Srt-N fragment. While Sti1-Srt-C could be labelled cleanly with a degree of labelling (DOL) of 100 %, the Sti1-Srt-N fragment persistently aggregated upon labelling with either ATTO 647 and Cy3b. Despite attempts including lowering the dye: protein ratio, adding the dye in a dilute solution and lowering the temperature, significant aggregation could not be eliminated and low DOLs were achieved. Nevertheless Cy3b-labelled Sti1-Srt-N and ATTO-647-labelled Sti1-Srt-C could be readily ligated in the presence of SrtA, leading to the formation of the double-fluorescently

labelled version of product 1 (ligation of the aggregated Sti1-Srt-N was also observed) (Figure 2.16). This demonstrates that Sti1 specifically labelled at two independent sites can indeed be generated, while attainment of the isolated protein will depend on elimination of the labelling impurities introduced with Sti1-Srt-N in future work.

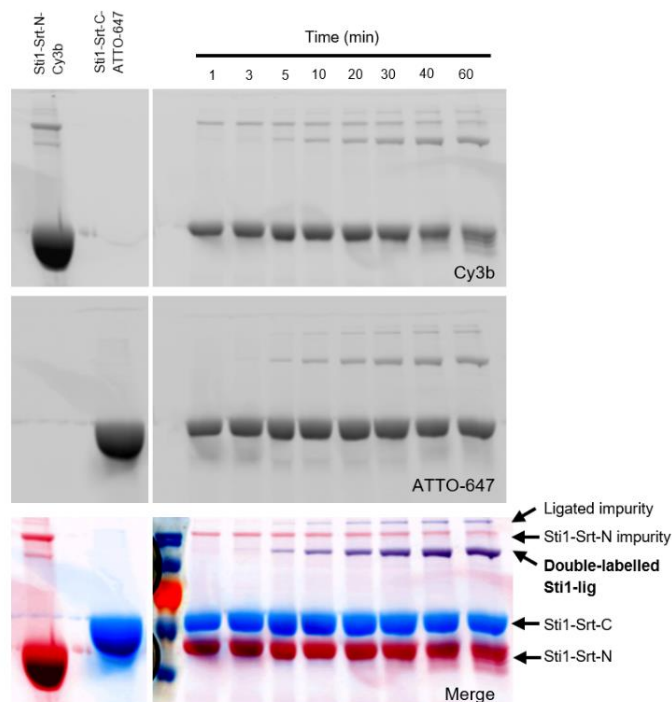


Figure 2.16. Formation of double labelled Sti1-lig. Cy3b-labelled Sti1-Srt-N and ATTO-647-labelled Sti1-Srt-C were ligated in the presence of SrtA to form double-labelled Sti1-lig and the reaction was followed by SDS gel electrophoresis. The gel was fluorescently imaged with excitation of Cy3b (upper) and ATTO-647 (middle) and gel scans were overlaid (lower). Common to both scans (purple), double-labelled Sti1-lig is formed over time, as well as a higher MW ligated impurity which is likely formed by ligation of Sti1-Srt-C to the higher MW Sti1-Srt-N impurity.

2.3 TPR domain swaps: function within the context of full-length Sti1

2.3.1 Design of Sti1 TPR domain-swapped constructs

The next part of the project aimed to further investigate the contributions of the Hsp70-binding domains TPR1 and TPR2B toward client maturation and complex formation with Hsp70 and Hsp90. In particular, it was asked whether TPR1 and TPR2B are functionally interchangeable

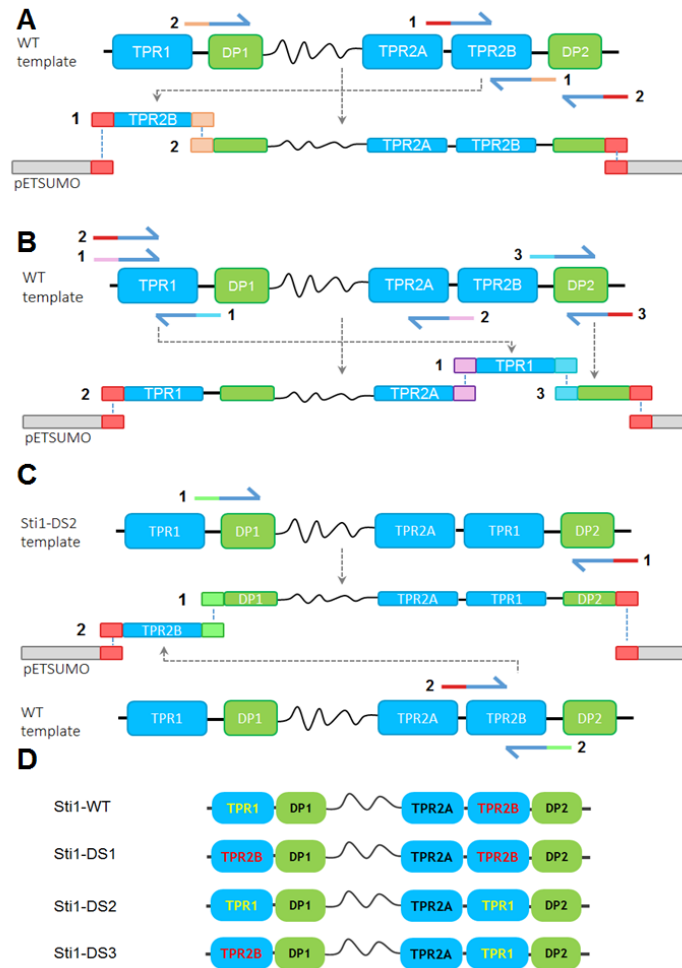


Figure 2.17. Generation of Sti1 domain-swapped constructs by SLIC cloning. The constructs (A) Sti1-DS1, (B) Sti1-DS2 and (C) Sti1-DS3 were generated from constituent fragments (numbered), which were themselves generated from the corresponding numbered primer pairs with designed overlaps. Sti1-WT template DNA was used to generate Sti1-DS1 and Sti1-DS2 while Sti1-DS3 was generated from a combination of WT and Sti1-DS2 template DNA. (D) Schematic representation of the resulting constructs with the exchanged domains highlighted, TPR1 in yellow and TPR2B in red.

and what role their positional context plays within the full-length Sti1 protein. To this end a series of domain-swapped constructs was generated in which TPR1 was replaced by TPR2B (Sti1-DS1), TPR2B was replaced by TPR1 (Sti1-DS2) or both domains were exchanged in position (Sti1-DS3) (Figure 2.17). The constructs were analysed in terms of their functioning and ability to form complexes with Hsp70 and Hsp90.

2.3.2 Functional analysis of Sti1 domain-swapped constructs

First, Sti1 domain-swapped constructs were assayed for their ability to inhibit yeast Hsp90 (Hsp82) ATPase activity using a regenerative ATPase assay. TPR2A-TPR2B has previously been identified as the minimal fragment of Sti1 necessary to completely inhibit Hsp82 ATPase activity, presumably by engaging in an interaction with the Hsp82 middle domain (Hsp82-MD) (Schmid *et al*, 2012). In accordance with this picture, full inhibition is observed with Sti1-DS1 in which TPR2A-TPR2B is intact, while no inhibition whatsoever is observed with Sti1-DS2 and Sti1-DS3, in which TPR2B has been replaced by TPR1 (Figure 2.18, B). These results therefore suggest that TPR1 cannot substitute for TPR2B in making the secondary interaction with the Hsp82-MD necessary to inhibit ATPase activity. Next the domain-swapped constructs were tested for their ability to support maturation of the glucocorticoid receptor (GR) in a model *in vivo* client maturation assay. $\Delta sti1$ *S. cerevisiae* cells display a drastically reduced ability to activate GR however this can be restored by supplementing them with plasmids containing wild-type Sti1 or specific variants thereof (Chang *et al*, 1997; Carrigan *et al*, 2004; Flom *et al*, 2006). The Sti1-DS1 construct was able to support higher than wild-type levels of GR activation (119%) while Sti1-DS2 and Sti1-DS3 resulted in slightly reduced GR activation levels of 83% and 70% respectively (Figure 2.18, C). The results for Sti1-DS2 and Sti1-DS3, which contain TPR1 in place of TPR2B, were surprising since previous work with Sti1 truncations and mutants has exhaustively demonstrated that an intact TPR2A-TPR2B-DP2 module is necessary to support near wild-type levels of GR activation. Further the overall structure of the module is thought to be important: DP2 has a fixed orientation with respect to TPR2B and disrupting the fixed S-shaped orientation between TPR2A-TPR2B led to a lower GR activation of around 55% (Schmid *et al*, 2012; Röhl *et al*, 2015). The current results suggest however that for this module an overall Hsp90-binding domain/ Hsp70-binding domain/ DP2 arrangement may be sufficient for *in vivo* GR activation. This is particularly interesting considering that this arrangement is unable to inhibit the ATPase activity of Hsp82 (Figure 2.18, B). While a tight regulation of Hsp90 conformational transitions through sequential co-chaperone binding has been shown to

be important for Hsp82 function (Li *et al*, 2011; Zierer *et al*, 2016), it may be that specific inhibition of Hsp82 ATPase activity by Sti1 is dispensable for client activation in this context.

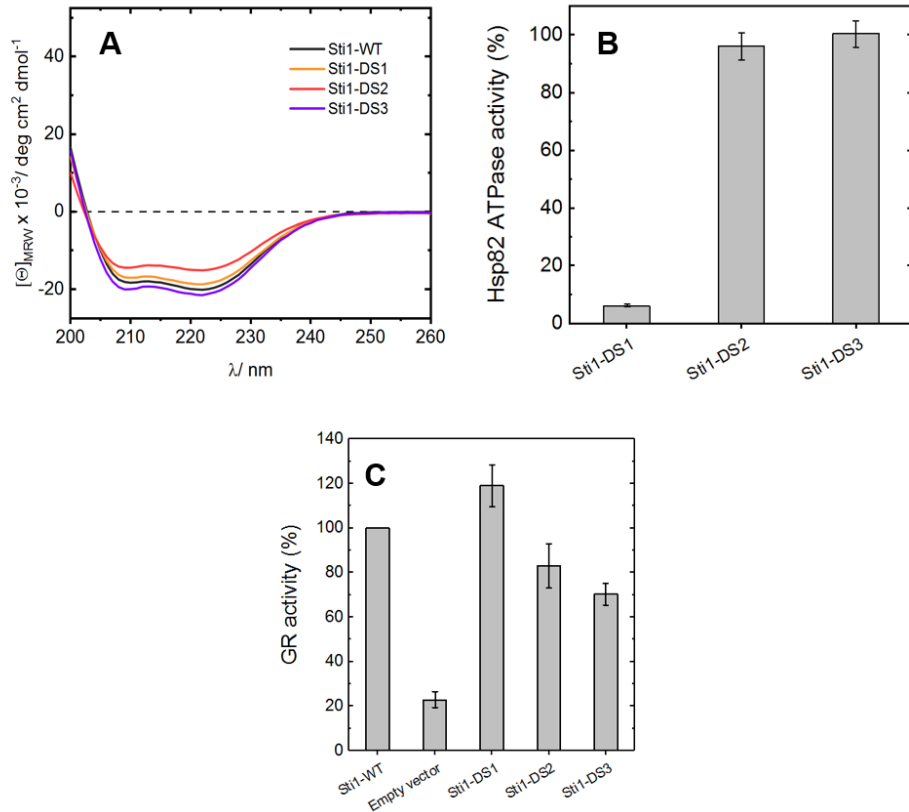


Figure 2.18. Functional analysis of Sti1 domain-swapped constructs. (A) Far-UV spectra of Sti1-WT (black), Sti1-DS1 (orange), Sti1-DS2 (red) and Sti1-DS3 (violet). (B) Ability of Sti1 domain-swapped constructs to inhibit Hsp82 ATPase activity measured by a regenerative ATPase assay. Activity is normalised to the level of inhibition in the presence of Sti1-WT. Error bars indicate the standard deviation of two independent experiments. (C) Ability of domain-swapped Sti1 constructs to support maturation of the GR client protein in Δsti1 *S. cerevisiae* cells, normalised to the level observed in the presence of Sti1-WT. Error bars indicate the standard deviation of six independent experiments.

2.3.3 Contributions of TPR domains to the binding of labelled Hsp70

To gain insight into the role of the TPR domains in complex formation, binding of domain-swapped Sti1 constructs to yeast Hsp70 (Ssa1) was analysed by AUC. When Sti1 constructs were titrated against randomly labelled Ssa1 up to an eight-fold excess, a concentration-dependent increase in S-value was observed, indicating formation of a binary complex at around 5.5 S (Figure 2.19) (Schmid *et al*, 2012). At the highest molar excess binary complexes formed with Sti1-WT sedimented at 5.4 S while those with Sti1-DS1 sedimented at 5.6 S, indicating a slightly compacted conformation, and those with Sti1-DS2 and Sti1-DS3 sedimented at 5.2 S, indicating slightly extended conformations. It is interesting that despite possessing two active Hsp70-binding TPR domains, Sti1 maximally binds Ssa1 in a 1: 1 complex. The fact that this is observed regardless of the identity or arrangement of the domains within the molecule shows that the effect is imposed by the overall architecture of Sti1, further indicating cooperation between the two modules.

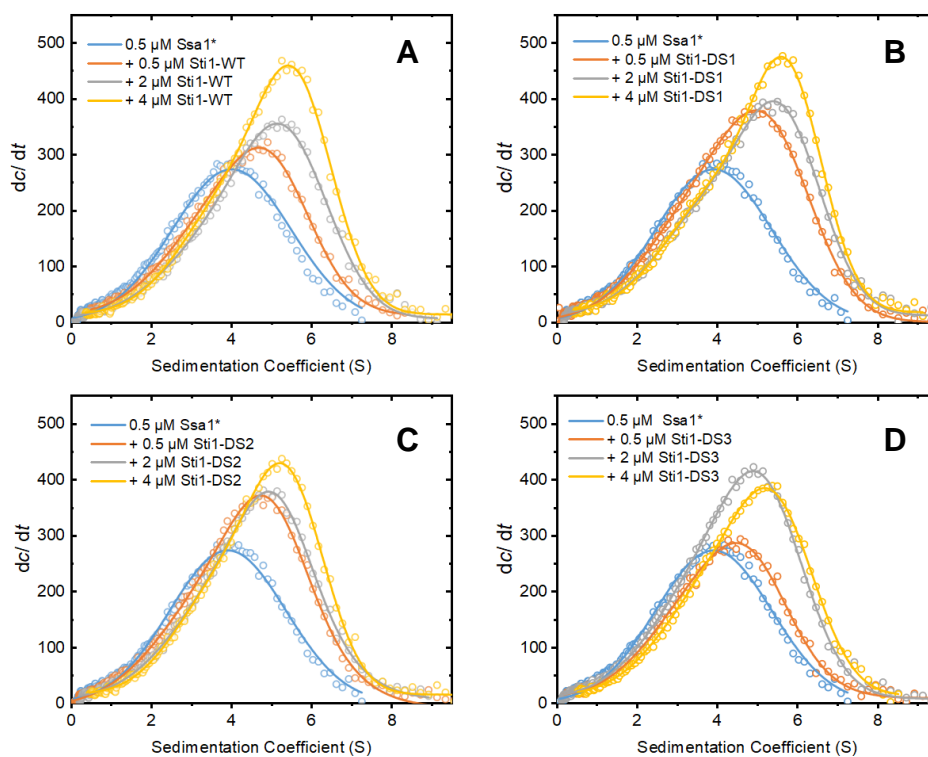


Figure 2.19. Complex formation between labelled Ssa1 and domain-swapped Sti1 constructs. 500 nM Ssa1* in the presence of increasing concentrations of (A) Sti1-WT, (B) Sti1-DS1, (C) Sti1-DS2 or (D) Sti1-DS3 was measured by sedimentation velocity AUC. Raw data (open circles) were converted to dc/dt plots and fit with gaussian distributions (lines).

The ability of Ssa1 to dimerise and whether this would affect binding to Sti1 was also investigated. Hsp70 has been shown to exist both as a monomer and a dimer in solution. While a consensus remains to be established, there is increasing evidence for the relevance of dimeric forms in complex formation and function (Morgner *et al*, 2015; Ebong *et al*, 2011; Sarbeng *et al*, 2015). The Hsp70 used in the current work, Ssa1 purified from *Pichia pastoris*, was found to exist as both monomers and dimers in solution, with the balance between the two being responsive to nucleotide, as analysed by AUC (Figure 2.20, A). ATP strongly promoted Ssa1 dimerisation, indicated by a peak shift to 6 S, while the slowly hydrolysing ATP analogue ATP γ S strongly favoured a monomeric form at 4 S. AMP-PNP (another non-hydrolysable ATP analogue) and ADP promoted intermediate distributions. Dimer formation in the presence of ATP was previously observed with *E.coli* DnaK and recently with human Hsp70 (Trcka *et al*, 2019; Qi *et al*, 2013). The current observation with the yeast system suggests that it is a conserved phenomenon.

Adding Sti1 to preformed Ssa1·ATP dimers however did not result in additional complex formation, further supporting the idea that Sti1 cooperatively binds only a single Hsp70 molecule (Figure 2.20, B). A recent study found that the co-chaperone Chip bound dimeric Hsp70·ATP while the co-chaperone Tomm34 interrupted dimers to bind only the monomeric form, similar to Sti1 in the current work (Trcka *et al*, 2019). These results suggest that Hsp70 dimerisation may play divergent roles in different co-chaperone settings.

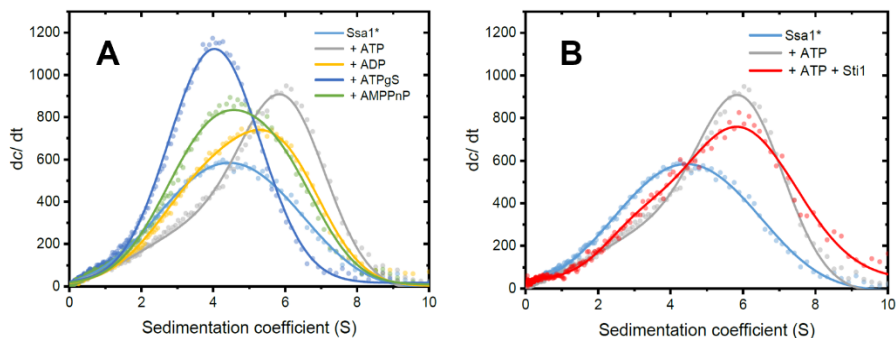


Figure 2.20. Nucleotide-dependent dimerisation of Ssa1. (A) 500 nM Ssa1* was analysed either alone or in the presence of 1 mM ADP, ATP, ATP γ S or AMPPnP by sedimentation velocity AUC. (B) Addition of 3 μ M Sti1-WT to 0.5 μ M Ssa1* in the presence of 1 mM ATP led to the formation of no new complexes.

2.3.4 TPR domain contributions to ternary complexes with Hsp90 and labelled Hsp70

Previous work with AUC has demonstrated the formation of ternary complexes between labelled Ssa1, unlabelled Hsp82 and unlabelled Sti1 as a peak sedimenting at 8 – 9 S. These are also observed when either TPR1 or TPR2B are inactivated, indicating that the complex can form with Ssa1 bound to either the N- or C-terminal module of Sti1 (Schmid *et al*, 2012; Röhl *et al*, 2015). When complex formation was analysed with the Sti1-DS1 construct, a large peak at 9 S and an overall sedimentation profile identical to Sti1-WT indicated normal ternary complex formation (Figure 2.21). With Sti1-DS2 and Sti1-DS3 however, no peak was observed in the 8 – 9 S range and a peak instead appeared at 6.5 - 6.8 S indicating formation of a new complex. Population of this peak seems to depend on the presence of TPR1 occupying the TPR2B position, which is common to Sti1-DS2 and Sti1-DS3, however its identity is difficult to attribute as it appears too small to support incorporation of a Hsp82 dimer. One possibility could be that this complex is composed of Sti1: Ssa1₂, with a single Ssa1 bound to each Sti1 module or with Ssa1 bound as a dimer. The formation of such a complex would then seem to depend on some non-specific, or transient influence of Hsp82 on Ssa1 or Sti1.

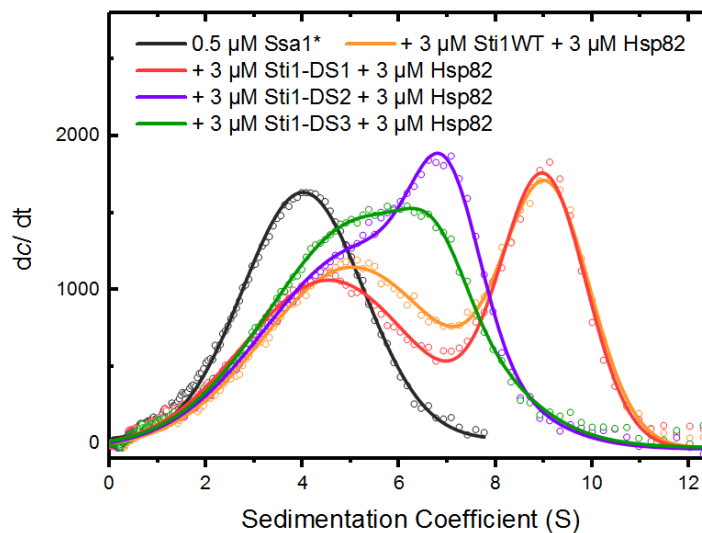


Figure 2.21. Complexes formed by labelled Ssa1* in the presence of Sti1 domain-swapped constructs and Hsp82. 500 nM Ssa1* was mixed with 3 μ M unlabelled Hsp82 and 3 μ M unlabelled Sti1-WT (orange), Sti1-DS1 (red), Sti1-DS2 (violet) or Sti1-DS3 (green) and complex formation measured by sedimentation velocity AUC. Raw data were analysed as dc/dt plots (open circles) and fit with Gaussian curves (solid lines).

2.3.5 Contributions of TPR domains to the binding of labelled Hsp90

To obtain further insight into complexes formed with the domain-swapped constructs, AUC experiments were carried out using a similar setup to the previous two sections, except using randomly labelled Hsp82 (Hsp82*) in place of labelled Ssa1. In these experiments a more detailed analysis of the sedimentation data by $c(S)$ distributions was made possible by the fact that Hsp82 could be labelled cleanly (residual amounts of free dye molecule could never be completely separated from Ssa1). Hsp82* alone sedimented at 4.1 S and upon addition of Sti1-WT a complete shift to a larger peak centred at 7.8 S and an intermediate peak centred at 6.2 S was observed (Figure 2.22). The larger peak was observed in a previous AUC study of Hsp82 and Sti1 and was assigned to a binary complex involving a single Hsp82 dimer and Sti1 molecule (Li *et al*, 2011). This study however used dc/dt analysis, in which the intermediate peak is obscured within a shoulder (see Figure 2.22). The same distribution is observed in the case of Sti1-DS1 although with a slight upward shift in the large peak to 8.2 S. A stark difference

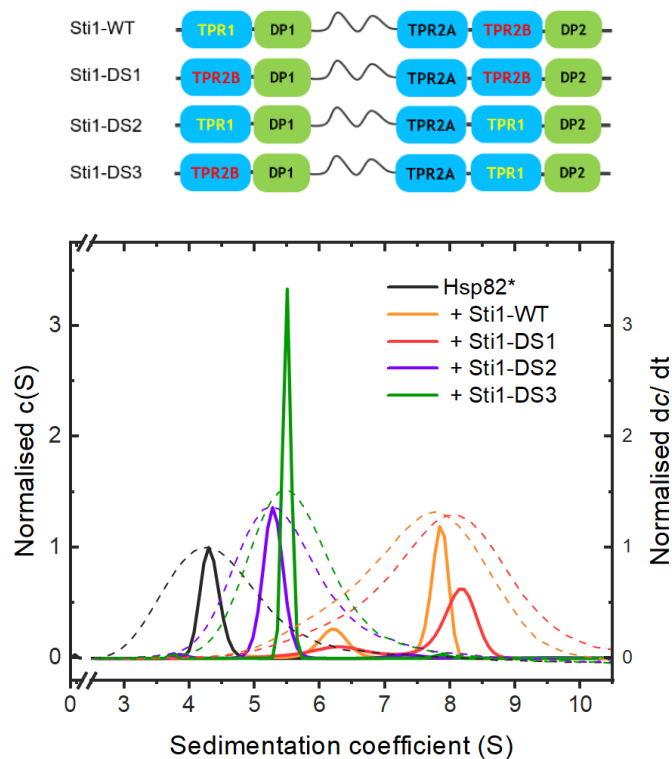


Figure 2.22. Complex formation between labelled Hsp82* and Sti1 domain-swapped constructs. Upper: schematic of Sti1 domain-swapped constructs. Lower: 500 nM labelled Hsp82* was mixed with 3 μ M Sti1-WT (orange), Sti1-DS1 (red), Sti1-DS2 (violet) or Sti1-DS3 (green) and measured by sedimentation velocity AUC. Raw data were analysed as dc/dt plots (dashed lines) or $c(S)$ distributions (solid lines).

is observed with Sti1-DS2 and Sti1-DS3, where Hsp82* appears entirely bound in intermediate complexes sedimenting at 5.2 S and 5.5 S respectively, with only very minor peaks visible in the 7 S to 8 S region.

There is conflicting evidence regarding the stoichiometry of Sti1-Hsp82 complexes. Some studies have found two Sti1 molecules per Hsp90 dimer (Prodromou *et al*, 1999; Hildenbrand *et al*, 2011; Hernández *et al*, 2002). However a stoichiometry of 1 Sti1 per Hsp82 dimer was found to completely inhibit Hsp82 ATPase activity and other studies have observed predominantly 1: 1 (Hsp82 dimer: Sti1) complexes with minor amounts of the 1: 2 complex (Li *et al*, 2011; Ebong *et al*, 2011; Southworth & Agard, 2011). The current results imply that both 1: 1 and 1: 2 complexes are possible between Hsp90 and Sti1, and that 1: 2 complexes are favoured. The formation of 1: 2 complexes seems to depend on the secondary Hsp82-MD – Sti1-TPR2ATPR2B interaction since they only occur with Sti1-WT and Sti1-DS1 in which TPR2B is in its wild type position (Figure 2.23, A). With Sti1-DS2 and Sti1-DS3, TPR2B is replaced by TPR1 and the secondary interaction is disrupted, meaning that Hsp82 would likely be bound solely through the primary MEEVD interaction. This would be consistent with the lower S-values observed for the Sti1-DS2 and Sti1-DS3 peaks compared to the intermediate peaks for Sti1-WT and Sti1-DS1, since such complexes, tethered only by the Hsp82 C-terminal tail, would be much more extended in solution (Figure 2.23, B). It is surprising that 1: 2 complexes cannot be formed when connected by the Hsp82 tail only, especially considering that that isolated Hsp82 C-terminal peptides bind to isolated TPR2A with a K_d of 300 nM (Schmid *et al*, 2012). However

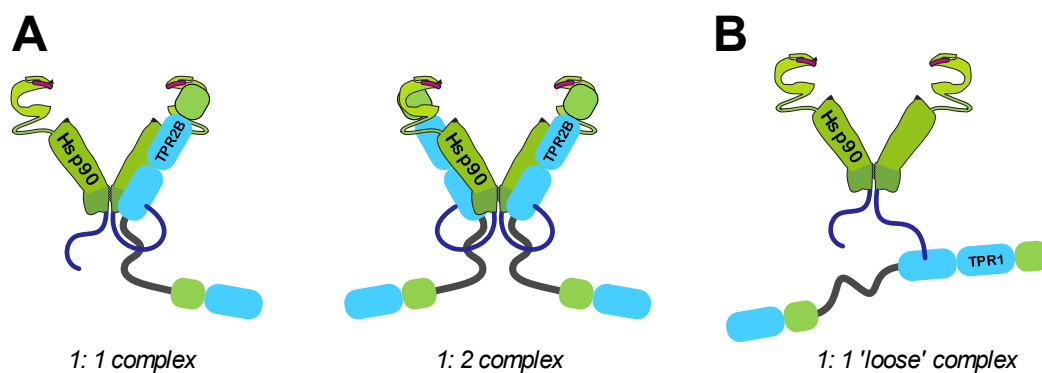


Figure 2.23. Model for association between Sti1 domain-swapped constructs and Hsp82. (A) With TPR2B in its wild type position (Sti1-WT and Sti1-DS1), both 1: 1 and 1: 2 (Hsp82 dimer: Sti1) complexes are formed. (B) With TPR1 in place of TPR2B (Sti1-DS2 and Sti1-DS3) the secondary interaction with Hsp90 is disrupted, resulting in loose 1: 1 complexes bound through the MEEVD only.

there is previous evidence to suggest that binding of TPR co-chaperones to the two tails in a Hsp82 dimer is not independent. In one study Hsp82 was found to preferentially form asymmetric ternary complexes with Hop (human Sti1) and the PPIase FKBP52, while all other combinations of binary and ternary complexes could freely interchange (Ebong *et al*, 2011). In another study asymmetric complexes were also found to form with Sti1 and the yeast PPIase Cpr6, against statistical expectations (Li *et al*, 2011). A possible explanation for the current results could be steric crowding beneath the Hsp82 dimer, however it could also be that a binding event at one tail is communicated allosterically through the dimer and influences binding at the other.

2.3.6 TPR domain contributions to ternary complexes with Hsp70 and labelled Hsp90

Having identified the existence of multiple modes of complex formation between Hsp82* and the Sti1 variants, the next step was to ask how these would be affected by the addition of Ssa1.

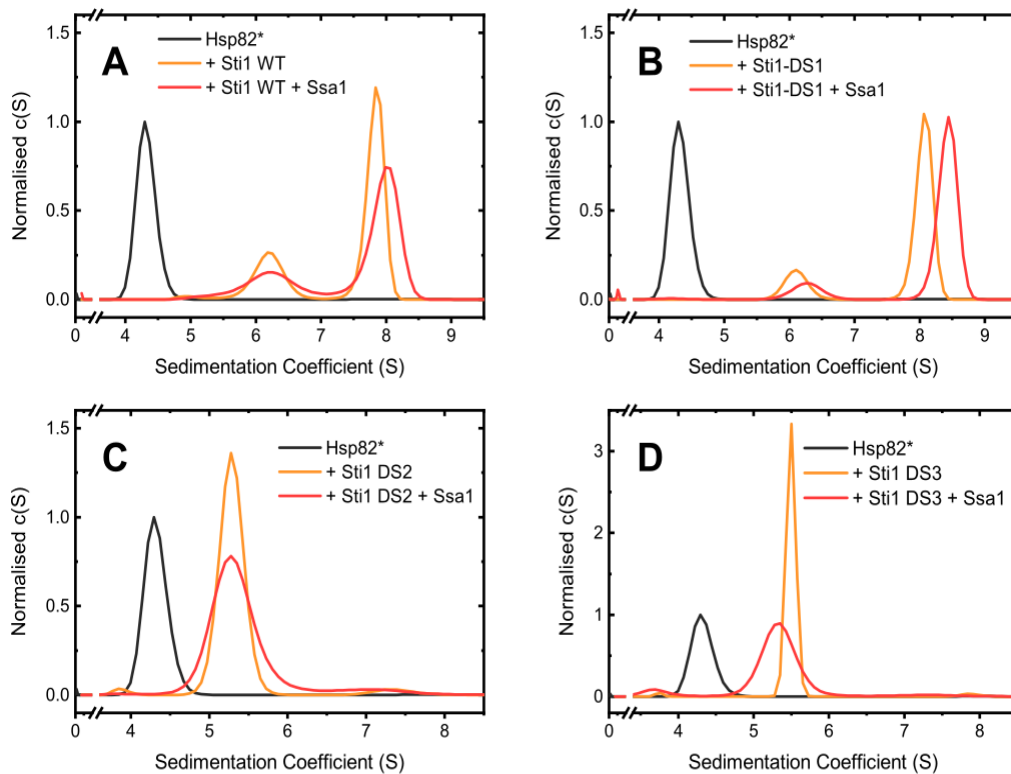


Figure 2.24. Complexes formed by labelled Hsp82* in the presence of Sti1 domain-swapped constructs and Ssa1. 500 nM Hsp82* was mixed with 3 μ M unlabelled Sti1 variant: (A) Sti1-WT, (B) Sti1-DS1, (C) Sti1-DS2 or (D) Sti1-DS3 in the absence (orange) or presence (red) of 3 μ M unlabelled Ssa1. Complex formation was measured by sedimentation velocity AUC and raw data were analysed as c(S) distributions.

Upon addition of excess unlabelled Ssa1, slight upwards shifts are seen in the larger peaks for Sti1-WT and Sti1-DS1 (Figure 2.24, A, B), while with Sti1-DS2 and Sti1-DS3 no new peaks appear and only a broadening of the intermediate peak is observed (Figure 2.24, C, D). The relatively small magnitude of the shift in the larger peaks of Sti1-WT and Sti1-DS1 suggests that rather than an incoming Ssa1 binding to form a Hsp82: Sti1₂: Ssa1 complex, it displaces one Sti1 molecule to form the Hsp82: Sti1: Ssa1 ternary complex, corresponding to the ternary complex peak previously observed with labelled Ssa1 (Section 2.3.4). The absence of a ternary complex peak for Sti1-DS2 and Sti1-DS3 shows that, as for Hsp82: Sti1₂ complexes, TPR2B in its wild-type position is a requirement for the formation of Hsp82: Sti1: Ssa1 ternary complexes. However the absence of a peak at 6.5 – 6.8 S for Sti1-DS2 and Sti1-DS3 is at odds with the appearance of peaks in this region observed with labelled Ssa1* (Figure 2.21). This appears to confirm that Hsp82 does not participate in these complexes, meaning that they are composed solely of Ssa1 and Sti1, possibly in a Ssa1: Sti1: Ssa1 or Sti1: Ssa1₂ configuration.

Regardless of the identity of the unique complexes observed with labelled Ssa1*, the current results suggest that an intact Hsp82-MD – TPR2ATPR2B interaction is necessary to form the Hsp82: Sti1: Ssa1 ternary complex, which implies that additional contacts between Ssa1 and Sti1-Hsp82 must be made once the interaction is engaged (Figure 2.25, A). Importantly, the results with Sti1-DS2 and Sti1-DS3 show that binding of Hsp82 and Ssa1 to Sti1 via the (M)EEVD interaction is not independent. When Hsp82 is bound solely through its MEEVD to TPR2A, subsequent binding of Ssa1 to the adjacent TPR1 on the C-terminal module, or to the TPR domain on the N-terminal module (regardless of whether it is TPR1 or TPR2B - Sti1-DS2 or Sti1-DS3 respectively) is precluded (Figure 2.25, B). For the latter condition to be fulfilled it must be the case that the two modules are in frequent contact on the timescale of Ssa1 and Hsp82 binding. Similarly, Ssa1 forms binary complexes with Sti1-DS2 and Sti1-DS3 (Figure 2.19, C, D), however configurations with Ssa1 bound to the N-terminal module would be unable to mediate the observed preclusion of Hsp82 binding to the C-terminal module, if the two modules were not in contact (Figure 2.25, C).

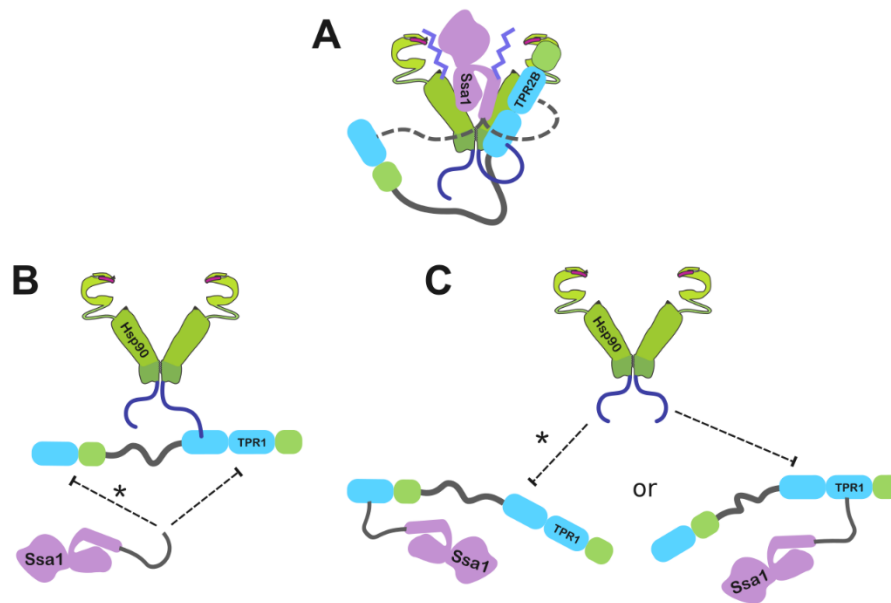


Figure 2.25. Scheme to demonstrate the interdependency of Sti1 EEVD binding.

(A) Ternary complexes are made possible by additional interactions taking place on the C-terminal module with Ssa1, following engagement of the Hsp82-MD with Sti1-TPR2B. (B) Hsp82 forms loose binary complexes with Sti1-DS2 and Sti1-DS3 which preclude binding of Ssa1. Since Hsp82 binds to the C-terminal module, additional inter-module communication is necessary to preclude Ssa1 binding to the N-terminal module (*). (C) Ssa1 forms binary complexes with Sti1-DS2 and Sti1-DS3 which preclude Hsp82 binding. The fact that no hypothetical ternary complexes with Ssa1 bound to the N-terminal module and Hsp82 to the C-terminal module are observed (*) indicates that EEVD binding is not independent.

Binary complex formation was also analysed between Hsp82* and Sti1-N39A and Sti1-N435A, in which the Ssa1-EEVD interaction with TPR1 or TPR2B respectively is inactivated. These gave rise to the same distributions seen with Sti1-WT and Sti1-DS1, consisting of an intermediate and large peak, again likely due to an intact Hsp82-MD – TPR2ATPR2B interaction (Figure 2.26). Ternary complexes have also previously been observed with these constructs using labelled Ssa1 and unlabelled Hsp82 (Schmid *et al*, 2012; Röhl *et al*, 2015). When ternary complex formation was analysed with labelled Hsp82* and unlabelled Ssa1, slight upward shifts in the large peaks of 0.7 S and 0.5 S respectively for Sti1-N39A and Sti1-N435A were observed, again suggesting displacement of one Sti1 molecule to form a more compact Hsp90-Sti1-Ssa1 complex (Figure 2.26).

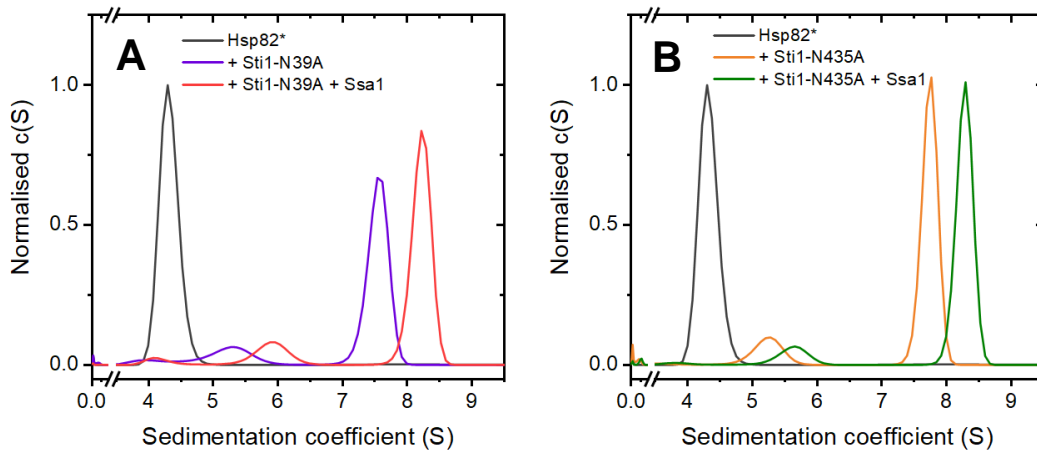


Figure 2.26. Ternary complex formation with labelled Hsp82*, unlabelled Ssa1 and Sti1 TPR-inactivated constructs. (A) Sedimentation velocity AUC was performed on 500 nM Hsp82* alone (black), with 3 μ M Sti1-N39A (violet), or additionally with 3 μ M Ssa1 (red). (B) as in (A) except using 3 μ M Sti1-N435A (orange), or additionally with 3 μ M Ssa1 (green). Raw data were fit to $c(S)$ distributions.

Taken together the results from this section highlight the importance of the Hsp82-MD – TPR2ATPR2B interaction in forming the ternary complex, as well as demonstrating that the MEEVD and EEVD interactions of Hsp82 and Ssa1 with Sti1 are not independent. In the absence of the Hsp82-MD – TPR2ATPR2B interaction (Sti1-DS2 and Sti1-DS3) binding of Ssa1 and Hsp82 is mutually exclusive, with the two modules of Sti1 communicating to bind either a single Ssa1 or Hsp82 molecule. This may represent a timing function, with Sti1 remaining in a preliminary binary state until the productive ternary complex can form (Figure 2.27, A). With TPR2B in its native position, ternary complexes are formed regardless of whether TPR1 or TPR2B are active (Sti1-N39A and Sti1-N435A) or of the identity of the N-terminal module (Sti1-DS1). This suggests that the key to ternary complex formation must be the ability of Ssa1 to make surface contact with Hsp82-Sti1 on the C-terminal module, in a compact conformation enabled by the Hsp82-MD – TPR2ATPR2B interaction. The N-terminal module may be able to transiently bind an incoming Ssa1 molecule, but only if the TPR2B – Hsp82-MD has been engaged and Ssa1 can be transferred to the C-terminal module, owing to the continuous communication between modules (Figure 2.27, B). Recently a weak interaction ($\sim 13 \mu$ M) between Ssa1 and a region in the Hsp82-MD has been demonstrated *in vitro* in the absence of Sti1, which may provide a basis for additional contacts formed on the C-terminal module (Kravats *et al*, 2018).

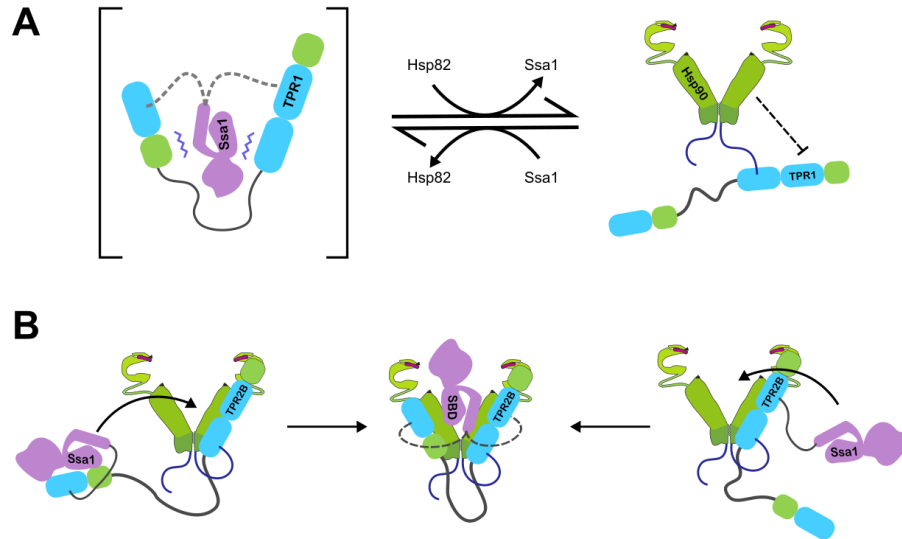


Figure 2.27. Ternary complexes depend on a native C-terminal module geometry. (A) In the absence of the Hsp82-MD – TPR2ATPR2B interaction mutually exclusive binding of Ssa1 and Hsp82 is maintained by inter-module communication. (B) Engagement of the Hsp82-MD – TPR2ATPR2B interaction brings about a conformation on the Sti1 C-terminal module compatible with ternary complex formation. Ssa1 can then be delivered into ternary complexes via the EEVD interaction with TPR1 or TPR2B.

2.3.7 Complex formation between Sti1 domain-swapped constructs and the Ssa1-SBD

As a final approach to interrogate TPR domain contributions to complex formation, an analysis of the interaction between domain-swapped Sti1 constructs and the substrate binding domain of Ssa1 (Ssa1-SBD) was conducted. First, binding of domain-swapped constructs to labelled Ssa1-SBD (Ssa1-SBD*) was analysed with fluorescence anisotropy (Figure 2.28, A). When TPR1 was substituted with TPR2B (Sti1-DS1) or TPR2B with TPR1 (Sti1-DS2), no significant change in affinity was observed. When they were both substituted at once however (Sti1-DS3), the affinity halved (Figure 2.28, B). This further highlights the importance of context within the overall architecture of Sti1, since a weaker affinity is observed with Sti1-DS3, in which both domains are active, than with Sti1-N39A or Sti1-N435A, in which only a single domain is active (see Figure 2.6 and Table 2.2, Section 2.1.2). Furthermore, substituting TPR1 with TPR2B or TPR2B with TPR1 respectively led to a slight increase or a slight decrease in the binding capacity B_{\max} , while substituting both at once significantly reduced B_{\max} to a level identical to the Sti1-N39A and Sti1-N435A constructs (Figure 2.28, C and see Section 2.1.2).

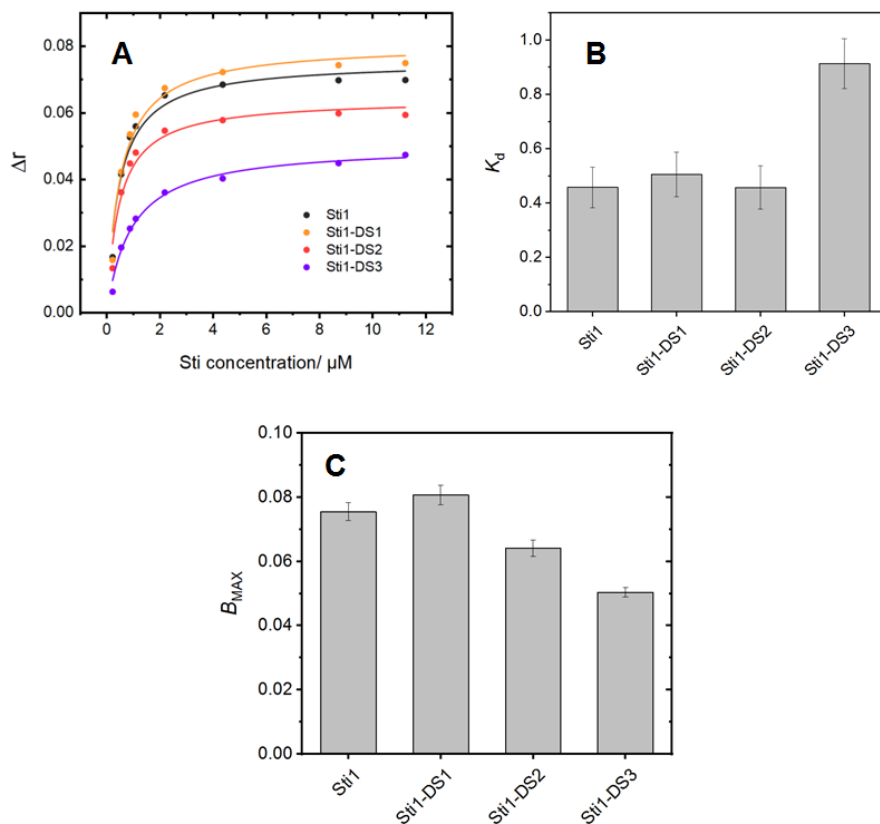


Figure 2.28. Affinities of Ssa1-SBD for Sti1 and domain-swapped variants. (A) 500 nM Ssa1-SBD* was incubated with increasing concentrations of Sti1-WT (black), Sti1-DS1 (orange), Sti1-DS2 (red) or Sti1-DS3 (violet) and binding measured by fluorescence anisotropy. (B, C) Dissociation constants derived from (A) with the fitting error shown.

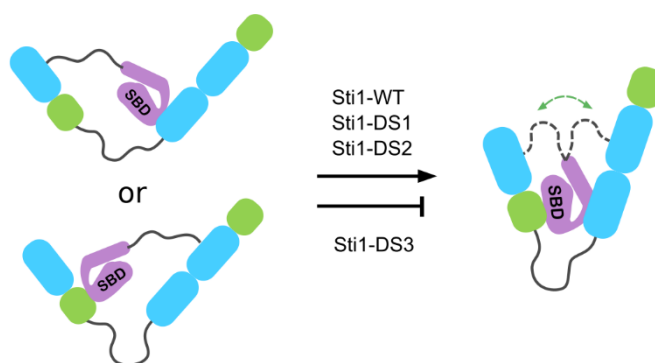


Figure 2.29. Optimal binding to Sti1 requires conformations which enable EEVD transfer between modules. These are accessible when at least one module possesses its native Hsp70-binding TPR domain (Sti1-WT, Sti1-DS1, Sti1-DS2). When TPR1 and TPR2B are exchanged in position (Sti1-DS3) the requisite conformation cannot be attained.

Taken together these results show that the defect in binding caused by inactivating either TPR domain can be rescued or even enhanced by substituting it with an active domain, but only when the TPR domain in the opposing module is in its native position. This indicates that one native module is sufficient to support the conformations enabling inter-module EEVD transfer, outlined in Sections 2.1.2 - 2.1.3, which contribute to binding. When both domains are exchanged in position, communication becomes disrupted and conformations enabling EEVD transfer cannot be accessed (Figure 2.29).

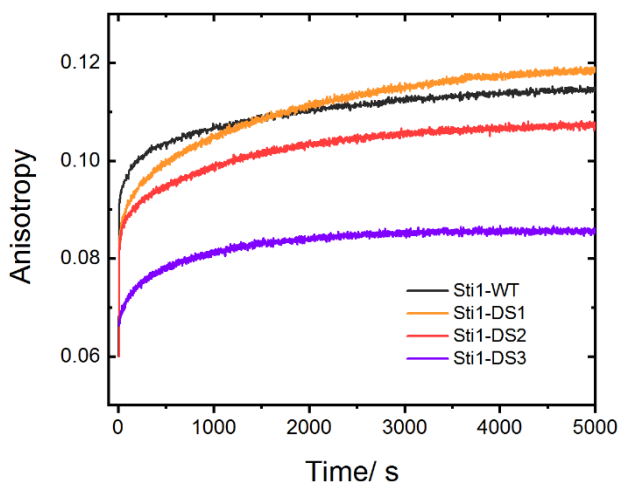


Figure 2.30. Association kinetics between Ssa1-SBD* and Sti1 domain-swapped variants measured by fluorescence anisotropy. 500 nM SBD* was mixed with 500 nM Sti1-WT (black), Sti1-DS1 (orange), Sti1-DS2 (red) or Sti1-DS3 (violet) and association measured as an increase in fluorescence polarization over time.

The kinetics of association between the Sti1 domain-swapped constructs and Ssa1-SBD* was also analysed using fluorescence anisotropy. While a quantitative analysis was precluded by the absence of a stopped-flow device, a qualitative comparison yielded interesting differences in the binding behaviour (Figure 2.30). The same multi-phase binding behaviour was observed as with the single TPR-inactivated constructs via anisotropy, as well as measured via the FRET interaction (Section 2.1.3). Sti1-WT, Sti1-DS1 and Sti1-DS2 all show a strong initial rapid binding while this is significantly impaired in Sti-DS3, whose association kinetics appear similar to the single TPR-inactivated constructs Sti1-N39A and Sti1-N435A (Section 2.1.3). It therefore appears that an active domain on both modules brings about a rapid binding phase, but that this is only possible when at least one domain is in its native position, and is interrupted when both domains are exchanged (Sti1-DS3). For Sti1-DS1 and Sti1-DS2, in addition to exhibiting defects

in the rapid initial binding, opposing effects are observed on the later phases of association, with the substitution of TPR2B for TPR1 (Sti1-DS1) leading to an even greater build-up of bound Ssa1-SBD* on a longer timescale. This may indicate that TPR2B is better able to participate in stabilising compacted interactions discussed in Section 2.1.3, which promote EEVD transfer.

Next complex formation between the Sti1 domain-swapped constructs and Ssa1-SBD* was analysed by AUC in a setup analogous to the experiments with labelled Ssa1 and labelled Hsp82 (Section 2.3.3 - 2.3.6). All constructs formed binary complexes with the Ssa1-SBD*, with the appearance of a single peak centred around 4.5 S (Figure 2.31). This demonstrates that, as is the case with full-length Ssa1, no arrangement of the TPR domains gives rise to a greater than 1: 1 binding with Ssa1-SBD. The S-values of the Sti1-DS2 and Sti1-DS3 binary complex peaks (both 4.3 S) were slightly lower than that of Sti1-WT (4.5 S), while that of Sti1-DS1 (4.7 S) was slightly higher, correlating with the trend in S values of binary complexes formed with full-length Ssa1

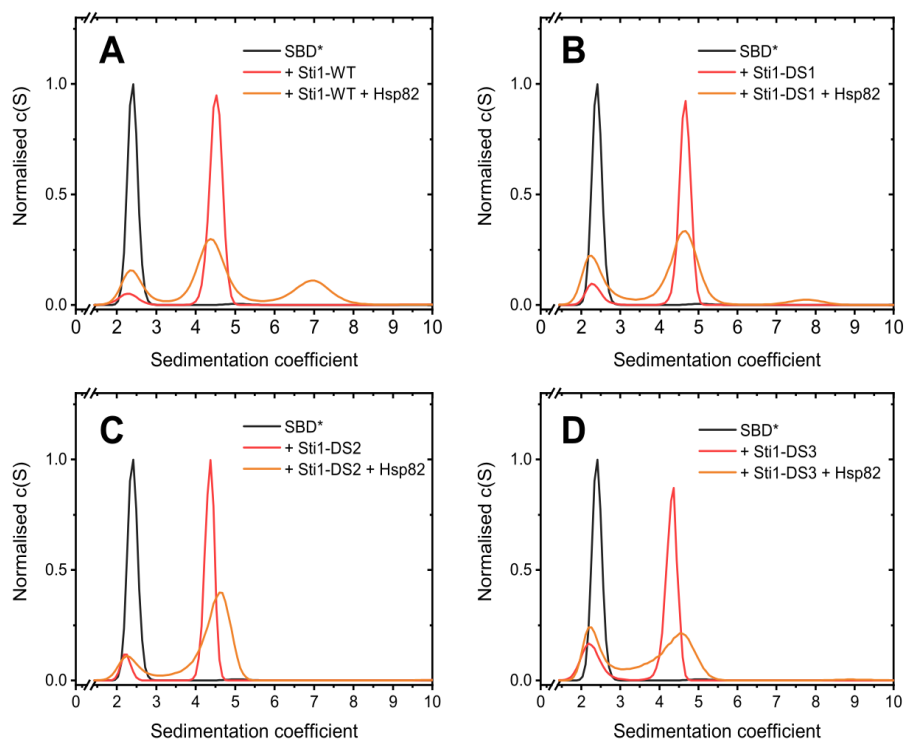


Figure 2.31. Complexes formed by SBD* in the presence of Sti1 domain-swapped constructs and Hsp82. 0.5 μ M SBD* was mixed with 3 μ M unlabelled Sti1 variant: (A) Sti1-WT, (B) Sti1-DS1, (C) Sti1-DS2 or (D) Sti1-DS3 in the absence (red) or presence (orange) of 3 μ M unlabelled Hsp82. Complex formation was measured by sedimentation velocity AUC and raw data were analysed as c(S) distributions.

(Section 2.3.3). This trend also correlates with the binding capacity measured with anisotropy (Figure 2.28, C) and may be a further indication that compact conformations promoting inter-domain transfer enhance Ssa1 binding. Upon addition of unlabelled Hsp82 ternary complexes are formed with Sti1-WT and Sti1-DS1 at 7.0 S and 7.8 S respectively, while only broadening of the binary complex peak is seen with Sti1-DS2 and Sti1-DS3 (Figure 2.31). This further corroborates the importance of an intact TPR2A-TPR2B in forming ternary complexes and shows that the network of interactions on the C-terminal module minimally involves Ssa1-SBD. Compared with full-length Ssa1 however, the amount of ternary complex formation with Sti1-WT is reduced, and is almost undetectable with Sti1-DS1 (see Figure 2.21 and Figure 2.31, A, B). This shows that further contacts with the NBD of Ssa1 are important in forming the ternary complex, and that in the absence of these, loading of the complex by TPR2B in the N-terminal module of the Sti1-DS1 construct is defective.

Binary complexes were also observed with Ssa1-SBD* in the presence of the unlabelled TPR-inactivated constructs Sti1-N39A and Sti1-N435A, respectively at 4.3 S and 4.4 S (Figure 2.32). Upon further addition of unlabelled Hsp82 ternary complexes were readily formed, as has previously been observed with labelled full-length Ssa1 (Schmid *et al*, 2012; Röhl *et al*, 2015). Formation of ternary complexes with the TPR2B-inactivated Sti1-N435A is particularly strong and displays the highest overall S value, at 8.1 S, indicating the highest degree of compaction. This may seem surprising given that complexes form at the C-terminal module. However it would be consistent with a conformation in which the Ssa1-SBD forms a complex at the C-

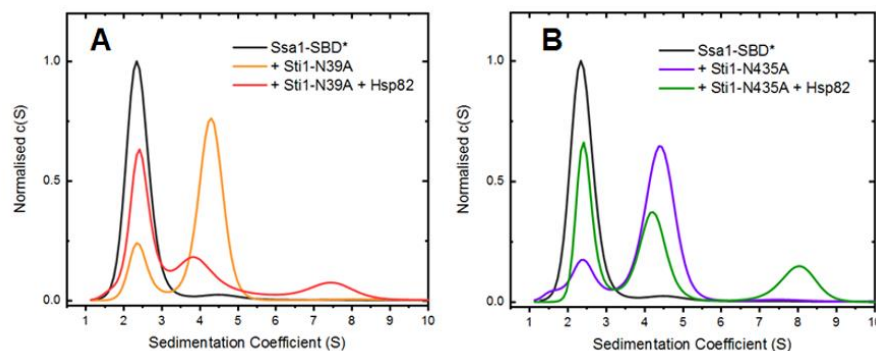


Figure 2.32. Ternary complex formation with SBD* in the presence of Sti1 TPR-inactivated constructs and Ssa1. (A) Sedimentation velocity AUC was performed on 500 nM SBD* alone (black), with 3 μ M Sti1-N39A (orange), or additionally with 3 μ M Hsp82 (red). (B) as in (A) except using 3 μ M Sti1-N435A (violet), or additionally with 3 μ M Hsp82 (green). Raw data were fit to $c(S)$ distributions.

terminal module, making surface contacts with Hsp82 and/ or TPR2A-TPR2B, yet with its EEVD bound exclusively to TPR1, effectively tethering the N-terminal module to the C-terminal module (Figure 2.33, A). This was the major configuration previously observed for Hsp82: Sti1: Ssa1 complexes by electron microscopy (See Figure 1.9 A) (Alvira *et al*, 2014). Ternary complexes with Sti1-N39A and Sti1-DS1 also displayed higher compaction (7.4 S and 7.8 S respectively) than Sti1-WT (6.9 S) suggesting that the Ssa1-SBD is fully occupied within the environment of the C-terminal module (Figure 2.33 B, C). This pattern is conserved in ternary complexes formed with labelled Hsp82 and full-length Ssa1, with Sti1-WT giving rise to the lowest S value of all constructs (Section 2.3.6). These results reveal a tendency towards compacted states, with Ssa1 fully located at the C-terminal module, if effective inter-module transfer is disrupted. Only with Sti1-WT where inter-module transfer may take place efficiently, is there an appreciable population of an extended conformation with Ssa1 bound solely to TPR1 (Figure 2.33, D).

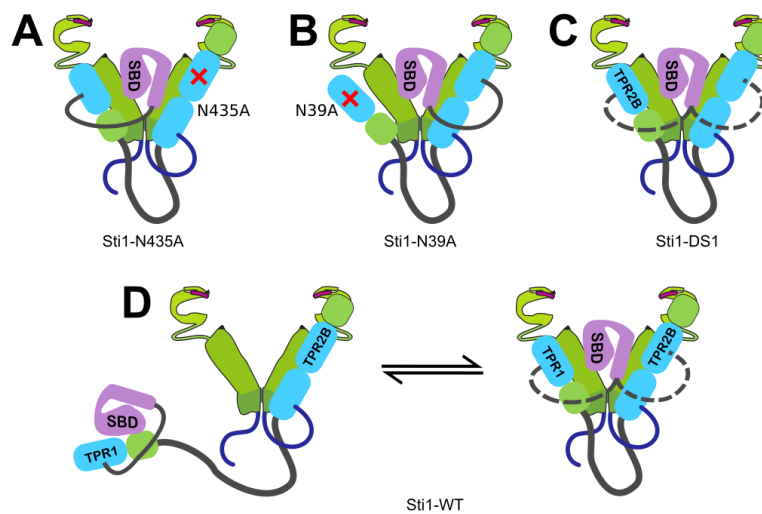


Figure 2.33. Conformations of ternary complexes formed with different Sti1 constructs. (A) Sti1-N435A forms compact conformations with Ssa1-SBD located at the C-terminal module and with the N-terminal module tethered to the C-terminal module. (B, C) With Sti1-N39A and Sti1-DS1 Ssa1-SBD is also located fully at the C-terminal module. (D) Ternary complexes with Sti1-WT can exist in an equilibrium between extended and compact conformations.

2.4 Complex formation with the client protein GR

2.4.1 Formation of GR-LBD-Hsp70-Hsp40 oligomeric complexes

In the final part of the project, the ability of yeast Hsp70 and Hsp90 to form complexes with a model client protein, the ligand binding domain of the glucocorticoid receptor (GR-LBD) was investigated, along with the contributions of the TPR domains of Sti1 to this process. Previous work with the human chaperones has established a picture in which Hsp70 binds to GR-LBD in the presence of Ydj1 (yeast Hsp40) and ATP and holds it in a partially unfolded state incapable of binding its hormone ligand. Subsequent binding of Hsp90 mediated by Hop (human Sti1) chaperones GR-LBD to a fully folded state capable of hormone rebinding (Kirschke *et al*, 2014). Furthermore Hsp90 alone has been shown to form a stable complex with GR-LBD (Lorenz *et al*, 2014). In the current work formation of complexes between the GR-LBD, yeast Hsp70 and Hsp90 was investigated by AUC.

Complex formation was first analysed in the presence of ATP using GR-LBD randomly labelled with ATTO-488 (GR-LBD*). GR-LBD* alone sedimented as a major peak at 2.6 S with a small shoulder at 1.6 S arising from a degradation product. Addition of Hsp82 resulted in a peak at 5.9 S indicating formation of a stable Hsp90-GR-LBD complex, as has been observed previously with his₆-tagged Hsp82 (Lorenz *et al*, 2014). Addition of Ydj1 alone resulted in a small peak at 4.7 S indicating formation of a Ydj1-GR-LBD binary complex, however no complex formation was observed when Ssa1 was added alone (Figure 2.34, A). When Ssa1 and Ydj1 were added together in the absence of ATP, a small peak appeared at 7 S in addition to the 4.7 S binary peak, potentially indicating the presence of a Ssa1-Ydj1-GR-LBD ternary complex. However when Ssa1 and Ydj1 were added in the presence of ATP, a dramatic shift to a large peak at 13.3 S was observed, indicating formation of a large oligomeric complex (Figure 2.34, B). In addition, two weakly populated peaks appeared at 8.7 S and 10.8 S, indicating the presence of multiple intermediate oligomeric forms. This large complex was unexpected given the relatively low molecular weight species observed so far, however its strong population and narrow peak width suggest it is stable and specific.

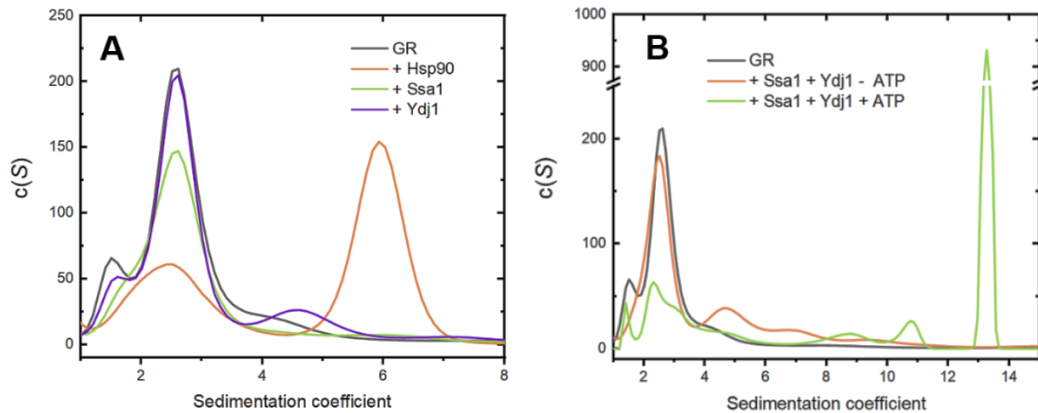


Figure 2.34. Complex formation between GR-LBD and yeast chaperones investigated by sedimentation velocity AUC. (A) 500 nM GR-LBD* was run alone (black) or mixed with 3 μ M Hsp82 (orange), 6 μ M Ssa1 (green) or 2 μ M Ydj1 (violet) in the presence of 2 mM ATP. (B) 500 nM GR-LBD* was mixed with 6 μ M Ssa1 and 2 μ M Ydj1 in the absence (orange) or presence (green) of 2 mM ATP. Raw data were fit to $c(S)$ distributions.

As mentioned in Section 2.3.3, the ability of Hsp70 to exist in dimeric and oligomeric states has been widely documented (Aprile *et al*, 2013; Sarbeng *et al*, 2015). While the precise role of Hsp70 oligomerisation remains unclear, there have been reports linking the phenomenon to chaperone activity, as well as studies observing the interaction of oligomeric Hsp70 with a substrate (Thompson *et al*, 2012; Angelidis *et al*, 1999; Sousa *et al*, 2016). The complex seen at 13.3 S in the current work may therefore suggest that Hsp70 oligomerisation also plays a role in the chaperoning of GR. A similar complex was observed by AUC with human Hsp70, Hsp90 and Hop, suggesting the phenomenon is conserved from yeast to man (unpublished data, Dr. Daniel Rutz, TU München).

Next it was asked what effect Hsp82 and Sti1 would have on the formation of the oligomeric complex. Addition of Hsp82 to the GR-LBD-Ydj1-Ssa1 mixture resulted in a minor downward shift of the major oligomeric peak to 13 S, as well as the appearance of an intermediate peak at 5.9 S, corresponding to the Hsp82-GR-LBD binary complex, and one at 8.8 S, corresponding to the smaller intermediate species observed with Ssa1 and Ydj1 alone (Figure 2.35). Addition of Sti1 to the GR-LBD-Ydj1-Ssa1 mixture also resulted in a slight shift of the major peak to 13 S, an intermediate peak at 8.9 S similar to with GR-LBD-Ydj1-Ssa1 alone or with Hsp82, and a new minor peak at 7 S. Adding Sti1 and Hsp82 together resulted in a broadening of the large oligomeric peak and pair of weakly populated peaks at 7 S and 9.5 S. In summary the effect of Hsp82 and Sti1 is to displace GR-LBD from the oligomeric complex resulting in intermediate

species and free GR-LBD. Sti1 caused the greatest GR-LBD displacement (highest level of free GR-LBD), potentially by sequestering Ssa1 in binary complexes incompatible with GR-LBD binding. Hsp82 on the other hand formed a stable binary complex with GR-LBD at the expense of the oligomeric complex. The Hsp82-GR-LBD binary complex was not observed when Hsp82 and Sti1 were added together, likely because Sti1 binds to Hsp82 to hold it in an open conformation incompatible with GR-LBD binding (Lorenz *et al*, 2014). In summary, under the conditions studied GR-LBD is able to assemble into an initial Ydj1-Ssa1-bound oligomeric state and a final Hsp82-bound state. Assembly takes place independently and rather than bridging the two states, Sti1 favours population of the initial state.

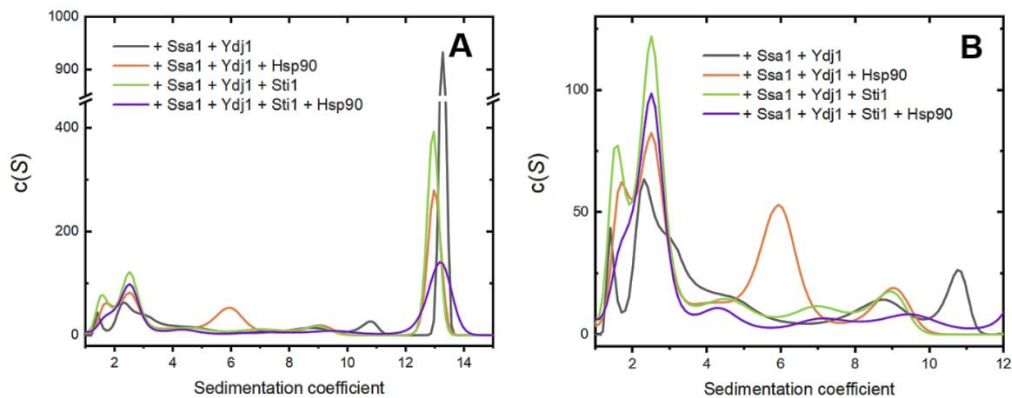


Figure 2.35. Influence of Hsp82 and Sti1 on the GR-LBD-Ydj1-Ssa1 complex investigated by sedimentation velocity AUC. (A) 3 μ M Hsp82 (orange) or 3 μ M Sti1 (green) or both together (violet) were added to a mixture of 500 nM GR-LBD*, 2 μ M Ydj1 and 6 μ M Ssa1 in the presence of 2 mM ATP. (B) Detailed view of the intermediate S value region from (A). Raw data were analysed as c(S) distributions.

Divergent effects were observed when GR-LBD-Ydj1-Ssa1 was supplemented with the Sti1 domain-swapped or domain-inactivated constructs in the presence of Hsp82 (Figure 2.36). With Sti1-DS1, Sti1-N39A and Sti1-N435A, slight upward shifts in the major peak were observed while Sti1-DS3 produced a similar distribution to that of Sti1-WT. With Sti1-DS2 on the other hand, an entirely new complex was formed at 11 S. Taken together these results demonstrate that Sti1 interacts with the GR-LBD-Ydj1-Ssa1 pre-complex in the presence of Hsp82, and that the activity and identity of TPR1 and TPR2B are important for the interaction. In particular, replacement of TPR1 with TPR2B (Sti1-DS1) results in binding to the complex while replacement of TPR2B with TPR1 (Sti1-DS2) results in disassembly of the complex into a lower molecular weight oligomeric species. The presence of all Sti1 constructs precluded the formation of the 5.9 S Hsp82-GR-LBD binary complex, demonstrating that Hsp82 is sequestered

from binding GR-LBD by Sti1 even when the interaction can only take place via the MEEVD interaction (Sti1-DS2 and Sti1-DS3). Interestingly disassembly of a similar GR-LBD-Ydj1-hHsp70 (human Hsp70) complex into a lower molecular weight complex was achieved with human Hsp90 and wild-type Hop (unpublished data, Dr. Daniel Rutz, TU München). This highlights a potential role for additional factors in connecting the initial oligomeric and final Hsp82-bound states in yeast, as a topic for further investigation.

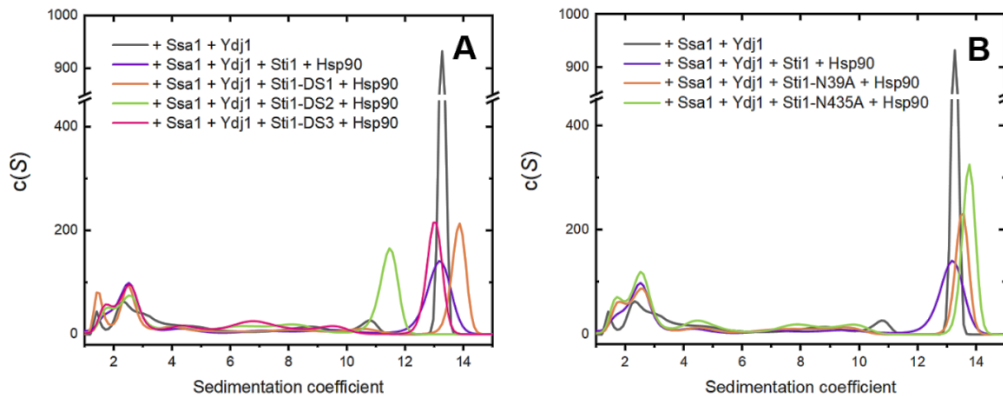


Figure 2.36. Influence of Hsp82 and Sti1 domain-swapped or TPR-inactivated constructs on the GR-LBD-Ydj1-Ssa1 complex investigated by sedimentation velocity AUC. (A) 3 μ M Sti1-WT (violet), Sti1-DS1 (orange), Sti1-DS2 (green) or Sti1-DS3 (pink) were added to a mixture of 500 nM GR-LBD*, 2 μ M Ydj1 and 6 μ M Ssa1 (black) in the presence of 2 mM ATP. (B) as in (A) except using 3 μ M Sti1-N39A (orange) or 3 μ M Sti1-N435A (green). Raw data were analysed as c(S) distributions.

2.4.2 Formation of quaternary GR-LBD complexes in the absence of ATP

In a final approach, the contribution of Sti1 TPR domains to complex formation with the GR-LBD was studied in the absence of ATP. These experiments used labelled Hsp82 to provide continuity with the identification of complexes from Sections 2.3.5 – 2.3.6. Hsp82* alone did not form a complex with GR-LBD in the absence of nucleotide (Figure 2.37). This is in line with a previous study which found that Hsp82 preferentially binds GR-LBD in a partially closed conformation promoted by ATP (Lorenz *et al*, 2014). In the presence of Sti1 and GR-LBD, Hsp82* formed only complexes with Sti1, with the same distribution of peaks centred at 6 S and 7.9 S as in the absence of GR-LBD, corresponding to the Hsp82: Sti1 and Hsp82: Sti1₂ complexes (Section 2.3.5). However when Sti1, GR-LBD and Ssa1 were added together, a complete shift to a peak at 9.3 S was observed, indicating formation of a Hsp82: Sti1: Ssa1: GR-LBD quaternary complex. Formation of this complex was furthermore independent of the cochaperone Ydj1. Hsp70: Hsp90: Hop: GR-LBD complexes have previously been identified in pull-down

experiments or isolated for EM analysis with the help of stabilising crosslinkers, however the current results show that the complex can assemble freely in solution in the absence of ATP and Ydj1 (Kirschke *et al*, 2014; Morishima *et al*, 2000; Alvira *et al*, 2014). This may be due to a stabilising influence of Ssa1 within the complex, inducing partial closure of Hsp82 and overcoming the effect of Sti1, which is to hold Hsp82 in an open conformation. However the absence of a strongly populated peak in this region under the ATP conditions studied in the previous section indicates that GR-LBD prefers to remain in the oligomeric pre-complex in the absence of additional factors.

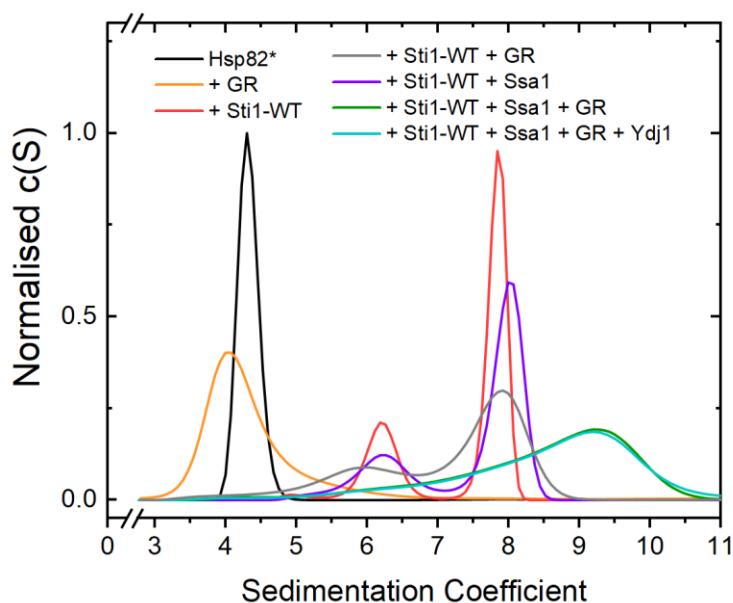


Figure 2.37. Formation of quaternary complexes with GR-LBD using labelled Hsp82 in the absence of ATP. Sedimentation velocity AUC was carried out on 500 nM Hsp82* alone or in the presence of the indicated protein combinations in the absence of ATP. GR-LBD was used at 1 μ M, Sti1-WT at 3 μ M, Ssa1 at 3 μ M and Ydj1 at 1 μ M. Raw data were analysed as c(S) distributions.

When complex formation was attempted with the Sti1 domain-swapped constructs in place of Sti1-WT, only Sti1-DS1 was able to promote formation of the 9.3 S quaternary complex (Figure 2.38, A), while with Sti1-DS2 and Sti1-DS3, Hsp82* remained bound in the previously observed binary complexes (Figure 2.38, B, C). Over and above the requirement for ternary complex formation with Ssa1, these results underscore the importance of TPR2B in its native position for the formation of quaternary complexes. However they also demonstrate that TPR2B can functionally replace TPR1 in the formation of quaternary complexes.

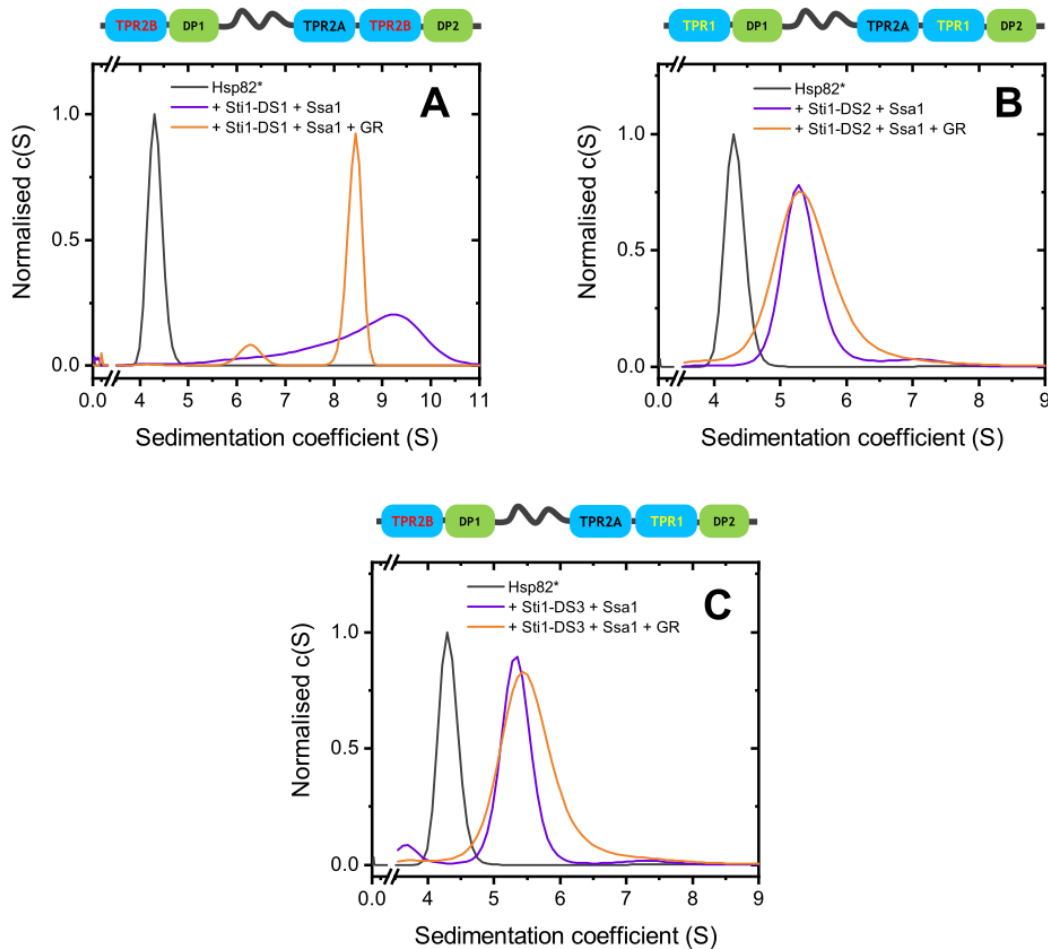


Figure 2.38. Complex formation with Sti1 domain-swapped constructs and GR-LBD using labelled Hsp82 in the absence of ATP. 0.5 μM Hsp82* (alone – black) was mixed with 3 μM Ssa1 and 3 μM Sti1 variant: (A) Sti1-DS1, (B) Sti1-DS2 or (C) Sti1-DS3 in the absence (orange) or presence (violet) of 1 μM GR-LBD. Complex formation was measured by sedimentation velocity AUC and raw data were analysed as $c(S)$ distributions.

Interestingly the TPR domain-inactivated constructs Sti1-N39A and Sti1-N435A did not support quaternary complexes under the same conditions, with only a broadening of the Hsp82: Sti1: Ssa1 ternary complex distributions observed upon addition of GR-LBD (Figure 2.39). The fact that Sti1-N435A did not support quaternary complex formation is in principle in line with the theory that the C-terminal module is the productive module of Sti1, which jointly binds Hsp70 and Hps90 through their EEVD motifs to enable transfer of GR. However the fact that no quaternary complexes were observed with Sti1-N39A contradicts the observation that TPR1 is dispensable for *in vivo* GR activation (Schmid *et al*, 2012). The results therefore reveal a novel role for TPR1 in complex formation with GR-LBD in a minimal reconstituted system. Taken together the above findings suggest that a network of contacts on the Sti1 C-terminal module

provided by the native Hsp82-MD – TPR2ATPR2B interaction, as well as an active TPR domain on both modules are necessary for quaternary complex formation *in vitro*. This provides further evidence for the communication between the modules in the assembly of the quaternary complex.

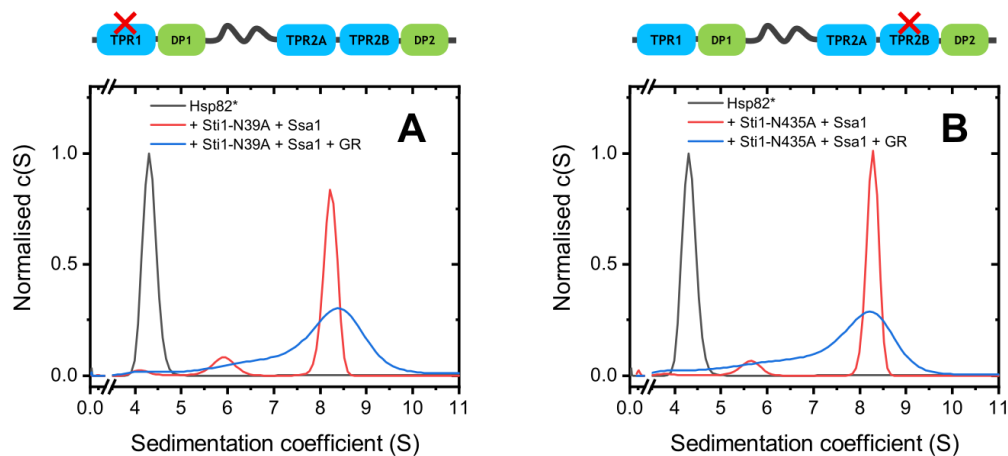


Figure 2.39. Complex formation with Sti1 TPR-inactivated constructs and GR-LBD using labelled Hsp82 in the absence of ATP. 0.5 μM Hsp82* (alone – black) was mixed with 3 μM Ssa1 and (A) 3 μM Sti1-N39A or (B) 3 μM Sti1-N435A in the absence (red) or presence (blue) of 1 μM GR. Complex formation was measured by sedimentation velocity AUC and raw data were analysed as $c(S)$ distributions.

Given the fact that Ssa1 was unable to bind GR-LBD in the absence of ATP and Ydj1 (Figure 2.34), it is unlikely that under the current conditions GR-LBD is delivered into quaternary complexes via the canonical route, involving an initial Ssa1-GR-LBD complex. A likely alternative mechanism is that a ternary complex is first formed between Ssa1, Sti1 and Hsp82, and that during formation the constituent Hsp82 is forced into a partially closed conformation capable of GR-LBD binding, effectively mimicking the partially closed conformation of Hsp82 in the presence of ATP. Indeed Hsp82 was observed to adopt a partially closed conformation in a previous cryo-EM reconstruction of the ternary complex (Alvira *et al*, 2014). This would demonstrate a new role for Ssa1 as a closing factor for Hsp82, similar to the co-chaperone p23. However the fact that ternary complexes are readily formed with Sti1-N39A and Sti1-N435A, but that neither are capable of binding GR-LBD, shows that the ternary complex must attain a particular binding-competent conformation dependent on the ability of Ssa1-EEVD to interact with both modules during assembly. In such a scheme it may be that initial interaction of Ssa1 with the N-terminal module is a necessary priming step on the pathway to formation of a complex on the C-terminal module with the requisite partially closed conformation (Figure

2.40, steps 1-3). It may also be that once a compacted ternary complex has been formed, a continuous transitioning of the Ssa1-EEVD between modules provides an allosteric basis for the GR-LBD binding-competent conformation (Figure 2.40, step 4). Taken together these results extend the phenomenon of Sti1 inter-module communication in Hsp70 binding elucidated in previous sections, showing that it also plays a role in complex formation with a model client protein.

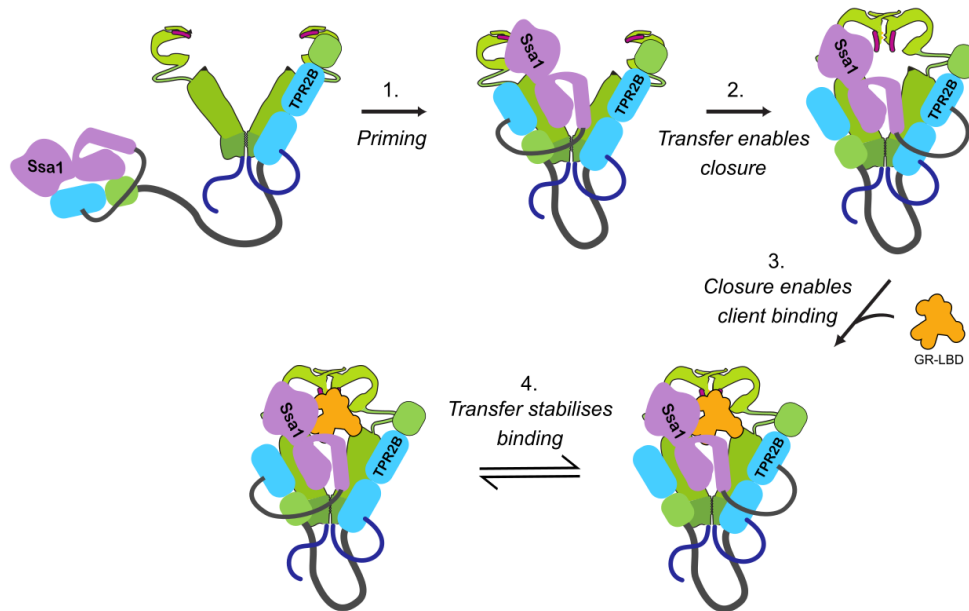


Figure 2.40. Sti1 Inter-module communication is required for quaternary complex formation. Both Sti1 modules are required to be active for quaternary complex formation, suggesting additional steps involving inter-module transfer. Initial Ssa1 binding to the N-terminal module followed by Ssa1-EEVD transfer may prime ternary complexes for client binding by inducing partial closure of Hsp82. Further inter-module Ssa1-EEVD transfer may stabilise quaternary complexes in a client binding-competent state.

Conclusions and Perspectives

3.1 TPR domain collaboration in EEVD binding revealed by FRET

Sti1 interacts with Ssa1 in a complex and dynamic manner, with contributions made from multiple domains in the Sti1 protein. A FRET system was designed to target the interaction between the TPR1 and TPR2B domains of Sti1, and the EEVD motif of the Ssa1-SBD (Section 2.1). This revealed that the EEVD binds to both domains while both are active, but has a slightly higher affinity for TPR2B. The use of alternately inactivated constructs showed that the two domains were not independent, and that the ability to bind to one enhanced binding to the other. These results implicate the existence of compacting conformations that connect the two domains, which are located on opposing modules connected by a flexible linker. The fact that the total binding capacity of Sti1 was less than the sum of the individual domains (Section 2.1.2), and that 1: 1 complexes are maximally formed with Ssa1-SBD (Section 2.3.1), suggests that such conformations promote transfer of the EEVD within the same complex, in preference to binding of a second Ssa1-SBD. Kinetic measurements of the FRET association between Ssa1-SBD and TPR1 and TPR2B revealed multiple phases, indicating the presence of additional conformational changes which contribute to the binding through each domain (Section 2.1.3). While the FRET association with TPR1 was relatively insensitive to the active status of TPR2B, the activity of TPR1 had a strong effect on association with TPR2B. When TPR1 was inactive, binding to TPR2B was faster but to a limited capacity, while when TPR1 was active, the Ssa1-SBD bound slower to TPR2B but ultimately to a greater capacity. This is consistent with a picture in which TPR1 loads Ssa1-SBD onto TPR2B in a regulated manner (Figure 3.1).

Future work should extend the system to full-length Ssa1 and investigate potential further contributions to binding from regions outside of the EEVD motif. Such contributions may already play a role with Ssa1-SBD due to differences in the interaction with TPR1- and TPR2B-inactivated Sti1 measured by FRET versus anisotropy. In addition, extending the system for study at the single molecule level would provide definitive information on the nature of interaction with both domains. In particular, a three-colour single molecule FRET setup involving a Ssa1-EEVD donor and a pair of acceptors at TPR1 and TPR2B, would allow for the

determination of sequential binding and provide greater detail on the conformations enabling EEVD transfer. Towards this end, a procedure was developed for generating a Sti1 molecule labelled specifically at TPR1 and TPR2B with two different dye molecules (Section 2.2). The method, involving *in vitro* ligation with the SrtA enzyme, was shown to produce a ligated Sti1 molecule which could be efficiently and cleanly isolated. The method was also used to produce a Sti1 molecule fluorescently labelled at the desired positions, however a final isolation of this was hampered by impurities arising from the labelling of one of the starting fragments. Future work should involve finding a suitable labelling strategy for this fragment, or for isolating the final product.

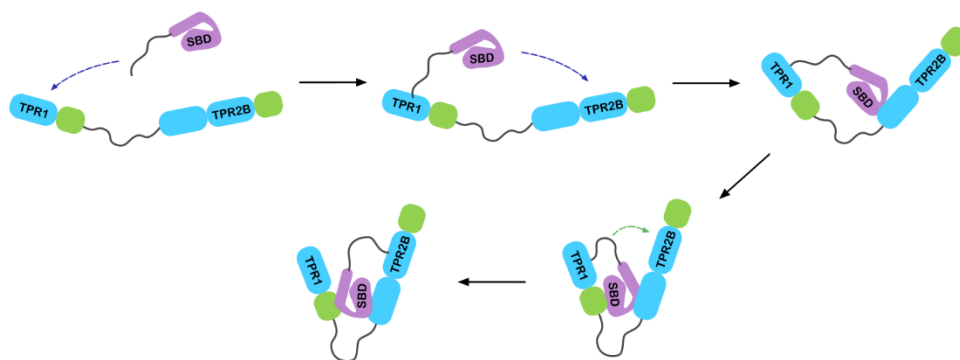


Figure 3.1 Sti1 binds Ssa1-SBD cooperatively with contributions from both modules connected by bridging conformations. Ssa1-SBD binds to both TPR1 and TPR2B of Sti1 and binding to one domain enhances binding to the other. TPR1 preferentially enhances binding to TPR2B through bridging conformations which promote EEVD transfer within the complex.

3.2 Collaboration in EEVD binding requires context within Sti1

The collaboration between TPR1 and TPR2B in binding the Ssa1-SBD was further investigated by studying whether each domain could substitute for the other within full length Sti1. These experiments highlighted the importance of context within Sti1, and revealed the need for at least one of the domains to be in its native position in order to achieve proper collaboration between them (Section 2.3.7). While replacement of TPR1 with TPR2B, or of TPR2B with TPR1 led respectively to an enhancement or defect in binding, substitution of both at once gave rise to a greater defect than when only one of them was active. This shows that the context of the domains within their native modules plays an important role in mediating the enhancement of

binding to one domain by the other. When TPR1 and TPR2B are exchanged in position, the bridging conformations that enable EEVD transfer become inaccessible. The results also show that Sti1 is more sensitive to a change in the C-terminal module, and that binding to this module may even be enhanced by a change to the N-terminal module.

3.3 New insights into the Sti1-Hsp90 interaction

Sti1 associates with Hsp82 via a primary interaction between Sti1-TPR2A and the C-terminal MEEVD motif of Hsp82, as well as a secondary interaction between surface on the Hsp82-MD and Sti1-TPR2A-TPR2B (Brinker *et al*, 2002; Schmid *et al*, 2012). Binding of Sti1 holds Hsp82 in an open conformation and engagement of the secondary interaction is necessary to inhibit its ATPase activity (Hessling *et al*, 2009; Lee *et al*, 2012). The current work demonstrated that TPR1 cannot functionally replace TPR2B in mediating Hsp82 ATPase inhibition (Section 2.3.2). This result confirms the importance of the rigid geometry that was found to exist for the native TPR2A-TPR2B segment (Schmid *et al*, 2012; Röhl *et al*, 2015). Indeed, when TPR2B is replaced by TPR1 within Sti1, it does not appear that the secondary interaction can be engaged at all, giving rise to complexes connected by the primary MEEVD - TPR2A interaction only (Section 2.3.5). Surprisingly, engagement of the secondary interaction conferred the ability to form ternary complexes with two Sti1 molecules bound per Hsp82 dimer, a point of contention within the literature. This points towards communication across the Hsp82 dimer, with engagement of the secondary interaction on one protomer inducing a conformation compatible with binding of a second Sti1 to the other. Importantly, no ternary complexes are seen connected by the MEEVD primary interaction only, showing that binding to the two tails in an Hsp82 dimer is not independent. While this may be an effect of steric hinderance, it may also be an indication of allosteric communication between the two tails across the Hsp82 dimer. Future work should incorporate other TPR co-chaperones such as Cpr6 in order to shed light on this phenomenon.

3.4 New insights into Hsp70-Sti1-Hsp90 ternary complex formation

The ability to simultaneously bind Hsp70 and Hsp90 is a central feature of Sti1. Work so far has established a picture in which ternary complexes are formed with the Hsp82-MEEVD motif bound to TPR2A and the Ssa1-EEVD bound to either TPR1 or TPR2B. Ternary complexes can be formed minimally with the TPR2A-TPR2B fragment of Sti1, while in the full-length protein, TPR1 and TPR2B contribute differently: inactivating TPR1 decreases ternary complex formation, dependent on the linker, while inactivating TPR2B enhances it (Schmid *et al*, 2012; Röhl *et al*, 2015). The current work reveals that the key determinant of ternary complex formation is the overall surface geometry of the Sti1 C-terminal module provided by a native TPR2B, which is disrupted when TPR2B is substituted for TPR1 (Section 2.3.6). This requirement correlates with the ability of Sti1 to form the secondary interaction with the Hsp82-MD, which suggests that engagement of this interaction creates a conformational environment on the C-terminal module which is necessary to receive and make key surface contacts with Ssa1. Such contacts at least partially include regions on the Ssa1-NBD, since compared with full-length Ssa1, ternary complex formation with the Ssa1-SBD was reduced in favour of binary complexes and free Ssa1-SBD (Section 2.3.7).

On the other hand, ternary complexes were not critically dependent on the N-terminal module, rather it played an auxiliary role in loading Ssa1 onto complexes formed on the C-terminal module. As was previously observed with full-length Ssa1, ternary complex formation with the Ssa1-SBD was enhanced when TPR2B was inactivated but diminished when TPR1 was inactivated (Section 2.3.7) (Schmid *et al*, 2012; Röhl *et al*, 2015). This is consistent with a picture in which binding to TPR1 on the N-terminal module is more effective in loading Ssa1 into the conformational environment of the C-terminal module, than when TPR2B must load itself. Ssa1 binding to the N-terminal module is however metastable and intimately depends on its ability to be transferred to the C-terminal module, since no ternary complexes form when the C-terminal structure is disrupted by replacement of TPR2B with TPR1. Sti1-WT consistently gave the most extended ternary complexes (Section 2.3.6 – 2.3.7) which may indicate native inter-domain communication is required to support states with Ssa1 bound to exclusively to the N-terminal module to an appreciable extent.

3.5 Sti1 contributions to GR maturation *in vivo*

The minimal unit within Sti1 necessary to support GR activation *in vivo* has previously been shown to be TPR2A-TPR2B-DP2, and deletion of TPR1 led to a level of activation identical with the wild-type (Schmid *et al*, 2012). The current work has shown that replacement of TPR1 with TPR2B led to increased *in vivo* GR activation, while replacement of TPR2B with TPR1, or substitution of both domains at once, supported reduced but still substantial activation levels (Section 2.3.2). The results with Sti1 in which TPR2B was replaced by TPR1 are surprising since the rigid orientation of TPR2A-TPR2B-DP2 is thought to be important for client activation (Schmid *et al*, 2012; Röhl *et al*, 2015). Furthermore these constructs were unable to form ternary complexes with Ssa1 and Hsp82, or quaternary complexes additionally with the GR-LBD under minimal *in vitro* conditions (Sections 2.3.6 – 7, Section 2.4.2). It may therefore be that additional factors within the cell are able to overcome the structural deficiency with these Sti1 variants. For example GR activity in yeast was recently shown to depend upon the co-chaperones Cpr6 and Sgt1, both of which additionally formed complexes with Hsp90-GR-LBD *in vitro* (Sahasrabudhe *et al*, 2017). It could therefore be that such factors impose conformational stability on Hsp82, analogous to the missing Hsp82-MD - TPR2A-TPR2B interaction, sufficient to allow client transient complex formation and client transfer (Figure 3.2).

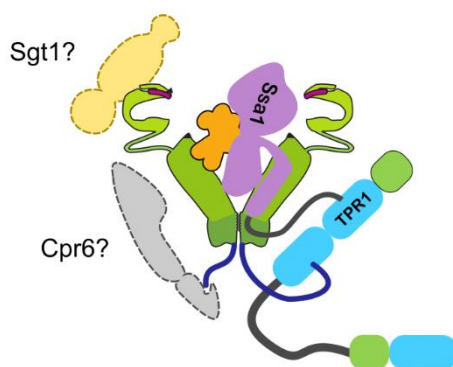


Figure 3.2 Additional factors may compensate for Sti1 structural deficiency. Sti1 in which TPR2B is replaced with TPR1 cannot assemble ternary or quaternary complexes *in vitro* yet supports GR activation *in vivo*. It may be that other co-chaperones involved in GR activation provide the conformational basis to allow transfer complexes to transiently form.

In the presence of ATP and the co-chaperone Ydj1, a previously unidentified large oligomeric complex is formed with GR-LBD and Ssa1, indicating a novel role for oligomerisation in the chaperoning of GR (Section 2.4.1). While Hsp82 formed a binary complex with GR-LBD in the presence of this oligomeric complex, Sti1 displaced GR-LBD from both the oligomeric complex and the binary complex with Hsp82. The domain-swapped Sti1 constructs had divergent effects in this setting, giving rise to distinct oligomeric complexes of both higher and lower molecular weight. Future work should be undertaken to investigate the role of oligomerisation in GR chaperoning, in addition to looking at additional factors such as the co-chaperones Cpr6 and p23/ Sba1, which may be able to bridge the initial oligomeric Ssa1-bound state and the final Hsp82-bound state. Such factors may also interact with the unique oligomeric complexes formed with domain-swapped Sti1 constructs in which TPR2B is replaced by TPR1, providing a basis for the observed GR activity with these constructs.

3.6 Sti1 inter-domain communication in GR-LBD quaternary complex formation

Previously immunoprecipitation was used to show that GR could be stably isolated in complexes that minimally contained Hsp70, Hsp90 and Hop (Dittmar *et al*, 1997; Dittmar & Pratt, 1997). More recently Hsp70: Hsp90: Hop: GR-LBD complexes were able to be isolated for EM analysis with the use of stabilising crosslinkers (Kirschke *et al*, 2014; Alvira *et al*, 2014). The current work demonstrated that a complex composed of yeast Hsp82, Ssa1, Sti1 and GR-LBD could assemble freely in solution, and revealed details of the contributions of Sti1 TPR domains to this process (Section 2.4.2). As was the case for ternary complexes, quaternary complexes with GR-LBD could not be formed when TPR2B was substituted with TPR1, but could readily be formed when TPR1 was substituted with TPR2B. This further highlights the importance of an intact surface geometry on the C-terminal module, with a subordinate role played by the N-terminal module. However unlike for ternary complexes, quaternary complex formation was critically dependent on the peptide binding groove activity the N-terminal module, demonstrating a role for this module in the assembly process. The results suggest a mechanism in which a preliminary interaction with the N-terminal module and subsequent Ssa1-EEVD transfer to the C-terminal module are necessary to attain a complex with the correct conformation for binding GR-LBD (Figure 3.3). Such a scheme is compatible with the observed

behaviour of TPR1 in loading the EEVD onto TPR2B in FRET experiments. The complex is expected to form under these minimal conditions due to the fact that Hsp82 can be induced into a partially closed state, as seen in a previous EM reconstruction (Alvira *et al*, 2014). This particular effect could be tested in future work using a previously established fret system for hsp82 closure (Hessling *et al*, 2009). Furthermore, studying the interaction of Ssa1 with TPR1 and TPR2B using three colour single molecule FRET, in the presence of Hsp82 and GR-LBD, would provide a fuller understanding of how the domains collaborate in the assembly process.

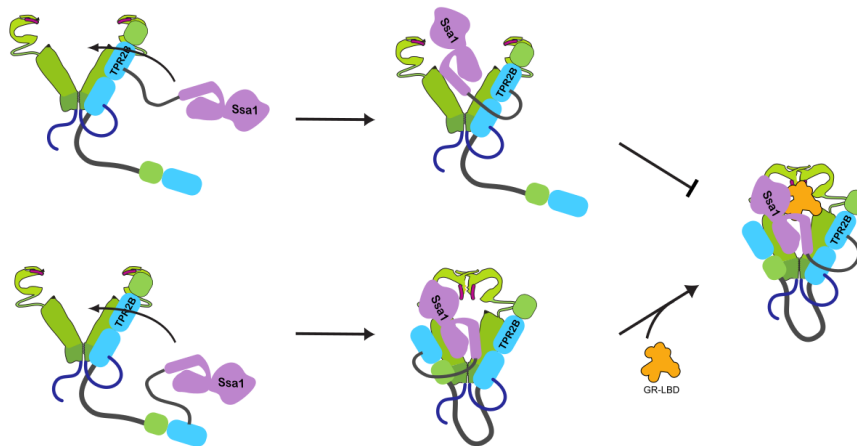


Figure 3.3 The N-terminal module affects C-terminal module conformation via EEVD transfer. Quaternary complexes with GR-LBD are formed on the C-terminal module, however assembly requires preliminary interaction of Ssa1 with the N-terminal module and the ability for the Ssa1-EEVD to transition between modules.

In summary this work has revealed new insights into the collaboration between Sti1 modules in Ssa1-EEVD binding, demonstrating a function for TPR1 to load TPR2B through bridging conformations which enable EEVD transfer. It has identified a critical importance on the geometry of the C-terminal module, necessary to enable Hsp82 to bind two Sti1 molecules as well as to form Hsp82: Ssa1: Sti1 ternary complexes. The N-terminal module has a role in loading Ssa1 into complexes on the C-terminal module, but cannot support independent binding of Ssa1 if the correct C-terminal environment is not established. This function of the N-terminal module turned out to be critical in forming quaternary complexes with GR-LBD under minimal conditions, revealing the importance of conformations involving communication between modules in assembling the client transfer complex. This dependence however appears to be

superseded in GR activation *in vivo*, where TPR1 is dispensable, and other co-chaperones may instead provide the necessary conformational environment to assemble transfer complexes. This may additionally be the case for Sti1 in which the structure of the C-terminal module is disrupted, which also supported *in vivo* GR activation. The underlying functional interplay between the C- and N-terminal modules demonstrated in this work may therefore represent an optimal functioning of the system, one which could become critically important in stress situations. Under such conditions chaperone and co-chaperone capacities are stretched and maximal folding efficiency is required. However the dependence of the C-terminal module on loading by the N-terminal module likely also plays a role in normal cellular functioning, where Hsp90 acts as a central protein folding hub, dynamically forming multiple complexes to process many clients at once. A preliminary interaction with the N-terminal module would provide useful temporary storage for an incoming client while the outgoing client is processed on the C-terminal module, particularly since different clients are likely to have different processing times.

Finally Hsp70 and Hsp90 represent major targets in cancer, and there is an increasing focus on their interactions and co-chaperones (Edkins, 2016). In particular, molecules which disrupt the interaction between Hsp90 and Hop have been demonstrated to have anti-cancer effects (Wang *et al*, 2016; Pimienta *et al*, 2011). In view of the current work, designing molecules to target Sti1 inter-module communication, the interaction of Hsp70 with TPR1, or the network of contacts formed on the C-terminal module could provide potentially fruitful new approaches. Indeed there is increasing interest in designing molecules that allosterically modulate Hsp70, Hsp90 and their complexes, allowing for fine-tuning rather than complete inhibition in therapeutic settings (Ferraro *et al*, 2019).

Materials and Methods

4.1 Materials and equipment

Chemical	Origin
Acrylamide (38 %, 2% Bisacrylamide)	Roth (Karlsruhe, Germany)
Agar, powder	Serva (Heidelberg, Germany)
Amino acids	Sigma-Aldrich (St. Louis, USA)
Ammoniumperoxodisulfate (APS)	Roche (Mannheim, Germany)
Ampicillin	Roth (Karlsruhe, Germany)
Adenosyl-imidodiphosphate (AMP-PNP)	Roche (Mannheim, Germany)
Adenosine-5'-diphosphate (ADP) disodium salt	Roche (Mannheim, Germany)
Adenosine-5'-triphosphate (ATP) disodium salt	Roche (Mannheim, Germany)
Bacto Agar	Difco (Detroit, USA)
Bacto Tryptone	Difco (Detroit, USA)
Bacto Yeast Extract	Difco (Detroit, USA)
Bromphenolblue S	Serva (Heidelberg, Germany)
Coomassie Brilliant-Blue R-250	Serva (Heidelberg, Germany)
Desoxynucleotide triphosphates (dNTPs)	Roche (Mannheim, Germany)
DNA stain G Serva	(Heidelberg, Germany)
1,4-Dithiothreitol (DTT)	Roth (Karlsruhe, Germany)
Ethylendiamintetraacidic acid (EDTA)	Merck (Darmstadt, Germany)
D(+)-Glucose	Merck (Darmstadt, Germany)
Glycerol 99% ICN	Merck (Darmstadt, Germany)
4-(2-hydroxyethyl)-1-piperazineethanesulfonic acid (HEPES)	Roth (Karlsruhe, Germany)
Imidazole	Sigma-Aldrich (St. Louis, USA)
Isopropanol	Roth (Karlsruhe, Germany)
Isopropyl- β -D-thiogalactopyranoside (IPTG)	Serva (Heidelberg, Germany)
Kanamycin	Roth (Karlsruhe, Germany)
LB Medium, Powder	Serva (Heidelberg, Germany)
Lithium Acetate	Roth (Karlsruhe, Germany)
2-Mercaptoethanol	Roth (Karlsruhe, Germany)

<i>o</i> -Nitrophenyl- β -D-galactopyranoside (ONPG)	Sigma-Aldrich (St. Louis, USA)
NADH	Roche (Mannheim, Germany)
Phosphoenol pyruvate	Roche (Mannheim, Germany)
Protease Inhibitor Mix HP	Serva (Heidelberg, Germany)
Radicicol	Sigma-Aldrich (St. Louis, USA)
Salmon Sperm DNA	Sigma-Aldrich (St. Louis, USA)
SERVA Blue R	Serva (Heidelberg, Germany)
Sodiumdodecylsulphate (SDS)	Roth (Karlsruhe, Germany)
N,N,N',N'-Tetramethylethylenediamin (TEMED)	Roth (Karlsruhe, Germany)
Tris-(Hydroxymethyl)-aminomethan (Tris)	Roth (Karlsruhe, Germany)
Tween 20	Merck (Darmstadt, Germany)
Yeast Extract SERVABACTER®, powder	Serva (Heidelberg, Germany)
Yeast Nitrogen Base (YNB)	Difco (Detroit, USA)
YPD medium, powder	Roth (Karlsruhe, Germany)

Kits and Markers

Origin

Serva DNA Stain G	Serva (Heidelberg, Germany)
PeqGold 1 kb DNA ladder	PeqLab (Erlangen, Germany)
Wizard® Plus SV Mini-Preps DNA Purification Kit	Promega (Madison, USA)
Wizard® SV Gel and PCR Clean-Up System	Promega (Madison, USA)
Low-range-molecular weight marker	Biorad (Munich, Germany)

Enzymes

Origin

All restriction enzymes	New England Biolabs (Ipswich, USA)
Pfu Polymerase	Promega (Madison, USA)
GoTaq polymerase	Promega (Madison, USA)
Phusion polymerase	New England Biolabs (Ipswich, USA)
Q5 polymerase	New England Biolabs (Ipswich, USA)
T4 DNA polymerase	New England Biolabs (Ipswich, USA)
T4 DNA ligase	New England Biolabs (Ipswich, USA)
DNase I	Roche (Mannheim, Germany)
Pyruvate Kinase (PK)	Roche (Mannheim, Germany)
L-Lactate dehydrogenase (LDH)	Roche (Mannheim, Germany)

Equipment	Origin
BP 121 S Analytical balance	Sartorius (Göttingen, Germany)
BL310 Analytical balance	Sartorius (Göttingen, Germany)
Hoefer Mighty Small II electrophoresis unit	GE Healthcare (Freiburg, Germany)
LKB-GPS 200/400 Power amplifier	GE Healthcare (Freiburg, Germany)
Pharmacia EPS 3500, 301, 1001 Power amplifier	GE Healthcare (Freiburg, Germany)
Centrifuges	
Avanti J25 (JA-10 and JA-25.50 rotor)	Beckman (Fullerton, USA)
Eppendorf Centrifuge 5418 R	Eppendorf (Hamburg, Germany)
Beckman ProteomeLab XL-A (TI-50 rotor)	Beckman (Fullerton, USA)
Chromatographic devices	
ÄKTA FPLC	GE Healthcare (Freiburg, Germany)
Jasco HPLC system	Shimadzu (Munich, Germany)
Chromatographic material	
HisTrap (FF or HP) Ni-NTA 5 ml	GE Healthcare (Freiburg, Germany)
Ressource Q	GE Healthcare (Freiburg, Germany)
Hydroxyapatite	Biorad (Munich, Germany)
Superdex 75 prep grade (16/60) and (26/60)	GE Healthcare (Freiburg, Germany)
Superdex 200 prep grade (16/60), (10/300) and (26/60)	GE Healthcare (Freiburg, Germany)
HiPrep 26/10 Desalting column	GE Healthcare (Freiburg, Germany)
Zeba spin desalting columns	Thermo Fisher (Waltham, USA)
PD10 desalting column	GE Healthcare (Freiburg, Germany)
Histrap spin columns	GE Healthcare (Freiburg, Germany)
Fluorescent Dyes	
ATTO 488 NHS ester	AttoTec (Siegen, Germany)
ATTO 488 maleimide	AttoTec (Siegen, Germany)
ATTO 550 maleimide	AttoTec (Siegen, Germany)
ATTO 647 maleimide	AttoTec (Siegen, Germany)
Cy3b maleimide	GE Healthcare (Freiburg, Germany)
5-Carboxyfluorescein (FAM) NHS	Invitrogen (La Jolla, USA)

Spectroscopic devices	Origin
Chirascan CD spectrometer	Applied Photophysics (Surrey, UK)
Varian Cary 50/100 Bio UV-Vis Spectrophotometer	Varian (Palo Alto, USA)
Fluoromax 3 spectrofluorimeter	Jobin Yvon Horiba (Edison, USA)
Fluorescence detection system (AUC)	Aviv Biomedical (Lakewood, USA)
TECAN Sunrise plate reader	Tecan (Männedorf, Switzerland)
Typhoon 9200 Variable Mode Imager	Amersham (Uppsala, Sweden)
Jasco FP-8500 spectrofluorimeter	Jasco, Groß-Umstadt, Germany
Additional equipment	Origin
Quartz Cuvettes	Hellma (Müllheim, Germany)
T100 Thermocycler	Biorad (Munich, Germany)
Incubator	Haake (Karlsruhe, Germany)
WTW pH Meter	WTW (Weilheim, Germany)
Eppendorf Thermomixer	Eppendorf (Hamburg, Germany)
Cell disruption machine Basic Z model	Constant Systems (Warwick, England)
Mixer Mill MM 400	Retsch (Haan, Germany)
Amicon stirred cells	Merck (Darmstadt, Germany)
Amicon Centrifugal Filter Units	Merck (Darmstadt, Germany)
Cellulose acetate filters, 0.45 µm	Sartorius (Göttingen, Germany)
Ultrafiltration Discs	Merck (Darmstadt, Germany)
Software & Web-based tools	Source
PrimerX	Lapid, C (bioinformatics.org/primerx)
Serial cloner	serialbasics.free.fr/Serial_Cloner
Clustal W sequence alignment	(Thompson et al., 1994)
Origin	OriginLab (Northhampton, USA)
ProtParam Tool	(Gasteiger et al., 2005)
Pymol	Schrödinger LLC (New York, USA)
SedView	(Hayes and Stafford, 2010)
Sedfit	(Schuck, 2000)
NEBuilder/ NEB tm calculator	nebuilder.neb.com
RF-Cloning design tool	RF-Cloning.org
UCSF Chimera	cgl.ucsf.edu/chimera/
MODELLER	(Sali & Blundell, 1993)

4.2 Primers

Primer	Sequence
Sti1_G88C_f	CGGTGCCGCCCACTTAGGTCTTTGCGATCTCGA
Sti1_G88C_r	TGCTTTCAGCTTCGTCGAGATCGCAAAGACCTAAG
Sti1_K478C_f	GGCCACCGCACAAATTGCTGTTTGCGAATATGCTTC
Sti1_K478C_r	ATCTAGTGTTTCCAAAGCGGAAGCATATTCGCAAACAGCAATTTGT
N435A fwd	GATGCTAGAGGATATTCTGCGAGAGCTGCTGCACTAGCG
N435A rev	CGCTAGTGCAGCAGCTCTCGCAGAATATCCTCTAGCATC
N39A fwd	GAAGTTTCTGAAACTCCAGCGCATGTTTTATATTCTAAC
N39A rev	GTTAGAATATAAAACATGCGCTGGAGTTTCAGAAACTTC
T1D1T2A_f	tcacagagaacagattggtgatccATGTCATTGACAGCCGATG
T1D1T2A_r	attcatcggcAGGGTTAACATACGCCTC
T1_f	tgtaaccctGCCGATGAATACAAACAAC
T1_r	tggtaccaggAACCTGATCCAATCCTTC
D2_f	ggatcaggttCCTGGTACCAGTAACGAAACC
D2_r	agtgggtggtggtggtgctcgagTTAGCGGCCAGTCCGGAT
4T1-D1-Link_r	cttctccgcCTCAATTTTAGAGTCATCTTCATC
4T2B_f	taaaattgagGCGGAGGAAGCCCGTCTT
4T2B_r	taacatacgcTTGGAATCTTTGTTGGCTTGCC
4ABlink-T2B-D2_f	aagattccaaGCGTATGTTAACCTGAAAAGGC
4ABlink-T2B-D2_r	agtgggtggtggtggtgctcgagTTAGCGGCCAGTCCGGAT
ds_p425_f	cggattctagaactagtgatccATGTCATTGACAGCCGATGAATAC
ds_p425_r	acataactaattacatgactcgagTTAGCGGCCAGTCCGGAT
pS_Hsp82_f	cagagaacagattggtgatccATGGCTAGTGAAACTTTTGAATTC
pS_Hsp82_r	cagtgggtggtggtggtgctcgagCTAATCTACCTCTTCCATTTCCG
StiSort_N_f	accgcaacagattggaggtATGTCATTGACAGCCGATG
StiSort_N_r	ctcgaattcggatcctctagtcgagttagtggtggtggtggtgctcgaggccggttccggcagCT TTGGCATGGAGTTTGATTG
StiSort_C_f	accgcaacagattggaggtggcAAAAGCACTGAACAAAAGAAAGATGC
StiSort_C_r	ctcgaattcggatcctctagTTAGCGGCCAGTCCGGAT

4.3 Plasmids

Plasmid	Cloning Site	Origin
pETSUMO-Sti1 C49S C66S C453S	BamHI/XhoI	Alina Röhl
pETSUMO-Sti1 C49S C66S C453S G88C	BamHI/XhoI	This work
pETSUMO-Sti1 C49S C66S C453S K478C	BamHI/XhoI	This work
pETSUMO-Sti1 C49S C66S C453S G88C N435A	BamHI/XhoI	This work
pETSUMO-Sti1 C49S C66S C453S N39A K478C	BamHI/XhoI	This work
pETSUMO-Sti1	BamHI/XhoI	Andreas Schmid
pETSUMO-Sti1 N39A	BamHI/XhoI	This work
pETSUMO-Sti1 N435A	BamHI/XhoI	This work
pETSUMO-DS1-T2B	BamHI/XhoI	This work
pETSUMO-DS1-D1T2AT2BD2	BamHI/XhoI	This work
pETSUMO-DS2-T1D1T2A	BamHI/XhoI	This work
pETSUMO-DS2-TPR1	BamHI/XhoI	This work
pETSUMO-DS2-D2	BamHI/XhoI	This work
pETSUMO-DS3-T2B	BamHI/XhoI	This work
pETSUMO-DS3-D1T2AT2BD2	BamHI/XhoI	This work
pETSUMO-Sti1-DS1	BamHI/XhoI	This work
pETSUMO-Sti1-DS2	BamHI/XhoI	This work
pETSUMO-Sti1-DS3	BamHI/XhoI	This work
p425-GPD-Sti1-WT	BamHI/XhoI	This work
p425-GPD-Sti1-DS1	BamHI/XhoI	This work
p425-GPD-Sti1-DS2	BamHI/XhoI	This work
p425-GPD-Sti1-DS3	BamHI/XhoI	This work
pSUMO-Sti1-SrtN		This work
pSUMO-Sti1-SrtC		This work
p413-GPD-hGR		Andreas Schmid
pUC Δ ss26x		JF Louivion
pETSUMO-Ydj1	BamHI/XhoI	Daniel Rutz
pICZA-6xHis-Ssa1	NheI/XhoI	Andreas Schmid
pET28-yHsp82	NdeI/XhoI	Klaus Richter
pETSUMO-yHsp82	BamHI/XhoI	This work
pET28-SUMO Protease		Oliver Lorenz
pETSUMO-Ssa1-SBD (aa392-642) E632C	BamHI/XhoI	Alina Röhl
pET28-SrtA		Abraham Lopez

4.4 Molecular biology

4.4.1 Primer design

Depending on the particular cloning method, a variety of different cloning tools were used. PrimerX was used for the general design and characterisation of mutagenic primers. The Agilent Stratagene quikchange tool was used to design primers for Quikchange mutagenesis. Primers for use with the restriction-free cloning method were designed using the RF cloning tool (rf-cloning.org). For SLIC cloning, either the NEBuilder assembly tool was used or a combination of NEB Tm calculator and the Serial Cloner program.

4.4.2 General PCR

For standard PCR the Phusion polymerase was used according to the manufacturer's instructions.

PCR Components		Primary PCR Conditions			
5x phusion Buffer	10 μ l	Denature	98°C	30 sec	1X
10 mM dNTP mix	1 μ l	Denature	98°C	8 sec	
10 μ M Fwd Primer	2.5 μ l	Anneal	55°C	20 sec	35 X
10 μ M Rev Primer	2.5 μ l	Extension	72°C	20 sec/kb	
Template DNA 100 ng	1 μ l	Extension	72°C	5 min	1 X
Phusion	0.5 μ l	Hold	4°C		
H ₂ O	To 50 μ l				

4.4.3 Restriction digestion and ligation

For standard cloning purposes (preparing the ends of PCR products, linearising vectors and isolating constructs for sub-cloning) target DNA was digested with the required restriction enzymes and accompanying buffers, according to the manufacturer's protocol. Generally, 1 μ g of DNA was digested with 0.5 μ l restriction enzyme (20 U/ μ l) at 37°C for 1 h. Cut plasmids were separated with preparative agarose gel electrophoresis before purification with Wizard® SV clean up kits while PCR product digestions were purified directly.

Ligations were performed using T4 DNA ligase with the appropriate buffer following the manufacturer's protocol. Generally, vector and insert were incubated in a 1: 3 molar ratio with 1 μ l T4 ligase in a total volume of 20 μ l for 20 min at room temperature.

4.4.4 Agarose gel electrophoresis

DNA separation was performed using 1 % (w/v) agarose gels cast with DNA stain G (2µl in 100 ml liquid agarose) in TAE buffer. Electrophoresis was carried out at a constant voltage of 120 V for 20 – 30 min. Bands were excised and purified with Wizard® SV clean up kits.

4.4.5 Site-directed mutagenesis

Site directed mutagenesis was used to introduce single point mutations based on the design of a reverse-complementary pair of primers containing a single codon mismatch. PCR primers were designed using the online Stratagene Quikchange mutagenesis tool and PCR was carried out with the pfu polymerase according to the manufacturer's protocol. This method generates a nicked, complementary synthetic plasmid containing a single mismatched codon. Following PCR, the mixture was incubated with 1 µl DpnI, which specifically degrades the methylated template DNA, before being directly transformed into Mach1 or XL1-Blue competent cells.

4.4.6 Restriction-free cloning

Restriction-free (RF) cloning ligation is variant of the many ligation-independent, PCR-based methods for creating user designed plasmids (van den Ent & Löwe, 2006). It allows for the insertion of any sequence into any region of a plasmid, independent of endogenous restriction or recombination sites. Briefly, a hybrid primer pair is designed which contains sequence complementary to a desired insert, the target plasmid, and optional spacers containing novel sequence. In a first round of PCR, the insert is amplified to create a megaprimer which is then used in a second round with the target plasmid serving as the template. The plasmid is amplified bidirectionally to generate a nicked hybrid product which, following DpnI digestion of the methylated parental template, can then be transformed into competent bacterial strains by normal methods.

In this work RF cloning was used as an alternative to Quikchange to introduce Sti1 G88C and K478C point mutations. Owing to the fact that the insert was completely synthesised by the primers, a shortened PCR method was used.

PCR Components		Primary PCR Conditions			
5x phusion Buffer	4µl	Denature	98°C	30 sec	1X
10 mM dNTP mix	0.4µl	Denature	98°C	8 sec	
5 ng Fwd Primer	x µl	Anneal	55°C	20 sec	5X
5 ng Rev Primer	x µl	Extension	72°	5 sec	
Phusion	0.2 µl	Hold	4°C		
H ₂ O	To 20µl				

Then 100 ng of the template plasmid was added and the following secondary program was run:

Secondary PCR Conditions			
Denature	98°C	30sec	1X
Denature	98°C	8sec	15X
Extension	72°	30sec/kb	
Final Extension	72°C	5min	1X

The reaction was then incubated with 1 µl DpnI for 2 h before transformation into *E. coli* (Mach1 or XL1-Blue).

4.4.7 SLIC cloning

Sequence- and ligation independent cloning (SLIC) is a simple ligation-independent cloning method that was used to create the Stt1 domain-swapped constructs and Stt1 sortase constructs (Jeong *et al*, 2012). A target plasmid is linearised by restriction digest, followed by the insertion of any sequence, or even multiple consecutive sequence fragments simultaneously by homologous recombination. Fragments are synthesised by PCR with primers designed to generate 5' and 3' custom overlaps homologous to the target plasmid, or to preceding or succeeding insert fragments in a multi-component assembly. Upon short incubation with T4 DNA polymerase in the absence of nucleotides, 3' - 5' exonuclease activity generates overhangs which may then anneal to form the entire nicked assembly. The overlapping region should generally be around 18 nt (increased for multi-component assemblies) and may include optional spacer sequence. PCR is carried out with Q5 polymerase according to the manufacturer's protocol, with Tms calculated with NEB Tm calculator. Generally, a 2x molar excess of insert over vector is sufficient for assemblies with a single insert. However a number of insert ratios may need to be tested for assemblies using multiple inserts. The whole reaction may be scaled up as necessary.

PCR Components

Linearised vector	100 ng
Insert 1	x μ l
⋮	⋮
Insert n	x μ l
NEB Buffer 2	1 μ l
10x BSA (NEB)	1 μ l
T4 DNApol (NEB)	0.4 μ l
H ₂ O	To 10 μ l

The above mixture is assembled on ice excluding the polymerase. The polymerase is then added and the reaction is allowed to stand on the bench for 2.5 min. The reaction is then put back on ice for 10 min before being directly transformed into *E. coli* Mach1 or XL1-Blue.

4.4.8 *E. coli* culture media
LB Medium

LB powder	20 g/l
Plates: add agar	15 g/ litre medium
Optional antibiotics:	
Ampicillin	100 μ g/ ml
Kanamycin	50 μ g/ ml

4.4.9 *S. cerevisiae* culture media
YPD Medium

YPD powder	50 g/l
Plates: add agar	20 g/ litre medium

CSM Medium

YNB	6.7 g/l
Glucose	20 g/l
1 M NaOH	1 ml
Selective amino acid mix	1 g
Plates: add agar	20 g/l

Selective amino acid mix

Adenine	0.5 g	Methionine	2.0 g
Arginine	2.0 g	Phenylalanine	2.0 g
Aspartic acid	2.0 g	Threonine	2.0 g
Histidine	2.0 g	Tryptophan	2.0 g
Leucine	10 g	Tyrosine	2.0 g
Lysine	2.0 g	Uracil	2.0 g

The amino acid mix must be homogenised in a mixer mill. Depending on the desired auxotrophic selection, certain components are omitted from the mix before addition to CSM media. In this work two types of CSM media were prepared, one lacking uracil and histidine, and the other lacking uracil, histidine and leucine.

4.4.10 *P. pastoris* culture media**MD Medium**

YNB	13.4 g/l
Sorbitol	20 g/l

4.4.11 Cultivation of *E. coli* strains

Strain	Genotype	Origin
<i>E. coli</i> One-Shot Mach1 (cloning)	F- Φ 80 <i>lacZ</i> Δ M15 Δ <i>lacX74</i> <i>hsdR</i> (rK-mK+) Δ <i>recA1398</i> <i>endA1 tonA</i>	Invitrogen (Gronigen, Netherlands)
<i>E. coli</i> XL1-Blue (cloning)	<i>recA1 endA1 gyrA96 thi-1</i> <i>hsdR17 supE44 relA1 lac</i> [F' <i>proAB lacI^qZ</i> Δ M15 Tn10 (Tet ^r)]	Stratagene (La Jolla, USA)
<i>E. coli</i> BL21-CodonPlus (DE3)-RIL (protein expression)	F- <i>ompT hsdS</i> (r _B ⁻ m _B ⁻) <i>dcm</i> ⁺ Tet ^r <i>gal</i> λ (DE3) <i>endA Hte</i> [<i>argU ileY leuW Cam^r</i>]	Stratagene (La Jolla, USA)

E. coli strains were streaked on LB-agar plates containing appropriate antibiotics (generally Ampicillin at 100 μ g/ml or Kanamycin at 50 μ g/ml) and incubated 37°C to achieve single colonies. Individual colonies were picked and grown in liquid LB at 37°C overnight. Liquid cultures up to 10 ml were incubated in a test tube roller while larger cultures were incubated in

flasks with shaking. Cell growth was monitored by measuring absorption at 600 nm (OD_{600}) with a UV-vis spectrophotometer (an OD_{600} of 1 equates to around 8×10^8 cells/ml). For long term storage, 500 μ l of bacterial culture was mixed with 500 μ l sterile 50 % glycerol before snap freezing and storage at -80°C .

4.4.12 Transformation of chemically competent *E. coli* strains

Chemical transformation is a method for introducing DNA to *E. coli* cells involving treatment with Ca^{2+} ions followed by a brief exposure to an elevated temperature. In this work, transformations were carried out with fresh aliquots of chemically competent cells available within the laboratory, prepared according to standard methods (Sambrook *et al*, 1989). 1-20 μ l plasmid DNA was mixed with 200 μ l and incubated for 15 min on ice. Cells were then exposed to a 42°C heat shock for 1 min followed by a further 2 min on ice. 1 ml of LB medium was added and the cells were shaken for 45 min - 1 hr at 37°C . The cells were sedimented, and the supernatant discarded, before resuspension of the pellet in around 50 μ l medium. The resuspended pellet was spread on prewarmed agar plates containing the appropriate antibiotics, and incubated at 37°C overnight.

4.4.13 Cultivation of yeast strains

Strain	Genotype	Origin
<i>S. cerevisiae</i> Y00000 (wild-type)	BY4741; MATa; his3 Δ 1; leu2 Δ 0; met15 Δ 0; ura3 Δ 0	Euroscarf (Frankfurt, Germany)
<i>S. cerevisiae</i> Y01803 (sti1 Δ)	BY4741; Mat a; his3 Δ 1; leu2 Δ 0; met15 Δ 0; ura3 Δ 0; YOR027w::kanMX4	Euroscarf (Frankfurt, Germany)
<i>P. pastoris</i> KM71H	aox1::ARG4; arg4	Invitrogen (Groningen, Netherlands)

Cultures of *S. cerevisiae* or *P. pastoris* were respectively streaked out onto CSM or YPD plates and incubated for two to three days at 30°C . Cell growth was monitored by measuring OD_{600} ($OD_{600} = 1$ equates to $\sim 2 \times 10^7$ *S. cerevisiae* cells or $\sim 5 \times 10^7$ *P. pastoris* cells). For long term storage, 700 μ l of bacterial culture was mixed with 300 μ l sterile 50 % glycerol before snap freezing and storage at -80°C .

4.4.14 Transformation of *S. cerevisiae* strains

Yeast cultures (5ml) were grown overnight at 30°C. The following day 1 ml of the culture was collected and briefly centrifuged to collect a pellet and the supernatant was discarded. The pellet was resuspended in 50 – 100 µl medium before adding 2 µl of 10 mg/ ml salmon sperm carrier DNA. 1 µg plasmid DNA was added before brief vortexing and addition of 0.5 ml PLATE mix. After vortexing again, 20 µl 1 M sterile DTT was added followed by vortexing. Cells were incubated for 6 – 8 hours or overnight on the benchtop without mixing, before being subjected to heat shock at 42°C for 30 min. Finally 50 – 100 µl is withdrawn from the bottom of the tube and plated onto appropriate CSM plates.

PLATE Mix

Sterile 45% PEG 4000	90 ml
1 M Li Oac	10 ml
1 M Tris-Cl (pH 7.5)	1 ml
0.5 M EDTA	0.2 ml

4.5 Protein expression and purification

4.5.1 Purification buffers

Ni-NTA buffers standard

Sodium phosphate, pH 7.5	50 mM
NaCl	300 mM
DTT	1 mM
Imidazole	A: - B: 300 mM

Ni-NTA buffers (Ydj1)

Sodium phosphate, pH 7.2	40 mM
NaCl	500 mM
β-Mercaptoethanol	2 mM
Glycerol	10 % (v/v)
Imidazole	A: 20 mM B: 300 mM

**Ni-NTA buffers
(His₆-Ssa1)**

HEPES, pH 7.5	40 mM
NaCl	350 mM
KCl	150 mM
MgCl ₂	20 mM
Glycerol	5 % (v/v)
B-mercaptoethanol	2 mM
ATP	1 mM
Imidazole	A: 10 mM B: 300 mM

Ni-NTA buffers (SrtA)

Tris, pH 8.0	50 mM
NaCl	150 mM
Glycerol	10 % (v/v)
Imidazole	A: - B: 300 mM

ResQ buffers

Sodium phosphate, pH 7.5	50 mM
NaCl	300 mM
EDTA	1 mM
KCl	A: 20 mM B: 1 M

HAT Buffers (His₆-Ssa1)

Potassium phosphate, pH 7.0	A: 10 mM B: 300 mM
-----------------------------	-----------------------

SEC Buffer

HEPES, pH 7.5	40 mM
KCl	150 mM
MgCl ₂	5 mM

4.5.2 Protein expression

Standard protein expression was carried out in *E. coli* BL21 DE3 cod+ cells. 50 ml LB pre-cultures containing appropriate antibiotics were inoculated with single colonies and incubated overnight at 37°C. Pre-cultures were each used to inoculate 4 -8 l of LB medium (50 ml per 2 l in 5 l flasks). Cells were grown to an OD600 of 0.6 – 0.8 before induction with 1 mM IPTG. Induction took place for 4h at 37°C (Hsp82) or 30°C overnight (all other proteins except Ydj1) and cells were harvested at 7000 rpm for 10 min at 8°C using a Beckman Avanti J25, JA10 rotor. Pellets were either immediately processed further or snap-frozen and stored at -80°C.

For Ydj1, cells were instead grown to an OD600 of 0.2 – 0.5 at 37°C before switching to 30°C and then grown further to OD600= 0.8. Expression was induced with 0.5 mM IPTG and took place for 4 h at 30°C.

Expression of Ssa1 was carried out in *P. pastoris* strain KM71H. 3x 50 ml YPD pre-cultures were inoculated with single colonies and incubated overnight at 30°C. Each pre-culture was used to inoculate 2 l of MD medium in 5 l baffled flasks (total 6 l) which were incubated for 24h at 30°C. Expression was induced by addition of 0.5 % methanol (v/v) and incubation for 24h at 29°C. After this period, a further of 0.5 % methanol (v/v) was added and cells were incubated for a further 24 h at 29°C. After this cells were harvested at 7000 rpm for 10 min at 8°C using a Beckman Avanti J25, JA10 rotor. Pellets were either immediately processed further or snap-frozen and stored at -80°C.

Note that protein expression in *P. pastoris* depends on the cell's ability to oxidise methanol, and that ideal expression is heavily dependent on proper aeration of the culture. Therefore it is recommended to use of baffled flasks, capped with sterile gauze cloth instead of aluminium and higher shaker speeds (200 rpm). In addition, protein expression is compromised at temperatures above 30°C and therefore a temperature of 29°C is recommended.

4.5.3 Cell disruption

Cell pellets were thoroughly resuspended in 70 – 100 ml of the first purification buffer, to which one aliquot of SERVA Protease Inhibitor Mix-HP and a pipette tip's-worth of DNase I powder were added. Resuspended cells were loaded into a Basic Z model cell disruptor and disrupted at 1.8 kbar (*E. coli*) or 2.6 kbar (*P. pastoris*) before centrifugation at 18,000 rpm for 45 min at 8°C (Beckman Avanti J25, JA-25.50 rotor). The cleared lysate was retained and insoluble pellet discarded.

4.5.4 Protein purification

Sti1WT and all its variants along with Ssa1-SBD and Ydj1 were expressed in the pETSUMO vector and were purified according to an identical protocol. In a first nickel affinity step, lysate was loaded onto HisTrap column (FF or HP) pre-equilibrated in NI-NTA buffer A at a flow rate of 3 ml/ min. The bound column was washed at 4 ml/ min with around 100 ml buffer A followed by 6% buffer B until baseline (generally ~100 ml), before protein was eluted with a step-increase to 100 % B. To the eluate, 200 µl 1 mg/ml sumo protease was added and was either incubated either for 1 hr at 4°C before exchange back into buffer A with a HiPrep 26/10 desalting column, or diluted 1:2 in buffer A and dialysed against 5 l buffer A overnight. To remove the cleaved His-SUMO tag, buffer-exchanged proteins were loaded onto a HisTrap FF/ HP column pre-equilibrated in NI-NTA A and the flow-through was collected. Proteins were then concentrated using Amicon stirred cells and/ or Amicon centrifugal filters to a volume of 5 ml before loading onto superdex 75 or 200 gel filtration columns pre-equilibrated in SEC buffer. For the purification of FRET proteins with exposed cysteines, 1 mM DTT was added to the SEC buffer. Gel filtration columns were run for 1 column volume at a rate of 1 ml/ min and fractions of 3 - 5 ml collected. Pure fractions as judged by SDS-PAGE were pooled, concentrated by centrifugation to a concentration of 50 µM to 100 µM and snap frozen in liquid nitrogen in aliquots before storage at -80°C.

For Hsp82, an additional ion exchange chromatography step was used. Following His-SUMO tag cleavage and separation in the second nickel affinity step, the protein was diluted to a maximum of 150 ml in ResQ buffer A or exchanged into ResQ buffer A using a HiPrep 26/10 desalting column. The protein was then loaded onto a 6 ml Resource Q ion exchange column pre-equilibrated in ResQ A before washing with 10 column volumes ResQ A at 4 ml/min. An initial gradient of 0 mM to 100 mM KCl was then applied over 10 ml, followed by a longer gradient of 100 mM KCl to 500 mM KCl over 150 ml during which the protein elutes. Following analysis

with SDS-PAGE, sample-containing fractions were concentrated and further purified by gel filtration chromatography as above on a superdex 200 column.

For the purification of Ydj1, special Ni-NTA buffers (Section 4.5.1) were used during the nickel affinity steps. For the purification of SrtA, special Ni-NTA buffers were used during the nickel affinity steps and to each of these β -Mercaptoethanol was added to 2 mM. SrtA Ni-NTA buffer A was then used as the buffer for the final gel-filtration step, without β -Mercaptoethanol. Cleavage of the His-tag from SrtA was carried out using TEV protease instead of SUMO protease at 4°C overnight.

His₆-tagged Ssa1 was purified without tag cleavage, and special Ni-NTA buffers were used. The lysate was loaded onto a HisTrap then washed with 150 ml Ni-NTA buffer A, 150 ml 6% buffer B, and eluted with a step gradient to 100 % buffer B. Eluted Ssa1 was exchanged into HAT buffer A using a HiPrep Desalting column before loading onto a Hydroxyapatite column preequilibrated in HAT buffer A. Elution was performed by applying a linear gradient from HAT buffer A to HAT buffer B over 270 ml (Ssa1 elutes at around 55 – 65 % HAT 2). Following analysis by SDS-PAGE, fractions containing Ssa1 in reasonable purity were pooled, concentrated and loaded onto a Superdex 200 gel filtration column preequilibrated in Gel Filtration buffer. Gel filtration and storage proceeded as above.

His₆-tagged Sumo protease was purified without tag cleavage in a single nickel affinity step followed by gel filtration chromatography as above. Following centrifugal concentration, the protein was exchanged into 25mM Tris, pH 8.0, 1% Igepal (v/v), 250mM NaCl, 0.5 mM DTT and 50% glycerol. GR-LBD was kindly provided by Dr. Frank Echtenkamp (TU, München), purified according to (Lorenz *et al*, 2014).

4.6 Protein biochemistry

4.6.1 SDS polyacrylamide gel electrophoresis

SDS polyacrylamide gel electrophoresis (PAGE) was used to separate proteins according to their molecular weight, following the protocol of Laemmli (Laemmli, 1970). Gels were always cast such that they contained two sections, an upper 5 % stacking gel to collect proteins for separation, and a lower separating gel with an acrylamide content ranging from 10 % – 15 % depending on the size of the protein to be separated. Proteins were mixed with 5 % Laemmli

buffer and boiled at 95°C for 5 min. For size comparison, BioRad low-range molecular weight marker. Gels were run in 1x SDS-PAGE buffer at 300 V, 30 mA for around 50 min before staining with Fairbanks A solution, and subsequent destaining with 10 % acetic acid.

5 % Stacking gel

40 % acrylamide 38:2 (w/v)	0.625 ml
2x stacking buffer (0.4 % SDS, 250 mM Tris, pH 6.8)	2.5 ml
H ₂ O	1.875 ml

10 - 15 % Separating gel

40 % acrylamide 38:2 (w/v)	2.5 - 3.75 ml
4x Separating buffer (0.8 % SDS, 1.5 M Tris, pH 8.8)	2.5 ml
H ₂ O	to 10 ml

5x Laemmli buffer

SDS	10 % (w/v)
Tris	300 mM
Glycerol	50 % (w/v)
Bromophenol Blue	0.05 % (w/v)
B-Mercaptoethanol	5 % (v/v)

SDS-PAGE Buffer (10x)

Tris	250 mM
Glycine	2 M
SDS	1 % (w/v)

Fairbanks A solution

Isopropanol	25 % (v/v)
Acetic acid	10 % (v/v)
SERVA Blue R	0.05 % (v/v)

4.6.2 Protein labelling

Proteins were labelled either site-specifically at cysteine residues using ATTO dyes and maleimide coupling, or randomly at lysine residues using the FAM dye with NHS-ester coupling. For cysteine variants purified in the presence of the reducing agent DTT, it was first removed with PD-10 or spin columns. Dye stocks were prepared fresh before each labelling reaction by dissolving a few pipette-scrappings in 20 μ l DMSO. Rough stock concentration was measured by diluting 1 μ l in 5 ml water. Proteins were first separated from DTT using a pD-10 desalting column with standard gel filtration buffer. Generally, a two- to threefold excess of dye was used over protein (generally 500 μ l - 1 ml total volume at around 100 μ M) and the reaction was incubated for 1- 2 hours at RT. Labelling with FAM was carried out at 4°C overnight. Excess free label was then separated using a PD-10 desalting column or by gel filtration using a superdex 200 10/300 column before concentration if necessary. The degree of labelling (DOL) and concentration of the labelled protein were determined by absorption spectroscopy according to the following equations:

$$DOL = \frac{A_{dye} \cdot \epsilon_{dye}}{(A_{280} - A_{dye} \cdot CF_{dye}) \cdot \epsilon_{protein}}$$
$$c_{protein} = \frac{A_{280} - (A_{dye} \cdot CF_{dye})}{\epsilon_{protein} \cdot d}$$

Where A_{280} is the absorbance due to protein at 280 nm, A_{dye} is the absorption maximum of the dye, $\epsilon_{protein}$ and ϵ_{dye} are the extinction coefficients of the protein and dye respectively, CF_{dye} is the correction factor provided by the manufacturer that accounts for dye absorbance at 280 nm.

4.6.3 Sortase-mediated in vitro protein ligation

Purified unlabelled or labelled fragments (around 1 - 2 mg) were incubated at a 1: 1 ratio, along with an amount of SrtA equal to twice that of a single fragment. Fragments were reacted for 2 hours in standard SEC buffer (no calcium) at room temperature before loading onto a 1 ml Ni-NTA column pre-equilibrated with standard Ni-NTA buffer A. After washing with 10 ml buffer A, the column is eluted with 2 ml standard Ni-NTA buffer B. SUMO protease is added (around 50 μ l of a 1 mg/ ml solution) and tag cleavage takes place over 20 minutes. The solution is exchanged into Ni-NTA buffer A using a PD-10 column and passed over a 1 ml Ni-NTA column pre-equilibrated with buffer A, whereupon the flow-through is collected. The solution is concentrated to a maximum of 500 μ l using an Amicon centrifugal filter before further

purification by size exclusion chromatography on an HPLC device fitted with a Superdex 200 10/ 300 gel filtration column. Proteins are flash frozen in liquid nitrogen and stored at -80°C.

4.7 Protein analytical methods

4.7.1 Circular dichroism spectroscopy

Circular dichroism (CD) spectroscopy is a technique used to analyse chiral, 'optically active' substances such as proteins, based on their differential ability to absorb left and right circularly polarised light (Johnson, 1990). The optical activity of proteins arises from the chirality of their peptide backbones (imparted by secondary structure) as well as from the side chains of aromatic amino acids (whose chirality is provided by their surrounding environment within the protein tertiary structure). Different wavelengths of light may be used to interrogate different structural features, with near-UV (250 – 300 nm) giving information on aromatic tertiary structure, and far-UV (190 – 250 nm) giving information on peptide secondary structure. In particular, α -helices give rise to characteristic minima at 208 and 222 nm while β -sheets produce a minimum at 218 nm.

The measured electromagnetic signal is converted to ellipticity (θ) measured in millidegrees (mdeg). Following buffer correction, the signal is conventionally converted into the mean residue weighted molar ellipticity ($[\theta]_{MRW}$) to allow for standard comparison between proteins, according to the following equation:

$$[\theta]_{MRW} = \frac{100 \cdot \theta}{l \cdot N \cdot c}$$

Where θ is the measured ellipticity in mdeg, l is the path length in cm, N is the number of peptide bonds ($N_{aa} - 1$) and c is the protein concentration in mM. In this work, to ensure proper folding of proteins, far UV measurements were carried out in CD buffer in a Chirascan Plus spectrometer according to the following parameters:

Parameter	Setting
start wavelength	260 nm
end wavelength	190 – 200 nm
resolution	0.1 nm
scan speed	20 nm/min
response	4.0 s
band width	1.0 nm
accumulations	10
cuvette thickness	0.1 cm
protein concentration	3 – 5 μ M

4.7.2 UV/ Vis spectroscopy

Protein concentration was determined by measuring absorption at 280 nm in 1 cm quartz cuvettes in a Cary-50 UV-Vis spectrophotometer. Concentrations were calculated according to the Beer-Lambert equation:

$$A_{280} = \varepsilon \cdot c \cdot l$$

where ε is the protein extinction coefficient, c is the protein concentration and l is the path length. Protein extinction coefficients were calculated using the ProtParam online tool.

4.7.3 Equilibrium FRET spectroscopy

Fluorescence resonance energy transfer (FRET) is a tool to study the interaction between two light-sensitive fluorophores. A donor fluorophore is excited at a specific wavelength and energy is transferred to an acceptor fluorophore through dipole-dipole coupling. Emission from the acceptor is measured at a specific wavelength and is dependent on the efficiency of energy transfer, which is itself dependent on the distance between the fluorophores. If fluorophores are placed on separate proteins which interact and yield a FRET signal, the intensity of that signal is a function of concentration and may thus be used to measure binding. Equilibrium FRET measurements were carried out with 200 nM ATTO 488-labelled Ssa1-SBD and increasing concentrations of ATTO 550-labelled Sti1 FRET construct on a Jobin Yvon Horiba Fluoromax 3 spectrofluorimeter using 2 nm slit widths. Before measurement samples were mixed in individual quartz cuvettes and incubated in the dark for 1 hour at 30°C in 10 mM potassium phosphate. Particular attention was paid when dispensing solutions into the bottom of the cuvette to minimise removal of material with the pipette tips. Samples were excited at 485 nm

and FRET emission spectra recorded, comprising a pair of donor and acceptor peaks centred respectively at 520 nm and 575 nm. The FRET efficiency was calculated using a ratiometric method, which involves division of the acceptor peak intensity (A_{485}) by the sum of donor peak intensity (D_{485}) and acceptor peak intensity. From the acceptor peak intensity, direct excitation of the acceptor as well as the contribution of the donor emission to the acceptor channel is first subtracted. To calculate the amount of acceptor that was directly excited at 485 nm, the sample was excited a second time at 550 nm, upon which only the acceptor is excited (Clegg *et al*, 1993). The acceptor peak intensity upon excitation at 550 nm (A_{550}) is multiplied by the ratio of molar extinction coefficients of the acceptor at 550 nm and 485 nm. This is a constant, termed x , and is determined from an absorption spectrum of the acceptor alone.

$$x = \frac{\varepsilon_{485}}{\varepsilon_{550}}$$

(for the highest concentration point, A_{550} was over detector saturation and was therefore calculated from a plot of A_{550} versus concentration for lower points). The contribution of donor to the acceptor channel is calculated by multiplying the FRET donor peak intensity (D_{485}) by the constant ratio of emission intensity at 575 nm (I_{575}) versus 520 nm (I_{520}), measured from an emission spectrum of the donor alone, an effective deconvolution.

$$y = \frac{I_{575}}{I_{520}}$$

Subtraction of both the calculated direct acceptor excitation ($x \cdot A_{550}$) as well as the donor contribution ($y \cdot D_{485}$) from the raw FRET acceptor peak intensity (A_{485}), yields the acceptor intensity arising from FRET only, A_{FRET} .

$$A_{FRET} = A_{485} - x \cdot A_{550} - y \cdot D_{485}$$

The FRET efficiency, E , is then calculated as:

$$E = \frac{A_{FRET}}{A_{FRET} - D_{485}}$$

To normalise for acceptor labelling, the FRET efficiency was divided by the DOL of the acceptor, before being plotted as a function of acceptor concentration and fit to a simple binding equation:

$$E = \frac{E_{max} x}{K_d + x}$$

4.7.4 Stopped-flow FRET spectroscopy

Kinetic FRET measurements were carried out using an Applied Photophysics SX18-MV stopped flow spectrometer with sample syringes equilibrated at 30°C. 1 μM Samples were rapidly mixed at a 1: 1 volume ratio to give a final concentration of 0.5 μM ATTO 488-labelled Ssa1-SBD and 0.5 μM ATTO 550-labelled Sti1 FRET construct in 10 mM potassium phosphate. FRET was measured as an increase in acceptor fluorescence using a fluorescence detector equipped with a 570 nm cut-off filter with 1 nm excitation and emission slit widths. Baseline fluorescence was calculated as the sum of separate measurements of donor mixed with buffer and the respective acceptor mixed with buffer. After subtracting baseline fluorescence and correcting for degree of labelling of the acceptor, the resulting traces were fit to triple exponential association curves:

$$y = A_1 \cdot (1 - e^{-k_1 t}) + A_2 \cdot (1 - e^{-k_2 t}) + A_3 \cdot (1 - e^{-k_3 t})$$

where the k_1 , k_2 and k_3 are the rate constants for the three exponential phases and A_1 , A_2 and A_3 are the respective amplitudes. Amplitude-weighted average rates were calculated as:

$$k_{av} = \frac{(k_1 A_1 + k_2 A_2 + k_3 A_3)}{(A_1 + A_2 + A_3)}$$

4.7.5 Fluorescence anisotropy

Fluorescence anisotropy is a tool that can be used to study the binding of fluorescent molecules and proteins by observing differences in the polarisation of emitted light (Lakowicz, 2006). When a fluorophore is excited with linearly polarised light, the polarisation of the emitted light will be retained provided that the fluorophore is immobile. For molecules tumbling in solution, some polarisation is lost (depolarisation) depending on how fast the molecule is rotating. Anisotropy, r , can be used to measure depolarisation and is given by the following equation:

$$r = \frac{I_{\parallel} - I_{\perp}}{I_{\parallel} + 2I_{\perp}}$$

where I_{\parallel} is the fluorescence intensity measured with vertically polarised excitation and vertically polarised emission, and I_{\perp} is the fluorescence intensity measured with vertically polarised excitation and horizontally polarised emission. When a fluorescently labelled molecule or protein binds an unlabelled partner, there is a corresponding decrease in its rotation. This is called the rotational correlation time and is related to the anisotropy by:

$$r = \frac{r_0}{1 + \frac{\tau}{\theta}}$$

where r is the anisotropy, r_0 is the anisotropy in the absence of rotation (constant), τ is the fluorescence lifetime of the fluorophore (constant) and θ is the rotational correlation time. Thus a decreasing correlation time upon binding is measured as an increase in anisotropy. Anisotropy was measured in 1 cm quartz cuvettes at 30°C in 10 mM potassium phosphate on a Jasco FP-8500 equipped with polarisers. For kinetic measurements 0.5 μM fluorescently labelled Ssa1-SBD was mixed with 0.5 μM of various Sti1 constructs. For titrations, 0.5 μM fluorescently labelled Ssa1-SBD was mixed with increasing concentrations of Sti1 construct and pre-incubated for 1 hour at 30°C before measurement. Anisotropy values were subtracted from the value with 0.5 μM Ssa1-SBD alone. Samples were excited at 490 nm and emission collected at 520 nm with 1 nm excitation and emission slit widths respectively and high sensitivity. Kinetics were fit to triple exponential association curves and titrations were fit to the following binding equation:

$$\Delta r = \frac{B_{\max} x}{K_d + x}$$

where Δr is the change in anisotropy, x is the concentration of Sti1 variant, B_{\max} is the maximal change in anisotropy and K_d is the dissociation constant.

4.7.6 Analytical ultracentrifugation

Analytical ultracentrifugation (AUC) is a powerful method used to evaluate the sizes, shapes and interactions of proteins and complexes based on their sedimentation behaviour within a centrifugal field (Lebowitz *et al*, 2002). It is advantageous in comparison to other methods owing to the rich amount of information that can be extracted without the need for immobilisation on a solid support. In sedimentation velocity (SV) experiments, samples are subjected to centrifugal force in an ultracentrifuge, and an appropriate detection system is used to monitor over time, the movement of sedimentation boundaries which correspond to distinct species (proteins, complexes, or interacting systems). Different mathematical analytical methods can then be used to transform the raw data into sedimentation coefficient distributions, from which information such a size, shape and number of species can be evaluated. With absorbance detection (280 nm), all proteins in the sample are detectable. With fluorescence detection generally a single protein component is labelled, and then only complexes that contain this protein are detectable. This offers the possibility to study mixtures of many

components and the increased sensitivity provides for a much greater range in the choice of sample concentrations.

In this work, SV experiments were carried out in a Beckmann ProteomeLab XL-A ultracentrifuge equipped with either absorbance or fluorescence detection systems. For experiments using fluorescence detection, 500 nM of the labelled protein was used along with varying amounts of unlabelled proteins. For absorbance experiments, the concentration of all proteins in the sample was designed so as to give a total A_{280} of between 0.2 and 1. Experiments were carried out at 42,000 r.p.m. in a Beckman TI-50 rotor at 20°C in 10mM potassium phosphate buffer, pH 7.5. Depending on the level of fidelity required, raw data was analysed with the time derivative method in the program SedView (Stafford, 1992), or the Lamm equation modelling method in the program Sedfit (Schuck, 2000).

4.8 Activity assays

4.8.1 Steady state regenerative ATP activity assay

A regenerative steady state assay was used to measure the ATPase activity of Hsp90 in the presence of various Sti1 constructs (Ali *et al*, 1993). This approach uses a coupled enzyme system consisting of pyruvate kinase (PK), lactate dehydrogenase (LDH) and the cofactors phosphoenolpyruvate (PEP) and NADH. ADP produced during the measured reaction is rapidly converted back to ATP, preventing product inhibition, and this is coupled to the oxidation of NADH, which can be measured as a decrease in absorbance at 340 nm. The premix below was made fresh before beginning each set of assays. For each sample, 100 μ l of premix was mixed with 2 μ M Hsp90 and 2 μ M Sti1 construct in a 120 μ l quartz cuvette and the reaction was started by addition of 2 mM ATP (total sample volume 140 μ l). Absorbance at 340 nm was measured on a Cary 50 Bio UV/VIS spectrometer at 30°C. After around 30 min 500 μ M radicicol was added to specifically inhibit Hsp90 ATPase activity, revealing any background ATPase activity due to contaminants. This activity was subtracted from the total to give the true Hsp90 ATPase activity.

ATPase assay buffer

Hepes pH 7.5	50 mM
KCl	50 mM
MgCl ₂	10 mM

ATPase Premix

ATPase assay buffer	8.656 ml
100 mM NADH	48 μ l
100 mM PEP	240 μ l
PK	12 μ l
LDH	44 μ l

The hydrolysis rates were calculated according to the following equation:

$$K_{hyd} = \frac{m}{d \cdot \varepsilon_{NADH} \cdot c}$$

4.8.2 Glucocorticoid receptor activity assay

To test the ability of different Sti1 constructs to support activation of the GR in vivo, a β -galactosidase assay was used (Johnson & Craig, 2000). In this a Δsti strain of *S. cerevisiae* is transformed with p413GPD-*hGR* (His selection), an expression plasmid coding for human GR, along with a reporter plasmid, pUCASS-26X (Ura selection), carrying the β -galactosidase gene following a GR response element, and finally a p425GPD expression plasmid (Leu selection) containing the Sti1 construct of interest, Sti1-WT, or empty as a control. Strains were inoculated in 400 μ l CSM (UHL) media in 96-deep-well plates in replicates of three to six and incubated overnight at 30°C. The next day cultures were diluted 1: 10 in CSM medium and induced with 10 μ M 11-Deoxycorticosterone (DOC) before being grown overnight again at 30°C with shaking. For normalisation of cell density 20 μ l of each induced culture was mixed with 80 μ l H₂O in clear-bottomed 96-well plates and OD measured at 600 nm. For activity measurement, 50 μ l of the induced culture was centrifuged directly in a 96-well black-bottomed plate for 5 min at 4500 rpm before the supernatant was discarded by taking the plate in hand and shaking out with a single flicking motion. Cell lysis was achieved by adding 150 μ l lysis buffer to the remaining pellets and incubating with constant shaking for 25 min at 900 rpm. The reaction was started by adding 50 μ l ONPG (4 mg/ml) per well and β -gal activity was determined spectrophotometrically at 420 nm wavelength for 20 min. Kinetic slopes were calculated and normalized to the OD₆₀₀ of induced cultures.

Lysis buffer

Sodium Phosphate, pH 7.5	100 mM
SDS	0.1 % (w/v)

Bibliography

- Ali J.A., Jackson A.P., Howells A.J. & Maxwell A. (1993). The 43-kilodalton N-terminal fragment of the DNA gyrase B protein hydrolyzes ATP and binds coumarin drugs. *Biochemistry* **32**: 2717–2724
- Ali M.M.U., Roe S.M., Vaughan C.K., Meyer P., Panaretou B., Piper P.W., Prodromou C. & Pearl L.H. (2006). Crystal structure of an Hsp90-nucleotide-p23/Sba1 closed chaperone complex. *Nature* **440**: 1013–7
- Alvira S., Cuéllar J., Röhl A., Yamamoto S., Itoh H., Alfonso C., Rivas G., Buchner J. & Valpuesta J.M. (2014). Structural characterization of the substrate transfer mechanism in Hsp70/Hsp90 folding machinery mediated by Hop. *Nat. Commun.* **5**: 5484
- Anfinsen C.B. (1973). Principles that govern the folding of protein chains. *Science* **181**: 223–30
- Angelidis C.E., Lazaridis I. & Pagoulatos G.N. (1999). Aggregation of hsp70 and hsc70 in vivo is distinct and temperature- dependent and their chaperone function is directly related to non-aggregated forms. *Eur. J. Biochem.* **259**: 505–512
- Aprile F.A., Dhulesia A., Stengel F., Roodveldt C., Benesch J.L.P., Tortora P., Robinson C. V., Salvatella X., Dobson C.M. & Cremades N. (2013). Hsp70 Oligomerization Is Mediated by an Interaction between the Interdomain Linker and the Substrate-Binding Domain. *PLoS One* **8**: e67961
- Baindur-Hudson S., Edkins A.L. & Blatch G.L. (2015). Hsp70/Hsp90 organising protein (Hop): Beyond interactions with chaperones and prion proteins. *Subcell. Biochem.* **78**: 1–22
- Beraldo F.H., Soares I.N., Goncalves D.F., Fan J., Thomas A.A., Santos T.G., Mohammad A.H., Roffé M., Calder M.D., Nikolova S., Hajj G.N., Guimaraes A.L., Massensini A.R., Welch I., Betts D.H., Gros R., Drangova M., Watson A.J., Bartha R., Prado V.F., et al (2013). Stress-inducible phosphoprotein 1 has unique cochaperone activity during development and regulates cellular response to ischemia via the prion protein. *FASEB J.* **27**: 3594–3607
- Bertelsen E.B., Chang L., Gestwicki J.E. & Zuiderweg E.R.P. (2009). Solution conformation of wild-type E. coli Hsp70 (DnaK) chaperone complexed with ADP and substrate. *Proc. Natl. Acad. Sci.* **106**: 8471–8476
- Boczek E.E., Reefschräger L.G., Dehling M., Struller T.J., Häusler E., Seidl A., Kaila V.R.I. & Buchner J. (2015). Conformational processing of oncogenic v-Src kinase by the molecular chaperone Hsp90. *Proc. Natl. Acad. Sci. U. S. A.* **112**: E3189-98
- Borkovich K.A., Farrelly F.W., Finkelstein D.B., Taulien J. & Lindquist S. (1989). hsp82 is an essential protein that is required in higher concentrations for growth of cells at higher temperatures. *Mol. Cell. Biol.* **9**: 3919–30
- Bose S., Weikl T., Bügl H. & Buchner J. (1996). Chaperone function of Hsp90-associated proteins. *Science* **274**: 1715–7

-
- Bracher A. & Verghese J. (2015). The nucleotide exchange factors of Hsp70 molecular chaperones. *Front. Mol. Biosci.* **2**: 10
- Braig K., Otwinowski Z., Hegde R., Boisvert D.C., Joachimiak A., Horwich A.L. & Sigler P.B. (1994). The crystal structure of the bacterial chaperonin GroEL at 2.8 Å. *Nature* **371**: 578–586
- Brinker A., Scheufler C., Von Der Mulbe F., Fleckenstein B., Herrmann C., Jung G., Moarefi I. & Hartl F.U. (2002). Ligand discrimination by TPR domains. Relevance and selectivity of EEVD-recognition in Hsp70 x Hop x Hsp90 complexes. *J. Biol. Chem.* **277**: 19265–75
- Bukau B., Weissman J. & Horwich A. (2006). Molecular Chaperones and Protein Quality Control. *Cell* **125**: 443–451
- Butler L.M., Ferraldeschi R., Armstrong H.K., Centenera M.M. & Workman P. (2015). Maximizing the Therapeutic Potential of HSP90 Inhibitors. *Mol. Cancer Res.* **13**: 1445–1451
- Carrigan P.E., Nelson G.M., Roberts P.J., Stoffer J., Riggs D.L. & Smith D.F. (2004). Multiple domains of the co-chaperone Hop are important for Hsp70 binding. *J. Biol. Chem.* **279**: 16185–93
- Carrigan P.E., Riggs D.L., Chinkers M. & Smith D.F. (2005). Functional comparison of human and Drosophila Hop reveals novel role in steroid receptor maturation. *J. Biol. Chem.* **280**: 8906–8911
- Chang H.C., Nathan D.F. & Lindquist S. (1997). In vivo analysis of the Hsp90 cochaperone Sti1 (p60). *Mol. Cell. Biol.* **17**: 318–25
- Chen S. (1998). Hop as an Adaptor in the Heat Shock Protein 70 (Hsp70) and Hsp90 Chaperone Machinery. *J. Biol. Chem.* **273**: 35194–35200
- Chiti F. & Dobson C.M. (2006). Protein Misfolding, Functional Amyloid, and Human Disease. *Annu. Rev. Biochem.* **75**: 333–366
- Clegg R.M., Murchie A.I., Zechel A. & Lilley D.M. (1993). Observing the helical geometry of double-stranded DNA in solution by fluorescence resonance energy transfer. *Proc. Natl. Acad. Sci. U. S. A.* **90**: 2994–8
- Craig E.A. (2018). Hsp70 at the membrane: driving protein translocation. *BMC Biol.* **16**: 11
- Demand J., Lüders J. & Höhfeld J. (1998). The carboxy-terminal domain of Hsc70 provides binding sites for a distinct set of chaperone cofactors. *Mol. Cell. Biol.* **18**: 2023–8
- Dill K.A. & Chan H.S. (1997). From Levinthal to pathways to funnels. *Nat. Struct. Mol. Biol.* **4**: 10–19
- Dill K. a, Ozkan S.B., Shell M.S. & Weikl T.R. (2008). The protein folding problem. *Annu. Rev. Biophys.* **37**: 289–316
- Dinner A.R., Sali A., Smith L.J., Dobson C.M. & Karplus M. (2000). Understanding protein folding via free-energy surfaces from theory and experiment. *Trends Biochem. Sci.* **25**: 331–9

- Dittmar K.D., Demady D.R., Stancato L.F., Krishna P. & Pratt W.B. (1997). Folding of the glucocorticoid receptor by the heat shock protein (hsp) 90-based chaperone machinery. The role of p23 is to stabilize receptor.hsp90 heterocomplexes formed by hsp90.p60.hsp70. *J. Biol. Chem.* **272**: 21213–20
- Dittmar K.D. & Pratt W.B. (1997). Folding of the glucocorticoid receptor by the reconstituted Hsp90-based chaperone machinery. The initial hsp90.p60.hsp70-dependent step is sufficient for creating the steroid binding conformation. *J. Biol. Chem.* **272**: 13047–54
- Döring K., Ahmed N., Riemer T., Suresh H.G., Vainshtein Y., Habich M., Riemer J., Mayer M.P., O'Brien E.P., Kramer G. & Bukau B. (2017). Profiling Ssb-Nascent Chain Interactions Reveals Principles of Hsp70-Assisted Folding. *Cell* **170**: 298–311.e20
- Doyle S.M. & Wickner S. (2009). Hsp104 and ClpB: protein disaggregating machines. *Trends Biochem. Sci.* **34**: 40–48
- Dragovic Z., Broadley S.A., Shomura Y., Bracher A. & Hartl F.U. (2006). Molecular chaperones of the Hsp110 family act as nucleotide exchange factors of Hsp70s. *EMBO J.* **25**: 2519–28
- Dutta R. & Inouye M. (2000). GHKL, an emergent ATPase/kinase superfamily. *Trends Biochem. Sci.* **25**: 24–8
- Ebong I. -o., Daturpalli S., Morgner N., Zhou M., Robinson C. V., Saraiva M.A. & Jackson S.E. (2011). Heterogeneity and dynamics in the assembly of the Heat Shock Protein 90 chaperone complexes. *Proc. Natl. Acad. Sci.* **108**: 17939–17944
- Echeverría P.C., Bernthaler A., Dupuis P., Mayer B. & Picard D. (2011). An Interaction Network Predicted from Public Data as a Discovery Tool: Application to the Hsp90 Molecular Chaperone Machine. *PLoS One* **6**: e26044
- Edkins A.L. (2016). Hsp90 Co-chaperones as Drug Targets in Cancer: Current Perspectives. In pp 21–54. Springer, Cham
- van den Ent F. & Löwe J. (2006). RF cloning: A restriction-free method for inserting target genes into plasmids. *J. Biochem. Biophys. Methods* **67**: 67–74
- Ferraro M., D'Annessa I., Moroni E., Morra G., Paladino A., Rinaldi S., Compostella F. & Colombo G. (2019). Allosteric Modulators of HSP90 and HSP70: Dynamics Meets Function through Structure-Based Drug Design. *J. Med. Chem.* **62**: 60–87
- Flaherty K.M., DeLuca-Flaherty C. & McKay D.B. (1990). Three-dimensional structure of the ATPase fragment of a 70K heat-shock cognate protein. *Nature* **346**: 623–628
- Flom G., Behal R.H., Rosen L., Cole D.G. & Johnson J.L. (2007). Definition of the minimal fragments of Sti1 required for dimerization, interaction with Hsp70 and Hsp90 and in vivo functions. *Biochem. J.* **404**: 159–67
- Flom G., Weekes J., Williams J.J. & Johnson J.L. (2006). Effect of mutation of the tetratricopeptide repeat and asparatate-proline 2 domains of Sti1 on Hsp90 signaling and interaction in *Saccharomyces cerevisiae*. *Genetics* **172**: 41–51
- Flynn G.C., Chappell T.G. & Rothman J.E. (1989). Peptide binding and release by proteins implicated as catalysts of protein assembly. *Science* **245**: 385–90

-
- Fouchaq B., Benaroudj N., Ebel C. & Ladjimi M.M. (1999). Oligomerization of the 17-kDa peptide-binding domain of the molecular chaperone HSC70. *Eur. J. Biochem.* **259**: 379–84
- Freeman B.C., Felts S.J., Toft D.O. & Yamamoto K.R. (2000). The p23 molecular chaperones act at a late step in intracellular receptor action to differentially affect ligand efficacies. *Genes Dev.* **14**: 422–34
- Freeman B.C., Toft D.O. & Morimoto R.I. (1996). Molecular chaperone machines: chaperone activities of the cyclophilin Cyp-40 and the steroid aporeceptor-associated protein p23. *Science* **274**: 1718–20
- Freiburger L., Sonntag M., Hennig J., Li J., Zou P. & Sattler M. (2015). Efficient segmental isotope labeling of multi-domain proteins using Sortase A. *J. Biomol. NMR* **63**: 1–8
- Gaiser A.M., Brandt F. & Richter K. (2009). The Non-canonical Hop Protein from *Caenorhabditis elegans* Exerts Essential Functions and Forms Binary Complexes with Either Hsc70 or Hsp90. *J. Mol. Biol.* **391**: 621–634
- Gasteiger E., Hoogland C., Gattiker A., Duvaud S., Wilkins M.R., Appel R.D. & Bairoch A. (2005). Protein Identification and Analysis Tools on the ExPASy Server. In *The Proteomics Protocols Handbook* pp 571–607. Totowa, NJ: Humana Press
- Gautschi M., Lilie H., Funfschilling U., Mun A., Ross S., Lithgow T., Rucknagel P. & Rospert S. (2001). RAC, a stable ribosome-associated complex in yeast formed by the DnaK-DnaJ homologs Ssz1p and zuotin. *Proc. Natl. Acad. Sci.* **98**: 3762–3767
- Gautschi M., Mun A., Ross S. & Rospert S. (2002). A functional chaperone triad on the yeast ribosome. *Proc. Natl. Acad. Sci. U. S. A.* **99**: 4209–14
- Genest O., Reidy M., Street T.O., Hoskins J.R., Camberg J.L., Agard D.A., Masison D.C. & Wickner S. (2013). Uncovering a region of heat shock protein 90 important for client binding in *E. coli* and chaperone function in yeast. *Mol. Cell* **49**: 464–73
- Gidalevitz T., Prahlad V. & Morimoto R.I. (2011). The Stress of Protein Misfolding: From Single Cells to Multicellular Organisms. *Cold Spring Harb. Perspect. Biol.* **3**:
- Goloubinoff P., Mogk A., Zvi A.P., Tomoyasu T. & Bukau B. (1999). Sequential mechanism of solubilization and refolding of stable protein aggregates by a bichaperone network. *Proc. Natl. Acad. Sci. U. S. A.* **96**: 13732–7
- Grammatikakis N., Lin J.H., Grammatikakis A., Tsiachlis P.N. & Cochran B.H. (1999). p50(cdc37) acting in concert with Hsp90 is required for Raf-1 function. *Mol. Cell. Biol.* **19**: 1661–72
- Hagn F., Lagleder S., Retzlaff M., Rohrberg J., Demmer O., Richter K., Buchner J. & Kessler H. (2011). Structural analysis of the interaction between Hsp90 and the tumor suppressor protein p53. *Nat. Struct. Mol. Biol.* **18**: 1086–1093
- Harrison C.J., Hayer-Hartl M., Di Liberto M., Hartl F. & Kuriyan J. (1997). Crystal structure of the nucleotide exchange factor GrpE bound to the ATPase domain of the molecular chaperone DnaK. *Science* **276**: 431–5
- Hartl F.U., Bracher A. & Hayer-Hartl M. (2011). Molecular chaperones in protein folding and proteostasis. *Nature* **475**: 324–332

-
- Haslbeck M., Franzmann T., Weinfurtner D. & Buchner J. (2005). Some like it hot: the structure and function of small heat-shock proteins. *Nat. Struct. Mol. Biol.* **12**: 842–846
- Hayes D.B. & Stafford W.F. (2010). SEDVIEW, real-time sedimentation analysis. *Macromol. Biosci.* **10**: 731–5
- Hernández M.P., Sullivan W.P. & Toft D.O. (2002). The assembly and intermolecular properties of the hsp70-Hop-hsp90 molecular chaperone complex. *J. Biol. Chem.* **277**: 38294–304
- Hessling M., Richter K. & Buchner J. (2009). Dissection of the ATP-induced conformational cycle of the molecular chaperone Hsp90. *Nat. Struct. Mol. Biol.* **16**: 287–293
- Hildenbrand Z.L., Xiao C., Herrera N., Molugu S.K., Bernal R.A. & Ramirez C. (2011). Hsp90 can Accommodate the Simultaneous Binding of the FKBP52 and HOP Proteins. *Oncotarget* **2**: 43–58
- Hoff K.G., Silberg J.J. & Vickery L.E. (2000). Interaction of the iron-sulfur cluster assembly protein IscU with the Hsc66/Hsc20 molecular chaperone system of Escherichia coli. *Proc. Natl. Acad. Sci. U. S. A.* **97**: 7790–5
- Horwitz J. (1992). Alpha-crystallin can function as a molecular chaperone. *Proc. Natl. Acad. Sci. U. S. A.* **89**: 10449–53
- Hundley H.A., Walter W., Bairstow S. & Craig E.A. (2005). Human Mpp11 J Protein: Ribosome-Tethered Molecular Chaperones Are Ubiquitous. *Science (80-.)*. **308**: 1032–1034
- Iwasaki S., Sasaki H.M., Sakaguchi Y., Suzuki T., Tadakuma H. & Tomari Y. (2015). Defining fundamental steps in the assembly of the Drosophila RNAi enzyme complex. *Nature* **521**: 533–536
- Jahn M., Rehn A., Pelz B., Hellenkamp B., Richter K., Rief M., Buchner J. & Hugel T. (2014). The charged linker of the molecular chaperone Hsp90 modulates domain contacts and biological function. *Proc. Natl. Acad. Sci.* **111**: 17881–17886
- Jarosz D.F. & Lindquist S. (2010). Hsp90 and Environmental Stress Transform the Adaptive Value of Natural Genetic Variation. *Science (80-.)*. **330**: 1820–1824
- Jeong J.-Y., Yim H.-S., Ryu J.-Y., Lee H.S., Lee J.-H., Seen D.-S. & Kang S.G. (2012). One-Step Sequence- and Ligation-Independent Cloning as a Rapid and Versatile Cloning Method for Functional Genomics Studies. *Appl. Environ. Microbiol.* **78**: 5440–5443
- Jiang J., Ballinger C.A., Wu Y., Dai Q., Cyr D.M., Höhfeld J. & Patterson C. (2001). CHIP Is a U-box-dependent E3 Ubiquitin Ligase. *J. Biol. Chem.* **276**: 42938–42944
- Jiang J., Maes E.G., Taylor A.B., Wang L., Hinck A.P., Lafer E.M. & Sousa R. (2007). Structural basis of J cochaperone binding and regulation of Hsp70. *Mol. Cell* **28**: 422–33
- Jiang J., Prasad K., Lafer E.M. & Sousa R. (2005). Structural Basis of Interdomain Communication in the Hsc70 Chaperone. *Mol. Cell* **20**: 513–524
- Johnson B.D., Schumacher R.J., Ross E.D. & Toft D.O. (1998). Hop modulates Hsp70/Hsp90 interactions in protein folding. *J. Biol. Chem.* **273**: 3679–86
-

-
- Johnson J.L. & Brown C. (2009). Plasticity of the Hsp90 chaperone machine in divergent eukaryotic organisms. *Cell Stress Chaperones* **14**: 83–94
- Johnson J.L. & Craig E.A. (2000). A Role for the Hsp40 Ydj1 in Repression of Basal Steroid Receptor Activity in Yeast. *Mol. Cell. Biol.* **20**: 3027–3036
- Johnson W.C. (1990). Protein secondary structure and circular dichroism: A practical guide. *Proteins Struct. Funct. Genet.* **7**: 205–214
- Kabbage M. & Dickman M.B. (2008). The BAG proteins: a ubiquitous family of chaperone regulators. *Cell. Mol. Life Sci.* **65**: 1390–1402
- Kampinga H.H. & Craig E.A. (2010). The HSP70 chaperone machinery: J proteins as drivers of functional specificity. *Nat. Rev. Mol. Cell Biol.* **11**: 579–592
- Kampinga H.H., Hageman J., Vos M.J., Kubota H., Tanguay R.M., Bruford E.A., Cheetham M.E., Chen B. & Hightower L.E. (2009). Guidelines for the nomenclature of the human heat shock proteins. *Cell Stress Chaperones* **14**: 105–111
- Kandasamy G. & Andréasson C. (2018). Hsp70–Hsp110 chaperones deliver ubiquitin-dependent and -independent substrates to the 26S proteasome for proteolysis in yeast. *J. Cell Sci.* **131**: jcs210948
- Kaushik S. & Cuervo A.M. (2012). Chaperone-mediated autophagy: a unique way to enter the lysosome world. *Trends Cell Biol.* **22**: 407–17
- Kirschke E., Goswami D., Southworth D., Griffin P.R. & Agard D.A. (2014). Glucocorticoid Receptor Function Regulated by Coordinated Action of the Hsp90 and Hsp70 Chaperone Cycles. *Cell* **157**: 1685–1697
- Kityk R., Kopp J. & Mayer M.P. (2018). Molecular Mechanism of J-Domain-Triggered ATP Hydrolysis by Hsp70 Chaperones. *Mol. Cell* **69**: 227–237.e4
- Kityk R., Kopp J., Sinning I. & Mayer M.P. (2012). Structure and dynamics of the ATP-bound open conformation of Hsp70 chaperones. *Mol. Cell* **48**: 863–74
- Kityk R., Vogel M., Schlecht R., Bukau B. & Mayer M.P. (2015). Pathways of allosteric regulation in Hsp70 chaperones. *Nat. Commun.* **6**: 8308
- Kluck C.J., Patzelt H., Genevaux P., Brehmer D., Rist W., Schneider-Mergener J., Bukau B. & Mayer M.P. (2002). Structure-Function Analysis of HscC, the *Escherichia coli* Member of a Novel Subfamily of Specialized Hsp70 Chaperones. *J. Biol. Chem.* **277**: 41060–41069
- Kravats A.N., Hoskins J.R., Reidy M., Johnson J.L., Doyle S.M., Genest O., Masison D.C. & Wickner S. (2018). Functional and physical interaction between yeast Hsp90 and Hsp70. *Proc. Natl. Acad. Sci.* **115**: E2210–E2219
- Kriehuber T., Rattei T., Weinmaier T., Bepperling A., Haslbeck M. & Buchner J. (2010). Independent evolution of the core domain and its flanking sequences in small heat shock proteins. *FASEB J.* **24**: 3633–3642
- Laemmli U.K. (1970). Cleavage of structural proteins during the assembly of the head of bacteriophage T4. *Nature* **227**: 680–685

-
- Lakowicz J.R. (2006). Principles of fluorescence spectroscopy Springer
- Lebowitz J., Lewis M.S. & Schuck P. (2002). Modern analytical ultracentrifugation in protein science: A tutorial review. *Protein Sci.* **11**: 2067–2079
- Lee C.-T., Graf C., Mayer F.J., Richter S.M. & Mayer M.P. (2012). Dynamics of the regulation of Hsp90 by the co-chaperone Sti1. *EMBO J.* **31**: 1518–28
- Leitner A., Joachimiak L.A., Bracher A., Mönkemeyer L., Walzthoeni T., Chen B., Pechmann S., Holmes S., Cong Y., Ma B., Ludtke S., Chiu W., Hartl F.U., Aebersold R. & Frydman J. (2012). The Molecular Architecture of the Eukaryotic Chaperonin TRiC/CCT. *Structure* **20**: 814–825
- Levinthal C. (1968). Are there pathways for protein folding? *J. Chim. Phys. Physico-Chimie Biol.* **65**: 44–45
- Levy Y. & Onuchic J.N. (2006). Water Mediation in Protein Folding and Molecular Recognition. *Annu. Rev. Biophys. Biomol. Struct.* **35**: 389–415
- Li J., Richter K. & Buchner J. (2011). Mixed Hsp90-cochaperone complexes are important for the progression of the reaction cycle. *Nat. Struct. Mol. Biol.* **18**: 61–66
- Li J., Richter K., Reinstein J. & Buchner J. (2013). Integration of the accelerator Aha1 in the Hsp90 co-chaperone cycle. *Nat. Struct. Mol. Biol.* **20**: 326–31
- Liberek K., Marszalek J., Ang D., Georgopoulos C. & Zylicz M. (1991). Escherichia coli DnaJ and GrpE heat shock proteins jointly stimulate ATPase activity of DnaK. *Proc. Natl. Acad. Sci. U. S. A.* **88**: 2874–8
- Lindquist S. & Craig E.A. (1988). The Heat-Shock Proteins. *Annu. Rev. Genet.* **22**: 631–677
- Lopez T., Dalton K. & Frydman J. (2015). The Mechanism and Function of Group II Chaperonins. *J. Mol. Biol.* **427**: 2919–2930
- Lorenz O.R., Freiburger L., Rutz D.A., Krause M., Zierer B.K., Alvira S., Cuéllar J., Valpuesta J.M., Madl T., Sattler M. & Buchner J. (2014). Modulation of the Hsp90 Chaperone Cycle by a Stringent Client Protein. *Mol. Cell*: 1–13
- Lu Z. & Cyr D.M. (1998). Protein folding activity of Hsp70 is modified differentially by the hsp40 co-chaperones Sis1 and Ydj1. *J. Biol. Chem.* **273**: 27824–30
- Makhnevych T. & Houry W.A. (2012). The role of Hsp90 in protein complex assembly. *Biochim. Biophys. Acta - Mol. Cell Res.* **1823**: 674–682
- Mao H., Hart S.A., Schink A. & Pollok B.A. (2004). Sortase-Mediated Protein Ligation: A New Method for Protein Engineering. *J. Am. Chem. Soc.* **126**: 2670–2671
- Marcinowski M., Höller M., Feige M.J., Baerend D., Lamb D.C. & Buchner J. (2011). Substrate discrimination of the chaperone BiP by autonomous and cochaperone-regulated conformational transitions. *Nat. Struct. Mol. Biol.* **18**: 150–158

-
- Martin S.F., Tatham M.H., Hay R.T. & Samuel I.D.W. (2008). Quantitative analysis of multi-protein interactions using FRET: Application to the SUMO pathway. *Protein Sci.* **17**: 777–784
- Mattoo R.U.H., Sharma S.K., Priya S., Finka A. & Goloubinoff P. (2013). Hsp110 is a bona fide chaperone using ATP to unfold stable misfolded polypeptides and reciprocally collaborate with Hsp70 to solubilize protein aggregates. *J. Biol. Chem.* **288**: 21399–21411
- Mayer M.P. & Bukau B. (2005). Hsp70 chaperones: cellular functions and molecular mechanism. *Cell. Mol. Life Sci.* **62**: 670–84
- Mayer M.P. & Bukau B. (2008). Regulation of Hsp70 Chaperones by Co-chaperones. In *Protein Folding Handbook* pp 516–562. WILEY
- Mayer M.P. & Gierasch L.M. (2019). Recent advances in the structural and mechanistic aspects of Hsp70 molecular chaperones. *J. Biol. Chem.* **294**: 2085–2097
- Mayr C., Richter K., Lilie H. & Buchner J. (2000). Cpr6 and Cpr7, two closely related Hsp90-associated immunophilins from *Saccharomyces cerevisiae*, differ in their functional properties. *J. Biol. Chem.* **275**: 34140–34146
- Mazmanian S.K., Liu G., Ton-That H. & Schneewind O. (1999). Staphylococcus aureus sortase, an enzyme that anchors surface proteins to the cell wall. *Science* **285**: 760–3
- McLaughlin S.H., Smith H.W. & Jackson S.E. (2002). Stimulation of the weak ATPase activity of human Hsp90 by a client protein 1 Edited by G. von Heijne. *J. Mol. Biol.* **315**: 787–798
- Meyer P., Prodromou C., Hu B., Vaughan C., Roe S.M., Panaretou B., Piper P.W. & Pearl L.H. (2003). Structural and functional analysis of the middle segment of hsp90: implications for ATP hydrolysis and client protein and cochaperone interactions. *Mol. Cell* **11**: 647–58
- Mogk A., Kummer E. & Bukau B. (2015). Cooperation of Hsp70 and Hsp100 chaperone machines in protein disaggregation. *Front. Mol. Biosci.* **2**: 22
- Mogk A., Schlieker C., Friedrich K.L., Schönfeld H.-J., Vierling E. & Bukau B. (2003). Refolding of Substrates Bound to Small Hsps Relies on a Disaggregation Reaction Mediated Most Efficiently by ClpB/DnaK. *J. Biol. Chem.* **278**: 31033–31042
- Montgomery D.L., Morimoto R.I. & Gierasch L.M. (1999). Mutations in the substrate binding domain of the Escherichia coli 70 kDa molecular chaperone, DnaK, which alter substrate affinity or interdomain coupling. *J. Mol. Biol.* **286**: 915–932
- Morgner N., Schmidt C., Beilstein-Edmands V., Ebong I.-O., Patel N.A., Clerico E.M., Kirschke E., Daturpalli S., Jackson S.E., Agard D. & Robinson C. V (2015). Hsp70 Forms Antiparallel Dimers Stabilized by Post-translational Modifications to Position Clients for Transfer to Hsp90. *Cell Rep.* **11**: 759–769
- Morishima Y., Murphy P.J.M., Li D.-P., Sanchez E.R. & Pratt W.B. (2000). Stepwise Assembly of a Glucocorticoid Receptor·hsp90 Heterocomplex Resolves Two Sequential ATP-dependent Events Involving First hsp70 and Then hsp90 in Opening of the Steroid Binding Pocket. *J. Biol. Chem.* **275**: 18054–18060

-
- Muona M., Aranko A.S., Raulinaitis V. & Iwai H. (2010). Segmental isotopic labeling of multi-domain and fusion proteins by protein trans-splicing in vivo and in vitro. *Nat. Protoc.* **5**: 574–587
- Nakamoto H., Fujita K., Ohtaki A., Watanabe S., Narumi S., Maruyama T., Suenaga E., Misono T.S., Kumar P.K.R., Goloubinoff P. & Yoshikawa H. (2014). Physical Interaction between Bacterial Heat Shock Protein (Hsp) 90 and Hsp70 Chaperones Mediates Their Cooperative Action to Refold Denatured Proteins. *J. Biol. Chem.* **289**: 6110–6119
- Nakatsukasa K., Huyer G., Michaelis S. & Brodsky J.L. (2008). Dissecting the ER-Associated Degradation of a Misfolded Polytopic Membrane Protein. *Cell* **132**: 101–112
- Neckers L. & Workman P. (2012). Hsp90 molecular chaperone inhibitors: are we there yet? *Clin. Cancer Res.* **18**: 64–76
- Nelson G.M., Huffman H. & Smith D.F. (2003). Comparison of the carboxy-terminal DP-repeat region in the co-chaperones Hop and Hip. *Cell Stress Chaperones* **8**: 125–33
- Nelson R.J., Ziegelhoffer T., Nicolet C., Werner-Washburne M. & Craig E.A. (1992). The translation machinery and 70 kd heat shock protein cooperate in protein synthesis. *Cell* **71**: 97–105
- Neupert W. & Herrmann J.M. (2007). Translocation of Proteins into Mitochondria. *Annu. Rev. Biochem.* **76**: 723–749
- Park S.J., Borin B.N., Martinez-Yamout M.A. & Dyson H.J. (2011). The client protein p53 adopts a molten globule-like state in the presence of Hsp90. *Nat. Struct. Mol. Biol.* **18**: 537–41
- Pimienta G., Herbert K.M. & Regan L. (2011). A Compound That Inhibits the HOP–Hsp90 Complex Formation and Has Unique Killing Effects in Breast Cancer Cell Lines. *Mol. Pharm.* **8**: 2252–2261
- Polier S., Dragovic Z., Hartl F.U. & Bracher A. (2008). Structural basis for the cooperation of Hsp70 and Hsp110 chaperones in protein folding. *Cell* **133**: 1068–79
- Pratt W.B. & Toft D.O. (1997). Steroid receptor interactions with heat shock protein and immunophilin chaperones. *Endocr. Rev.* **18**: 306–360
- Prodromou C., Roe S.M., O'Brien R., Ladbury J.E., Piper P.W. & Pearl L.H. (1997). Identification and structural characterization of the ATP/ADP-binding site in the Hsp90 molecular chaperone. *Cell* **90**: 65–75
- Prodromou C., Siligardi G., O'Brien R., Woolfson D.N., Regan L., Panaretou B., Ladbury J.E., Piper P.W. & Pearl L.H. (1999). Regulation of Hsp90 ATPase activity by tetratricopeptide repeat (TPR)-domain co-chaperones. *EMBO J.* **18**: 754–62
- Qi R., Sarbeng E.B., Liu Q., Le K.Q., Xu X., Xu H., Yang J., Wong J.L., Vorvis C., Hendrickson W.A., Zhou L. & Liu Q. (2013). Allosteric opening of the polypeptide-binding site when an Hsp70 binds ATP. *Nat. Struct. Mol. Biol.* **20**: 900–7
- Ratzke C., Nguyen M.N.T., Mayer M.P. & Hugel T. (2012). From a Ratchet Mechanism to Random Fluctuations Evolution of Hsp90's Mechanochemical Cycle. *J. Mol. Biol.* **423**: 462–471
-

-
- Raviol H., Sadlish H., Rodriguez F., Mayer M.P. & Bukau B. (2006). Chaperone network in the yeast cytosol: Hsp110 is revealed as an Hsp70 nucleotide exchange factor. *EMBO J.* **25**: 2510–2518
- Reid B.G., Fenton W.A., Horwich A.L. & Weber-Ban E.U. (2001). ClpA mediates directional translocation of substrate proteins into the ClpP protease. *Proc. Natl. Acad. Sci. U. S. A.* **98**: 3768–72
- Reissmann S., Joachimiak L.A., Chen B., Meyer A.S., Nguyen A. & Frydman J. (2012). A Gradient of ATP Affinities Generates an Asymmetric Power Stroke Driving the Chaperonin TRiC/CCT Folding Cycle. *Cell Rep.* **2**: 866–877
- Retzlaff M., Hagn F., Mitschke L., Hessling M., Gugel F., Kessler H., Richter K. & Buchner J. (2010). Asymmetric Activation of the Hsp90 Dimer by Its Cochaperone Aha1. *Mol. Cell* **37**: 344–354
- Richter K., Haslbeck M. & Buchner J. (2010). The heat shock response: life on the verge of death. *Mol. Cell* **40**: 253–66
- Richter K., Muschler P., Hainzl O., Reinstein J. & Buchner J. (2003). Sti1 is a non-competitive inhibitor of the Hsp90 ATPase. Binding prevents the N-terminal dimerization reaction during the atpase cycle. *J. Biol. Chem.* **278**: 10328–33
- Röhl A., Rohrberg J. & Buchner J. (2013). The chaperone Hsp90: Changing partners for demanding clients. *Trends Biochem. Sci.* **38**: 253–262
- Röhl A., Toppel F., Bender E., Schmid A.B., Richter K., Madl T. & Buchner J. (2014). Hop/Sti1 phosphorylation inhibits its co-chaperone function. *EMBO Rep.* **16**: 240–249
- Röhl A., Wengler D., Madl T., Lagleder S., Toppel F., Herrmann M., Hendrix J., Richter K., Hack G., Schmid A.B., Kessler H., Lamb D.C. & Buchner J. (2015). Hsp90 regulates the dynamics of its cochaperone Sti1 and the transfer of Hsp70 between modules. *Nat. Commun.* **6**: 6655
- Rosam M., Krader D., Nickels C., Hochmair J., Back K.C., Agam G., Barth A., Zeymer C., Hendrix J., Schneider M., Antes I., Reinstein J., Lamb D.C. & Buchner J. (2018). Bap (Sil1) regulates the molecular chaperone BiP by coupling release of nucleotide and substrate. *Nat. Struct. Mol. Biol.* **25**: 90–100
- Ruckova E., Muller P., Nenutil R. & Vojtesek B. (2012). Alterations of the Hsp70/Hsp90 chaperone and the HOP/CHIP co-chaperone system in cancer. *Cell. Mol. Biol. Lett.* **17**: 446–458
- Rüdiger S., Freund S.M. V., Veprintsev D.B. & Fersht A.R. (2002). CRINEPT-TROSY NMR reveals p53 core domain bound in an unfolded form to the chaperone Hsp90. *Proc. Natl. Acad. Sci. U. S. A.* **99**: 11085–90
- Rüdiger S., Germeroth L., Schneider-Mergener J. & Bukau B. (1997). Substrate specificity of the DnaK chaperone determined by screening cellulose-bound peptide libraries. *EMBO J.* **16**: 1501–7
- Rutherford S.L. & Lindquist S. (1998). Hsp90 as a capacitor for morphological evolution. *Nature* **396**: 336–342

-
- Sahasrabudhe P., Rohrberg J., Biebl M.M., Rutz D.A. & Buchner J. (2017). The Plasticity of the Hsp90 Co-chaperone System. *Mol. Cell* **67**: 947–961.e5
- Saibil H. (2013). Chaperone machines for protein folding, unfolding and disaggregation. *Nat. Rev. Mol. Cell Biol.* **14**: 630–42
- Sali A. & Blundell T.L. (1993). Comparative Protein Modelling by Satisfaction of Spatial Restraints. *J. Mol. Biol.* **234**: 779–815
- Sambrook J., Fritsch E.F. & Maniatis T. (1989). Molecular cloning: a laboratory manual Cold Spring Harbor Laboratory
- Sarheng E.B., Liu Q., Tian X., Yang J., Li H., Wong J.L., Zhou L. & Liu Q. (2015). A functional DnaK dimer is essential for the efficient interaction with Hsp40 heat shock protein. *J. Biol. Chem.* **290**: 8849–62
- Scheufler C., Brinker A., Bourenkov G., Pegoraro S., Moroder L., Bartunik H., Hartl F.U. & Moarefi I. (2000). Structure of TPR domain-peptide complexes: critical elements in the assembly of the Hsp70-Hsp90 multichaperone machine. *Cell* **101**: 199–210
- Schirmer E.C., Glover J.R., Singer M.A. & Lindquist S. (1996). HSP100/Clp proteins: a common mechanism explains diverse functions. *Trends Biochem. Sci.* **21**: 289–96
- Schmid A.B., Lagleder S., Gräwert M.A., Röhl A., Hagn F., Wandinger S.K., Cox M.B., Demmer O., Richter K., Groll M., Kessler H. & Buchner J. (2012). The architecture of functional modules in the Hsp90 co-chaperone Sti1/Hop. *EMBO J.* **31**: 1506–17
- Schopf F.H., Biebl M.M. & Buchner J. (2017). The HSP90 chaperone machinery. *Nat. Rev. Mol. Cell Biol.* **18**: 345–360
- Schröder H., Langer T., Hartl F.U. & Bukau B. (1993). DnaK, DnaJ and GrpE form a cellular chaperone machinery capable of repairing heat-induced protein damage. *EMBO J.* **12**: 4137–44
- Schuck P. (2000). Size-distribution analysis of macromolecules by sedimentation velocity ultracentrifugation and Lamm equation modeling. *Biophys. J.* **78**: 1606–1619
- Shiau A.K., Harris S.F., Southworth D.R. & Agard D.A. (2006). Structural Analysis of E. coli hsp90 Reveals Dramatic Nucleotide-Dependent Conformational Rearrangements. *Cell* **127**: 329–340
- Shomura Y., Dragovic Z., Chang H.-C., Tzvetkov N., Young J.C., Brodsky J.L., Guerriero V., Hartl F.U. & Bracher A. (2005). Regulation of Hsp70 function by HspBP1: structural analysis reveals an alternate mechanism for Hsp70 nucleotide exchange. *Mol. Cell* **17**: 367–79
- Smith D.F. (2004). Tetratricopeptide repeat cochaperones in steroid receptor complexes. *Cell Stress Chaperones* **9**: 109–21
- Smock R.G., Blackburn M.E. & Gierasch L.M. (2011). Conserved, disordered C terminus of DnaK enhances cellular survival upon stress and DnaK in vitro chaperone activity. *J. Biol. Chem.* **286**: 31821–31829
-

-
- Sondermann H., Scheufler C., Schneider C., Hohfeld J., Hartl F.U. & Moarefi I. (2001). Structure of a Bag/Hsc70 complex: convergent functional evolution of Hsp70 nucleotide exchange factors. *Science* **291**: 1553–7
- Sousa R., Liao H.-S., Cuéllar J., Jin S., Valpuesta J.M., Jin A.J. & Lafer E.M. (2016). Clathrin-coat disassembly illuminates the mechanisms of Hsp70 force generation. *Nat. Struct. Mol. Biol.* **23**: 821–829
- Southworth D.R. & Agard D. a (2011). Client-loading conformation of the Hsp90 molecular chaperone revealed in the cryo-EM structure of the human Hsp90:Hop complex. *Mol. Cell* **42**: 771–81
- Spieß C., Meyer A.S., Reissmann S. & Frydman J. (2004). Mechanism of the eukaryotic chaperonin: protein folding in the chamber of secrets. *Trends Cell Biol.* **14**: 598–604
- Stafford W.F. (1992). Boundary analysis in sedimentation transport experiments: A procedure for obtaining sedimentation coefficient distributions using the time derivative of the concentration profile. *Anal. Biochem.* **203**: 295–301
- Stennett E.M.S., Ciuba M.A. & Levitus M. (2014). Photophysical processes in single molecule organic fluorescent probes. *Chem. Soc. Rev.* **43**: 1057–1075
- Stepanova L., Leng X., Parker S.B. & Harper J.W. (1996). Mammalian p50Cdc37 is a protein kinase-targeting subunit of Hsp90 that binds and stabilizes Cdk4. *Genes Dev.* **10**: 1491–502
- Swain J.F., Dinler G., Sivendran R., Montgomery D.L., Stotz M. & Gierasch L.M. (2007). Hsp70 Chaperone Ligands Control Domain Association via an Allosteric Mechanism Mediated by the Interdomain Linker. *Mol. Cell* **26**: 27–39
- Taipale M., Jarosz D.F. & Lindquist S. (2010). HSP90 at the hub of protein homeostasis: emerging mechanistic insights. *Nat. Rev. Mol. Cell Biol.* **11**: 515–528
- Taipale M., Krykbaeva I., Koeva M., Kayatekin C., Westover K.D., Karras G.I. & Lindquist S. (2012). Quantitative analysis of Hsp90-client interactions reveals principles of substrate recognition. *Cell* **150**: 987–1001
- Takagi F., Koga N. & Takada S. (2003). How protein thermodynamics and folding mechanisms are altered by the chaperonin cage *Proc. Natl. Acad. Sci. U. S. A.* **100**: 11367
- Thompson A.D., Bernard S.M., Skiniotis G. & Gestwicki J.E. (2012). Visualization and functional analysis of the oligomeric states of Escherichia coli heat shock protein 70 (Hsp70/DnaK). *Cell Stress Chaperones* **17**: 313–27
- Thompson J.D., Higgins D.G. & Gibson T.J. (1994). CLUSTAL W: improving the sensitivity of progressive multiple sequence alignment through sequence weighting, position-specific gap penalties and weight matrix choice. *Nucleic Acids Res.* **22**: 4673–4680
- Thulasiraman V., Yang C.F. & Frydman J. (1999). In vivo newly translated polypeptides are sequestered in a protected folding environment. *EMBO J.* **18**: 85

- Trcka F., Durech M., Vankova P., Chmelik J., Martinkova V., Hausner J., Kadek A., Marcoux J., Klumpler T., Vojtesek B., Muller P. & Man P. (2019). Human Stress-inducible Hsp70 Has a High Propensity to Form ATP-dependent Antiparallel Dimers That Are Differentially Regulated by Cochaperone Binding. *Mol. Cell. Proteomics* **18**: 320–337
- Ungermann C., Neupert W. & Cyr D.M. (1994). The role of Hsp70 in conferring unidirectionality on protein translocation into mitochondria. *Science* **266**: 1250–3
- Valpuesta J.M., Martín-Benito J., Gómez-Puertas P., Carrascosa J.L. & Willison K.R. (2002). Structure and function of a protein folding machine: the eukaryotic cytosolic chaperonin CCT. *FEBS Lett.* **529**: 11–6
- Vaughan C.K., Mollapour M., Smith J.R., Truman A., Hu B., Good V.M., Panaretou B., Neckers L., Clarke P.A., Workman P., Piper P.W., Prodromou C. & Pearl L.H. (2008). Hsp90-Dependent Activation of Protein Kinases Is Regulated by Chaperone-Targeted Dephosphorylation of Cdc37. *Mol. Cell* **31**: 886–895
- Verba K.A., Wang R.Y.-R., Arakawa A., Liu Y., Shirouzu M., Yokoyama S. & Agard D.A. (2016). Atomic structure of Hsp90-Cdc37-Cdk4 reveals that Hsp90 traps and stabilizes an unfolded kinase. *Science (80-.).* **352**: 1542–1547
- Walsh N., Larkin A., Swan N., Conlon K., Dowling P., McDermott R. & Clynes M. (2011). RNAi knockdown of Hop (Hsp70/Hsp90 organising protein) decreases invasion via MMP-2 down regulation. *Cancer Lett.* **306**: 180–189
- Wandinger S.K., Suhre M.H., Wegele H. & Buchner J. (2006). The phosphatase Ppt1 is a dedicated regulator of the molecular chaperone Hsp90. *EMBO J.* **25**: 367–376
- Wang J., Lee J., Liem D. & Ping P. (2017). HSPA5 Gene encoding Hsp70 chaperone BiP in the endoplasmic reticulum. *Gene* **618**: 14–23
- Wang W., Liu Y., Zhao Z., Xie C., Xu Y., Hu Y., Quan H. & Lou L. (2016). Y-632 inhibits heat shock protein 90 (Hsp90) function by disrupting the interaction between Hsp90 and Hsp70/Hsp90 organizing protein, and exerts antitumor activity *in vitro* and *in vivo*. *Cancer Sci.* **107**: 782–790
- Wayne N. & Bolon D.N. (2007). Dimerization of Hsp90 is required for *in vivo* function: Design and analysis of monomers and dimers. *J. Biol. Chem.* **282**: 35386–35395
- Weber-Ban E.U., Reid B.G., Miranker A.D. & Horwich A.L. (1999). Global unfolding of a substrate protein by the Hsp100 chaperone ClpA. *Nature* **401**: 90–93
- Wegele H., Wandinger S.K., Schmid A.B., Reinstein J. & Buchner J. (2006). Substrate transfer from the chaperone Hsp70 to Hsp90. *J. Mol. Biol.* **356**: 802–811
- Whitesell L. & Lindquist S.L. (2005). HSP90 and the chaperoning of cancer. *Nat. Rev. Cancer* **5**: 761–772
- Wisén S., Bertelsen E.B., Thompson A.D., Patury S., Ung P., Chang L., Evans C.G., Walter G.M., Wipf P., Carlson H.A., Brodsky J.L., Zuiderweg E.R.P. & Gestwicki J.E. (2010). Binding of a small molecule at a protein-protein interface regulates the chaperone activity of hsp70-hsp40. *ACS Chem. Biol.* **5**: 611–22

-
- Xu R., Ayers B., Cowburn D. & Muir T.W. (1999). Chemical ligation of folded recombinant proteins: segmental isotopic labeling of domains for NMR studies. *Proc. Natl. Acad. Sci. U. S. A.* **96**: 388–93
- Xu Z., Horwich A.L. & Sigler P.B. (1997). The crystal structure of the asymmetric GroEL–GroES–(ADP)7 chaperonin complex. *Nature* **388**: 741–750
- Young J.C., Hoogenraad N.J. & Hartl F.U. (2003). Molecular chaperones Hsp90 and Hsp70 deliver preproteins to the mitochondrial import receptor Tom70. *Cell* **112**: 41–50
- Zanata S.M., Lopes M.H., Mercadante A.F., Hajj G.N.M., Chiarini L.B., Nomizo R., Freitas A.R.O., Cabral A.L.B., Lee K.S., Juliano M.A., Oliveira E. de, Jachieri S.G., Burlingame A., Huang L., Linden R., Brentani R.R. & Martins V.R. (2002). Stress-inducible protein 1 is a cell surface ligand for cellular prion that triggers neuroprotection. *EMBO J.* **21**: 3307
- Zhang H., Amick J., Chakravarti R., Santarriaga S., Schlanger S., McGlone C., Dare M., Nix J.C., Scaglione K.M., Stuehr D.J., Misra S. & Page R.C. (2015). A Bipartite Interaction between Hsp70 and CHIP Regulates Ubiquitination of Chaperoned Client Proteins. *Structure* **23**: 472–482
- Zhu X., Zhao X., Burkholder W.F., Gragerov A., Ogata C.M., Gottesman M.E. & Hendrickson W.A. (1996). Structural analysis of substrate binding by the molecular chaperone DnaK. *Science* **272**: 1606–14
- Zierer B.K., Rübhelke M., Toppel F., Madl T., Schopf F.H., Rutz D.A., Richter K., Sattler M. & Buchner J. (2016). Importance of cycle timing for the function of the molecular chaperone Hsp90. *Nat. Struct. Mol. Biol.* **23**: 1020–1028
- Zimmerman S.B. & Trach S.O. (1991). Estimation of macromolecule concentrations and excluded volume effects for the cytoplasm of *Escherichia coli*. *J. Mol. Biol.* **222**: 599–620
- Zuiderweg E.R.P., Hightower L.E. & Gestwicki J.E. (2017). The remarkable multivalency of the Hsp70 chaperones. *Cell Stress Chaperones* **22**: 173–189

Publications

Röhl, A., Wengler, D., Madl, T., Lagleder, S., Toppel, F., Herrmann, M., Hendrix, J., Richter, K., **Hack, G.**, Schmid, A., Kessler, H., Lamb, D. C., Buchner, J., Hsp90 regulates the dynamics of its cochaperone Sti1 and the transfer of Hsp70 between modules. *Nature Communications*, 2015, 6, 6655.

Acknowledgements

I would like to thank Prof. Johannes Buchner for his advice and support and for giving me the opportunity to carry out my PhD thesis in an exciting research environment. I would like to thank Klaus Richter, Daniel Rutz, Jannis Lawatscheck and Benedikt Weber for assistance with measurements and useful scientific discussions. I would also like to thank Margot Rubinstein and Martin Haslbeck for helping keep things running smoothly.

Special shout-outs go to all the past and present members of the Buchner Lehrstuhl, as well as those from the Lang and Feige labs who made it such a fun place to work over the years. In no particular order: Bene, Patzi, Chris, Mari-Lena, Sandrine, Pamina, Jannis, Max, Nico, Tuan, you guys were great. I would also like to thank my old office mates Vinay and Hannah for many useful and interesting scientific discussions.

I would further like to thank the Verbands des Chemischen Industrie along with the Deutsche Forschungsgemeinschaft for financial support and finally I would like to thank all my friends and family for support through difficult times.